Diamond Structures for Advanced Electronics

A. C. Pakpour-Tabrizi

Department of Electronic and Electrical Engineering

University College London

A thesis submitted for the degree of

Doctor of Philosophy

2017 March

Declaration

I, A C Pakpour-Tabrizi herewith declare that I have produced this paper without the prohibited assistance of third parties and without making use of aids other than those specified; notions taken over directly or indirectly from other sources have been identified as such.

The thesis work was conducted from 2013 to 2017 under the supervision of R B Jackman at UCL.

Abstract

Although diamond is slowly becoming an advanced technology there is contradictory information and misunderstanding surrounding the fundamental electronic attributes of the material system. In particular, the properties of boron doped diamond for electronics on quantum length scales has yet to be fully understood or utilized within devices.

In this thesis, new insight into the electronic band structure of boron doped diamond on nano and macro scales is found and novel planar boron doped nanowires are fabricated electronically probed and a new type of side gated diamond nanowire transistor conceived.

High quality single crystal diamond with thin δ-shaped boron-doped epilayers have been thought to offer a viable approach towards transistors that can operate at high speed, high power and high temperatures. δ-doping diamond has been conjectured to achieve high mobilities and carrier concentrations, properties of real interest for electronic applications. Taking advantage of diamond's thermal and electronic properties, thin films can be incorporated into realistic nanoscale devices more easily than the parent bulk system. Using angle-resolved-photoemission spectroscopy (ARPES), the electronic structure of bulk and thin films ($\approx$ 2 nm) of boron-doped diamond are uncovered. Surprisingly, the ARPES measurements do not reveal any significant differences for these systems, irrespective of their physical dimensionality. This suggests that it is possible to grow nearly atomic-scale structures whilst still preserving the properties of bulk diamond, facilitating the use of thin films diamond for devices which necessitate nearly atomic-scale components.

Using a range of techniques such as Secondorary Ion Mass, Angle Resolved Photo-emission and Raman Spectroscopy we compare thin boron doped

delta layers (BDDδl) and effectively infinite, thick bulk Boron doped diamond. We see remarkably little electronic difference and hints of low dimensional transport in both films. Using photo-lithography and Reactive Ion Etching processes, macro scale devices are fabricated, these are characterized using Hall effect techniques. For the first time, lateral boron doped diamond nanowires are defined using electron beam lithography. These nanowires are then processed into a variety of novel transistor like devices, showing exciting emergent quantum properties as well as classical transistor like behaviour.

In developing the techniques and methods to fabricate structures in diamond we find a variety of processes require optimisation and develop a skill base to handle small and sometimes fragile substrates and process them into devices.

Dear Reader,

I dedicate this thesis (mostly) to my mum and dad. They taught me to think and more importantly led me to enjoy doing. They are kind, loyal and wise, canny and bound by no unjust rule other then to try to be good in any situation (where good is mostly defined by our family unit but also by the world in which we would like to live). If when I grow up I'm one quarter of the person each of you are, I'll be half the person you are collectively and that would be a fine thing. My sister and brother, Soraya, Veera and as yet unborn bump... I like to say I bequest this science to you as you are the future... But can′t say it with a straight face. Also, Soraya and Veera are already better doctors then I can ever hope to be. Lae, I'm sorry I'm yet to take the career you always thought I would follow. Reading this perhaps you will be reminded that I am always trying.

I also should wax lyrical about Richard and the gang who have been in the DEG throughout my PhD; Rob, Sonny and Joe. It has been a privilege to work/play with friends. We collectively have lived stories great and terrible, you have inspired, motivated/unmotivated, distracted and focussed me, you've me made nearly raise my voice (I've definitely gone to a rather stern tone a couple of times). Right now you are so important to me... And looking into some dystopian future as our lives ebb and flow around the ideas and motives that guide us through time and space... you will continue to be important but we may see each other less. But as sure as my hair is too long, every now and then we will spend quality time together and do new great and terrible things.

The rest of the DEG are all lovely as well. Friends and colleagues.

Richards guidance and management style gave me the opportunity to work with numerous brilliant people all over the world. Justin, Chris, Mark to name but a few of the more senior ones. Hopefully you are all rather dryly acknowledged in the acknowledgements. Others I may have in inadvertently or purposely forgotten. If its a big deal lets do something worth publishing together to correct my omittance.

Yes My Ninjas?

Holbeach Tigers.

Swordsmithing and Juggling, Music festivals and tree chopping. Swimming.

To Pink flamingos, perfectly sized dogs, white sock art, walking on byabooballidopawhoop and the great cat hunts of lore. To all the things I will never write down. To crossing the vast Fen plains by mobility scooter. And Climbing those things that people didn't even realise were there to be climbed. To a jab from the hip, free grange wood and what′s more, to all the people, the memories past and future that will keep me, and have kept me warm.

Thank you all. Especially Olive, my other sweet release.

Regards,

Alex Too.

Acknowledgements

I would like to acknowledge my collaborators, and colleagues. Particularly, the DEG led by Prof R. B. Jackman London Centre for Nanotechnology and Department of Electronic and Electrical Engineering, University College London, 17-19 Gordon Street, London WC1H 0AH, U.K.

The team that worked directly with me on the ARPES project: F. Mazzola, J. W. Wells, Alex Schenk and Ann Julie Holt of Norwegian University of Science and Technology (NTNU), J.A. Miwa, F. Arnold, M. Bianchi, P. Hofmann and Sanjoy Mahatha of Aarhus University, Denmark as well as Johan Adell for the support at the beamline I4. Phil King, Thomas Frederiksen and Ion Errea for the valuable discussions about the data acquisitions and their understanding.

I gratefully acknowledge Diamond Microwave Ltd (www.diamondmw.com) for access to the delta-doped diamond samples grown under contract by Element Six Ltd (www.e6.com) and for essential help from Dr Richard Lang and Dr Richard Balmer respectively. Likewise the bulk doped samples were grown at the Cardiff Diamond Foundry, under the supervision of Prof Oliver A Williams and Dr Souman Mandal (www.astro.cardiff.ac.uk) who assisted by me.

For working with me while I was at Yale generally Prof, Mark Reed but also his students who worked with me on: the Silicon Nanowire project Mary Mu, the DEP project Shari Yosinski and low dimensional transport Zac Kobos and Sonya Sawtelle.

And last but not least, Diamond Microwave and the UKs Engineering and Physical Sciences Research Council (EPSRC) are also thanked for the award of a PhD CASE award to APT, and EPSRC for an award to one of the applicants (RBJ) for financial support of the work (EP/H020055/1).

Contents

List of Figures

1

Introduction

Diamond is a remarkable material. However, its many remarkable qualities are nearly all double edged swords, the material is difficult to produce and challenging to process. That said, in the years since synthetic diamond was first proven significant progress has been made. It is now possible to buy high quality diamond and the know how exists to introduce a range of impurities and to harness the extensive opportunities the diamond material system offers.

Chapters 1-3 set the historical and technical background to this thesis, describing the underlying chemistry and physics as well as the experimental techniques used in the results chapters.

Chapter 4 descries the growth of a thick heavily boron dope single crystal diamond film and initial characterisation to prove that it is in fact high quality single crystal diamond. Raman spectroscopy is used as an indicator of the bulk diamond quality as well as to indicate the presence of considerable boron impurities. Secondary-ion mass spectrometry (SIMS) is then used to confirm the doping concentration and film thickness. Alternating current magnetic susceptibility (ACMS) at cryogenic temperature is then used to show a phase transition to a superconducting state. This thick heavily-doped film is then compared to a delta-doped film.

Chapter 5 concerns Angle Resolved Photo-emission. This is a surface science technique capable of giving considerable information about the electronic structure of a material. In chapter 5 extensive synchrotron-based x-ray experiments are presented,

combining data taken at 4 different synchrotrons over 5 different beam times. It is shown that boron doped diamond maintains bulk-like electronic properties even when the doping distribution ($10^{20}B/cm^3$ peak doping level) is reduced to a few nanometres full width half maximum (FWHM). Experimentally measured electronic band structures of unprecedented resolution across a wide incident photon energy range are presented.

Chapter 6 contains macroscopic transport measurements on delta-doped diamond from my PhD sponsors and compares these to results from an alternative grower and to so called intrinsic substrates. These results suggest that multiple conduction paths may convolute the results and that the Hall mobility may not be a good indicator for device performance.

Chapter 7 demonstrates that Ohmic nanowires can be patterned using Electron Beam Lithography. Wires with dimensions of 15-20 nm wide and due to the delta doping profile of the substrate (itself a unique material), 1-2 nm thick can be reproducibly fabricated. These structures will be utilised as the cornerstone of a variety of exciting quantum devices.

2

Diamond

2.1 Making Diamond. From Meteors to Methane

The material we call diamond was named by the ancient Greeks $\alpha\delta\acute{\alpha}\mu\zeta(Ad\acute{a}mas)$ meaning something along the lines of "unbreakable" (see capt Adama BSG). Beyond its lustre as a shiny harbinger of doom diamond is a well studied material system consisting of SP^3 bonded carbon arranged in a tetrahedral lattice, it has two basis atoms in a unit cell.

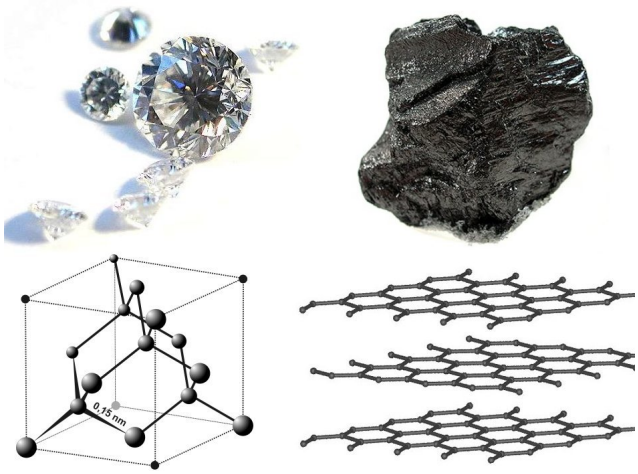

Figure 2.1: Diamond and graphite are two of the many ways carbon can organise itself taken from ref[1]

Natural diamond such as the material found in the famous Kimberlite and Lamporite pipes is thought to have been made near the Earth's mantle some 150km below

the Earth's surface. At this depth the temperature and pressure are high enough for the metastable state of carbon we call diamond to form (see Fig. 2.2). In this scenario the diamond crystals are then pushed up to the surface or near surface by a geological event such as a volcanic eruption. Diamond can also be formed from events where instantaneous, high pressures and temperatures are seen such as meteor strikes which can produce impact diamonds.

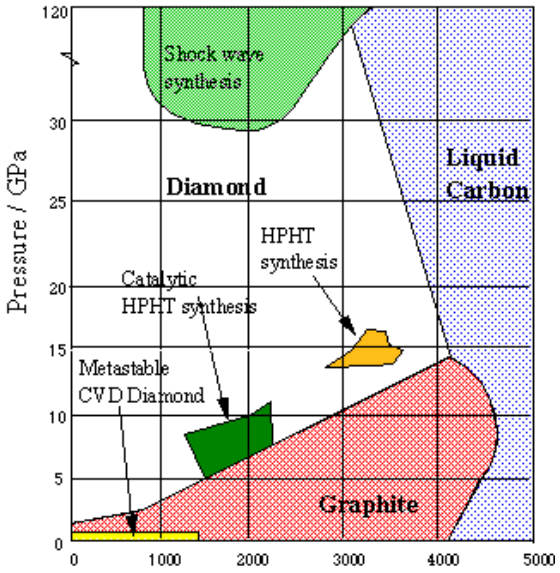

Figure 2.2: Phase diagram and potential growth mechanisms for diamond and graphite. Taken from [2]

This is not a satisfactory state of affairs if the material system's potential is to be harnessed by modern science. Its a tad slow, and the defects that give fancy diamonds their colour are unpredictably included in varying levels. It is these dopants/impurities that we must harness and understand if we are to take advantage of diamond as an electronic material. Clearly, to make electronic, technologically useful diamond material we must look to other methods of diamond production then volcanoes or meteors.

Diamond has a wide band gap and when there are low levels of impurities, is essentially an electrical insulator with spectacular physical properties: it is one of the hardest materials existing in nature, it has one of the highest thermal conductivities among the elements of the periodic table, a very high tolerance to application of strong electric fields and, contrary to standard semiconductors, it is robust against radiation damage,

a property which makes it suitable for use in hostile radiation environments [23, 24]. Altogether, these properties make diamond an appealing candidate for electronic applications, especially when acceptor species such as boron atoms are introduced into the system, adding 'metallicity' to the aforementioned properties.

2.2 An Introduction to Diamond Growth in the Laboratory

As seen in Fig. 2.2 there are several ways to be in the right part of the phase diagram to form diamond. Initial work on synthesising diamond was done under something of a cloak of secrecy due to the cold war, so exactly when things happened is hard to say. Independently, scientists in the Soviet Union and the west developed different technologies to grow diamond (anecdotally, the Soviets developed their detonation nano diamond in at least three independent labs that had no knowledge of one another). The General Electric Company (GEC) were the first to sell commercial HPHT (High preasure High Temperature) synthetic diamond in 1956. Two years earlier they had filed a patent for CVD (Chemical Vapour Deposition) of diamond [25]. The Russian approach during the late 50s and early 60s was somewhat different: they developed a process and material that we call Detonation Nano-Diamond (labelled shock-wave synthesis in Fig. 2.2).

2.2.1 High Pressure High Temperature, HPHT Single Crystal Diamond Substrate Growth

HPHT diamond substrates of both typeIIa and typeIa/b (with nitrogen impurity levels lower the 0.3%, and higher nitrogen impurity levels respectively) have in the last few years become easier to access and have improved significantly in key areas such as quality (in terms of growth zones and defect density), reproducibility and price. There are now commercial growers in Europe, America and Asia. HPHT material is mostly grown from seed material (diamond grit) in a carbon rich environment with a metal catalyst. The chamber is heated to above 2500K, melting the solvent. This is done at pressures in the GPa range. The carbon from the carbon source can now be transported to the diamond seed where it can, at the correct pressure and temperature form large diamond crystals [26]. For our purposes these rough diamonds are then laser cut and

polished by CMP (chemical mechanical polishing) until a high degree of smoothness is achieved.

2.2.2 Detonation Nano-Diamond and other diamond nano-particles

By detonating a mix of RDX and TNT in an oxygen-poor detonation chamber the atmosphere will, for a fraction of a second be in the right place in the carbon phase diagram to form Detonation Nano-Diamonds DNDs. These DNDs will be covered in graphitic carbon and other impurities. To remove these a series of aggressive physical and chemical cleaning steps are used to refine the residue down to 5-10nm diamond nanoparticles. These nanoparticles can then be used as seed material for homo-epitaxial growth of diamond on non-diamond substrates.

2.2.3 Microwave Enhanced Chemical Vapour Deposition, MEPCVD High Purity Single and Polycrystalline growth

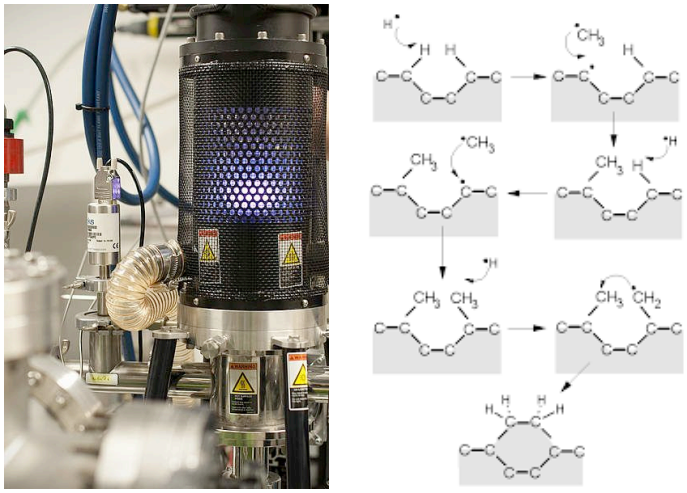

Figure 2.3: 1.5kW diamond growth system bult by SEKI Diamond Systoms and standard model for diamond growth proposed by James Butler among others taken from [3]

By creating a hydrogen plasma with a microwave generator it is possible to cheat nature and grow diamond in a metastable quasi-epitaxial manner. Most work is homo-growth although there is a small but important effort to work on heteroepitaxial growth[3]. It has been postulated that the polishing process actually does a lot of

damage to the crystal lattice in the first 10μm or so. Several groups are working on pre-CVD growth treatments to help with this[22].

2.3 Diamond as an Electronic Material

2.3.1 What are electronic bands

A crystalline material is made up of a periodic lattice of atoms. It is well known that in a single atom the electrons can only have discrete quantised energy levels and that when a number of atoms come together to form a crystal some of the electrons are tightly bound to the atoms. These electrons remain localised and their energy levels near constant, these energy levels are called the valence band. The valence electrons are usually integral to bonding. The electrons do not, however, have to stay localised. If they are given energy they can probabilistically move between nearby atoms causing electronic conduction. The allowed energy levels form bands and the amount of energy required to promote an electron from the valence band to the conduction band is called the band gap. In metals the Fermi-level crosses the valance band and there are free electrons able to move and carry charge across a potential difference.

In semiconductors the gap between the valence and conduction bands is small enough that thermal or electromagnetic excitations can promote a carrier from the valance to the conduction band. By introducing dopants that either have an excess of holes or electrons the band gap can be engineered, creating donor states which are mid gap and can be more easily accessed from either the conduction or valence bands (n and p-type respectively). A p-type semiconductor has an excess of holes, these holes usually come from a trivalent impurity such as boron or gallium.

The Fermi level sometimes referred to as electron chemical potential, E_F is the highest available electron energy level at absolute zero. The position of the Fermi level with the relation to the conduction band is a crucial factor in determining electrical properties. For an intrinsic crystalline material E_F should sit mid gap, for an n-type material it will be closer to the conduction band whereas for a p-type material the Fermi level will be closer to the valance band.

2.3.2 All about the Surface. Band Bending in Diamond

The band structure at or near the surface of diamond is very sensitive to the surface chemistry. This allows considerable scope for band gap engineering. It also means that care and consideration must be taken during any processing as it may fundamentally alter the physics at the surface (see Fig. 2.42.62.52.6 2.7).

At the start of the semiconductor revolution Schottky and Mott described the rectifying effect observed in metal-semiconductor interfaces using a band bending concept [27] [28]. When a metal is put into contact with a semiconductor, charge transfer will occur. Fig.2.4 shows idealised schematics for energy bands between an n-type semi conductor and a metal. If the work function of the metal ϕ_m is larger then the work function of the semiconductor ϕ_s, $\phi_m > \phi_s$ electrons will be drawn from the semiconductor to the metal until the Fermi levels for each material align.

When in contact and at equilibrium, a Helmholtz double layer is formed at the metal/semiconductor interface, where, due to electrostatic induction the metal has an excess of electrons and negative charge while the semiconductor is positively charged near the interface. As there are relatively few free carriers in a semiconductor this induced charge can not be compensated or screened and the a so called space charge region is formed.

In the n-type semiconductor, when $\phi_m > \phi_s$, the electrons are depleted in the space charge region, and this region is therefore called the depletion layer and is characterized by excess positive charge. When $\phi_m < \phi_s$, as shown in the right side of Fig.2.7, the electrons are accumulated in the space charge region due to the electron transfer from the metal to the semiconductor, and this region is called the accumulation layer. In general, when the Fermi level of the metal is below that of the semiconductor, charge will flow to the metal causing the semiconductor Fermi level to decrease, and vice versa[4]. The continuous shift in the bands due to charge transfer is called band bending.

So, when $\phi_m > \phi_s$ in an n-type semiconductor, a potential barrier is formed at the metal−semiconductor interface, this is called the Schottky barrier (ϕ_{SB}),

$$\phi_{SB} = \phi_m - \chi_s \tag{2.1}$$

where χ_s =electron affinity of the semiconductor. When $\phi_m < \phi_s$, in an n-type semiconductor, there is no Schottky barrier and the metal−semiconductor contact is

ohmic.

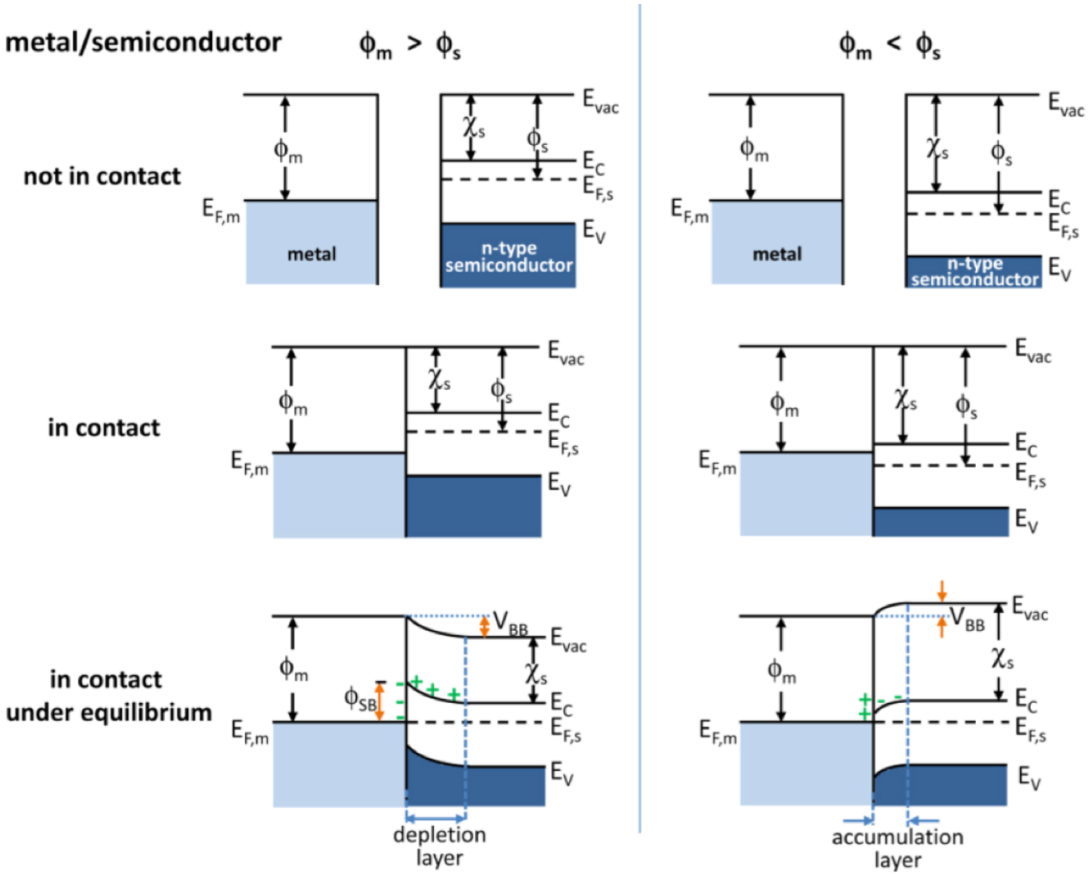

Figure 2.4: Energy band diagrams of metal and n-type semiconductor contacts. Evac, vacuum energy; Ec, energy of conduction band minimum; Ev, energy of valence band maximum; ϕ_m, metal work function; ϕ_s, semiconductor work function; χ_s =electron affinity of the semiconducto; $E_{f,s}$, Fermi level of semiconductor; ϕ_{sb}, is the Schottky Barrier height, V_{BB}, valence band barrier height. Taken from [4].

Fig.2.5 shows how a similar band bending effect can be caused by a nearby electric field. For simplicity this diagram assumes that the work functions of the electrode and the semiconductor are the same. The electric field is created by putting a voltage between the semiconductor and electrode. Due to the lack of free charges in the semiconductor the field can penetrate beyond the surface of the semiconductor, modulating the electronic properties of the channel. This is the fundamental effect utilised to make a transistor. Even without an external electric field the surface states caused by the reconstruction of a truncated crystal can cause band bending as described in Fig.2.6.

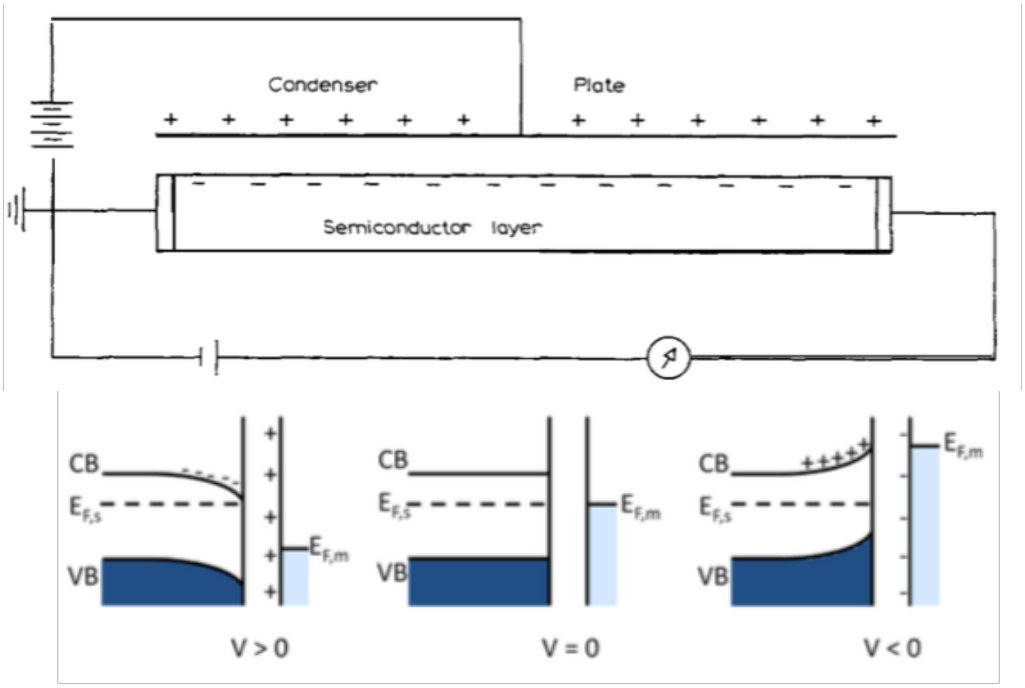

Figure 2.5: Schematic diagram of a field-effect experiment for an n-type semiconductor with no surface states. Adapted from Bardeens Nobel lecture [5] and [4].

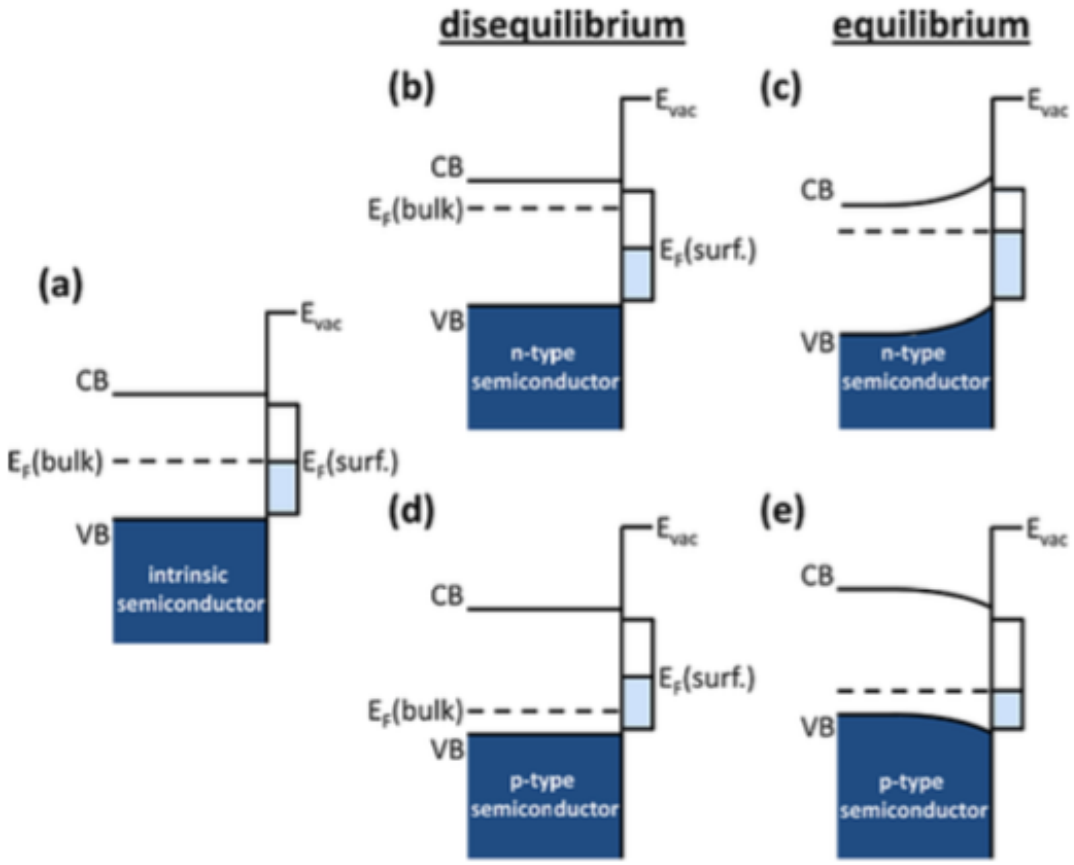

Figure 2.6: Schematic electron energy levels near the surface of a clean semiconductor: (a) undoped (intrinsic) semiconductor; (b) disequilibrium and (c) equilibrium between n-type bulk and its surface; (d) disequilibrium and (e) equilibrium between p-type bulk and its surface. There are different methods for solving the Schrodinger equation at surface to theoretcally deifing the electronic band structure, these are beyond the scope of this work.Taken from [4].

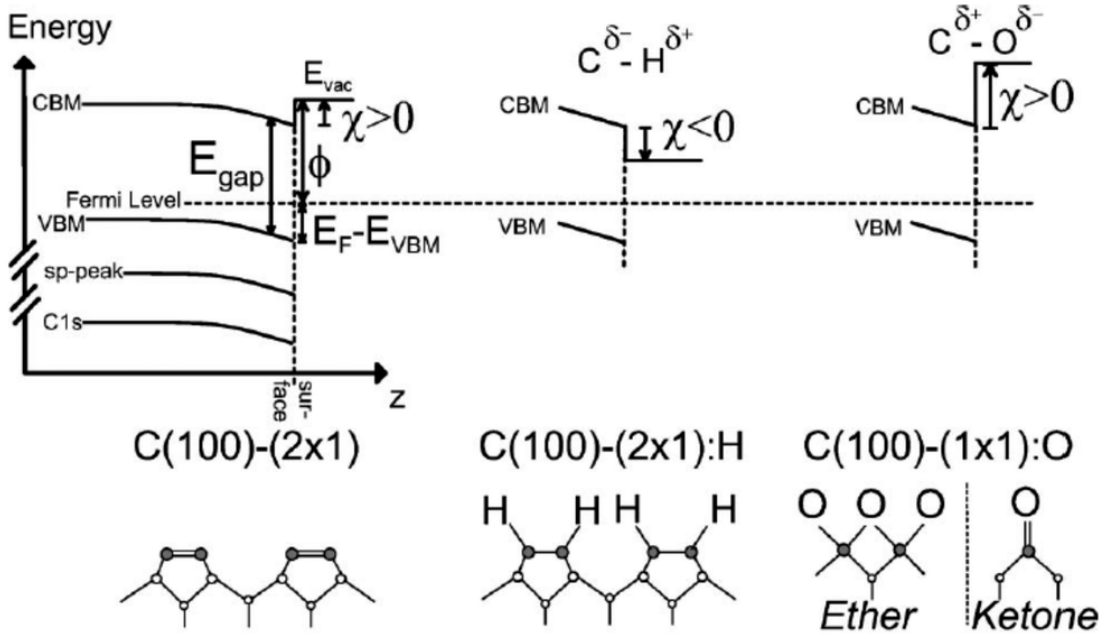

Figure 2.7: The band structure of diamond is very sensitive to the surface chemistry. Here we see how different moieties affect the bands and resultant - electron affinity. The relative elecronegativity of the surface molecule to carbon is proportional to this shift. Taken from [6].

2.3.2.1 Hydrogen Surface Conductivity

It was observed that when the diamond surface is covered with a majority of hydrogen moieties and an adsorbate such as water the system will show a high surface conductivity. The adsorbate is essentila for the charge transfer to occur. After much discussion the consensus has settled on a surface model which relies on the band bending possible in diamond as well as charge transfer of electrons from the diamond into the absorbate forming a 2D hole gas [29]. Although this is a very interetsing effect it has found little functional use as it is not a very stable system. The surface chemistry will over time degrade, becoming a mix of carboxylic groups, and the conductivity will decrease. The system is also vulnerable to changes in atmospheric conditions. However, it must always be kept in mind that it is a possible conduction mechanism. The difference in

activation energy, around 0.02ev [30] for a surface channel as opposed to a boron dopant which is in the range 0.7eV [31] and nitrogen which is a N type donor and is reported to have an activation energy near 1.7eV [32] allow experimental routes to distinguish between conduction mechanisms.

2.3.2.2 Oxygen Moieties, Pinning the Fermi-level

If the surface of diamond is covered with oxygen or fluorine , both of which have high electronegativities the Fermi-level of the band structure at the interface between the diamond and the atmosphere is pinned. On intrinsic diamond this means the wide band gap is maintained without any intermediate states, and no surface conductivity is possible [33]. This can be useful to define conductive and non-conductive areas on intrinsic material [34] and to simplify measurements on bulk doped diamond samples where surface conductivity may confuse measurements.

2.3.3 Doping Diamond During Growth

Boron is an electron acceptor and, given its small atomic radius can be easily incorporated substitutionally into the diamond lattice. This leads to an effective hole-doping, which makes diamond metallic [35]. Boron can be substitutionally incorporated into diamond [36] during growth by adding a boron precursor into the mix either as a gas or a solid. The deep donor level of boron and issues arising from threading propagation during growth, twining and growth zone formation (by which I mean regions where growth is mostly on some other growth plane then the one intended), an increase in graphitic content with thick films due to the CVD chamber sooting up, crystal lattice stress caused by all of the above and the incorporation of an atom which although close to the same size as carbon is not exactly the same size, leads to lots of scattering sites and carrier traps that ultimately make heavily boron doped diamond have either high mobilities and low carrier concentration or high carrier concentration and low mobilities. This is not ideal for a lot of electronic applications.

Doping diamond by substitutional incorporation of boron atoms into the carbon lattice is nowadays a mature technology and boron doped diamond can be purchased from a number of supliers. Doping concentrations from semiconducting to metallic levels are possible and the resolution in dopant positioning can be controlled down to

the nanometer scale [37, 38]. Even though the predicted mobility and carrier concentration enhancements theorised for δ-doped diamond have yet to be experimentally demonstrated, making boron-doped diamond at the nanometer scale still offers several advantages over the bulk counterpart: given its reduced size, it can be better integrated into a real miniaturized system, the costs are reduced and patterning metallic architectures with nearly atomic scale control over the dopant concentration is possible.

2.3.4 Delta Doping of Diamond

δ-doping is a technique known since the eighties for incorporating high concentrations of dopants into semiconductors and its use has widely spread into the semiconductor industry, in particular for doping silicon for electronic applications. The name 'δ-doping' originates from the idea of placing a narrow dopant profile in a semiconducting material, creating a structure whose impurity concerntration tends towards an atomically sharp plane within an intrinsic bulk crystal this resembles a δ-function [39]. More generically, δ-doping consists of doping a material with donor or acceptor species in a narrow region (from less than 1 nm to several nanometres), engineering a spatially confined layer of dopants, usually into the bulk of a material. Such a dopant profile is responsible for an effective n- or p-type doping of the host material, depending on whether the doping species are donor or acceptor species, respectively [39, 40]. The structures obtained by δ-doping are therefore hybrid systems with electronic properties dictated by the complex interplay of quantum size effects, spin and charge ordering and the overlap between the host material and the dopants' atomic-wavefunctions. δ-doping is a well established method for doping solid state systems such as silicon and has found widespread use in technology, leading to the establishment of an intriguing route to realize working atomic-scale devices [41, 42, 43], whilst constituting a test-bed for investigating quantum effects in solid state systems [44, 45, 46].

After vast efforts were spent the diamond community is generally of the opinion that Delta doping in diamond has been and will be a failure. My sponsor reported record Hall mobilities as high as 900 cm^2/Vs although could only achieve device mobilities which were significantly lower [7]. This makes the current technology as reported not well suited to high frequency high power devices.

The main samples on which this thesis hinge are the 100 or so samples that are the remenant of that project. Mostly they have surface consisting of δ-doped diamond

with the doped epilayer being of different thicknesses [7]: by using this doping approach metallic p-type 'thin' diamond samples where the full width half maximum of the dopant distribution is ≈ 2 nm an example is shown in Fig. 2.8.

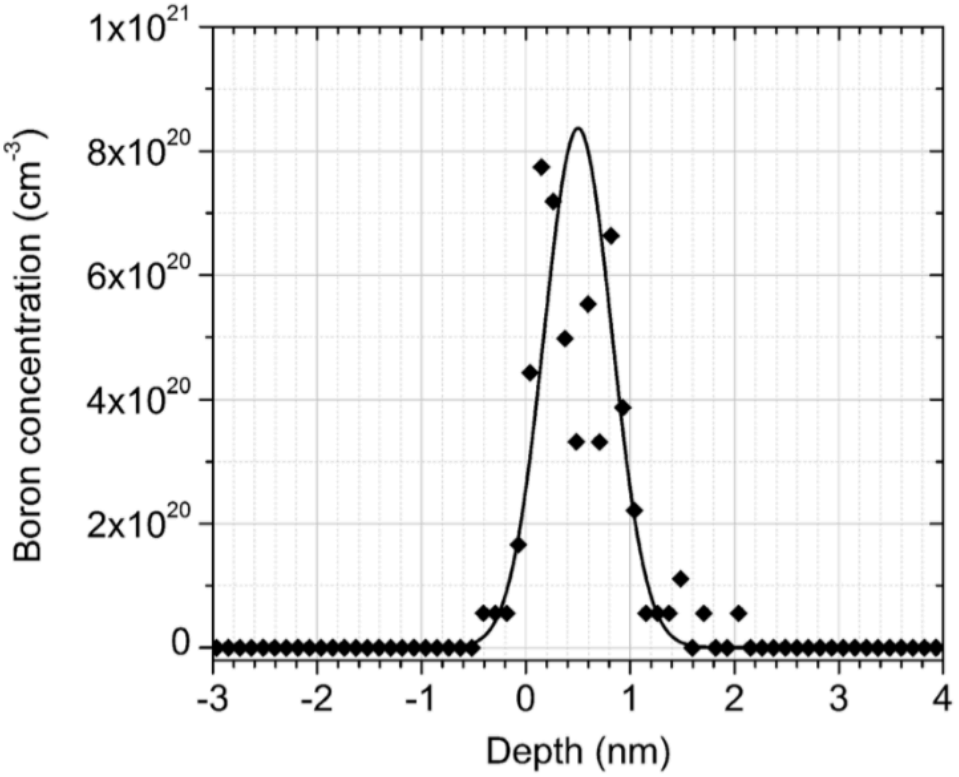

Figure 2.8: A plot of the boron profile of an example delta layer measured by ERDA showing a full width at half maximum of 1nm. Solid line represents a Gaussian fit to the measured data, the boron from depth $<$ 0nm is a measurement artefact[7].

2.3.5 Contacts to Diamond

To realise an electronic device contacts must be patterned on the semiconductor surface to allow either charge to be injected and sunk or voltages to be applied. In most material systems this somewhat of a black art and the nature of the interfaces between different materials is a deep subject. Diamond is no exception, and although there is a wealth of literature on contacts to diamond there is no absolute consensus as to what makes for the best metallisation and process treatments. The community has generally settled on a few metals used for contacts depending on the nature of the device and the constraints

of cost and equipment availability.

2.3.5.1 Ohmic

A perfect ohmic contact is one where there is no recertification of charge at the interface between two materials. i.e. current will increase linearly with applied voltage obeying Ohm's law (V=IR, Voltage = Current.Resistance). This can be challenging on p-type diamond as it is required that the workfunction of the metal be greater than or equal to the sum of the electron affinity and band gap of the semiconductor.

Refractory metals that can form a carbide such as Ti, Mo and Ta have been shown to make an Ohmic contacts with contact resistances on the order of $\rho_c = 4.93 \times 10^{-6}$ $\Omega\ cm^2$ [47] [48]. The series resistances decrease after annealing, with a reduction in ρ_c of one or two orders of magnitude after an anneal for longer the 5 mins at temperatures greater then 400C. Palladium (Pd) $\rho_c = 4.93 \times 10^{-7}$ $\Omega\ cm^2$ annealed at 400C has also been shown to make an Ohmic contact. [49].

Usually, a gold capping layer will be evaporated over the carbide forming layer; this allows wire bonding and/or probing with mechanical probes. The most common layers of metals are Ti/Pt/Au & Cr/Au, where the Pt works as a diffusion barrier.

By working with heavily doped diamond Ohmic contacts can be easily made. As the doping concentration decreases this becomes more difficult. Either way a tunnel contact is formed, the difference in the doping levels changes the semiconductor (diamond) barrier height relative to the metal[47]. The metallic or near-metallic doping of the diamond means that, although there is a barrier at the surface, statistically a large number of carriers can be injected through a few nanometres of a depletion region into the device without observing significant non-linear phenomena.

2.3.5.2 non-Ohmic

Aluminium can be used to form a Schottky-type contact with barrier heights anywhere between 0.8 and 2.2V [50][51][52], although it has been shown that the barrier heights will decease and the contact will become Ohmic after anneals at or above 700K[53].

2.3.6 Field Effect Transistors

The word transistor is a portmanteau of the words transfer and resistor, this word describes the device's basic purpose as a transistor can modulate the resistance between

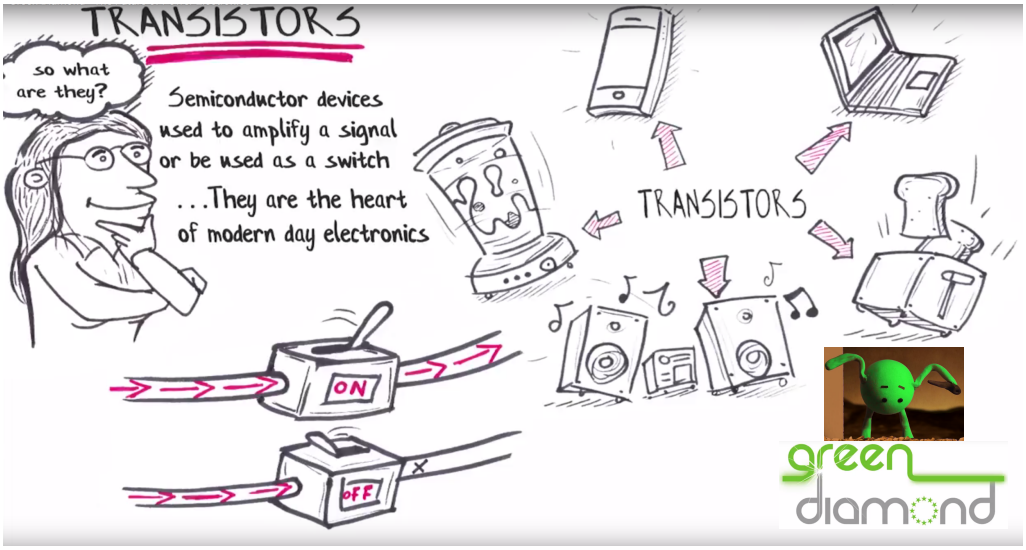

Figure 2.9: Overly simplifed description of a transistor used in GreenDiamond video (directed by author)[8]

two nodes (the channel) by a signal at a third node (the gate). It is generally accepted that Bardeen, Brattain and Shockley demonstrated the first solid state transistor in 1947: after this, the development of transistors at Bell labs and other universities and private institutions continued at a prodigious rate and heralded the start of the semiconductor age, which I posit we now live in. Transistors are integral components in a huge variety of modern technologies. Often they are used as switches or to amplify signals and nearly all of our modern conveniences will contain at least one... probably millions.

Over the last 60 years vast resources have been spent on transistor research and there are now many varieties of transistor-like devices that operate in different ways for different purposes. This thesis will concern itself with p-type conductivity in devices that are most similar to the metal-oxide-semiconductor field-effect transistor (often referred to as a MOSFET, MOS-FET, or MOS FET)

An electric field can cause free electrons (or holes) to conduct a current along a path, this is called drift. The current density due to these drifting carriers is the sum of the electron and hole velocities ν_h and ν_p. q is the elemental charge and n is the

number of the carriers.

$$J = qn\nu_p + qn\nu_h \tag{2.2}$$

When the electric field, E, is small, the carrier velocity is proportional to E. The constant of proportionality is called the mobility, μ.

$$J = qn\mu_p E + qn\mu_h E \tag{2.3}$$

At high E the carrier velocity saturates and is limited by scattering processes. In fact the mobility is affected by a number of constraints. Generally, the mobility of electrons in a semiconductor is significantly higher then the mobility of holes. As hole conduction happens in the valence band with valance electrons that are closer to the nucleus, holes generally have a higher effective mass and are scattered or trapped more readily.

The field-effect mobility can be extracted from the transconductance and gate capacitance using Eq.2.4 , where L_g and W_g are the gate length and width, C_{ox} is the dielectric capacitance, g_m is the peak transconductance, andV_{DS} is the voltage drop under the gate [54].

$$\mu_{FE} = L_g g_m/(w_g C_{ox} V_{DS}) \tag{2.4}$$

2.3.7 NanoWires and NanoWire devices

Semiconductor nanowires have been fabricated in material systems as varied as silicon [55] and WS_2 [56]. The high surface area to volume ratio makes them ideal for devices such as biosensors [57] or double, triple and even all-around gate nanowire transistors [58]. All of these devices utilise a range of things that can happen when devices become this small. In a nanowire, balistic transport is possible [59]. This is were a carrier is transported through the wire without scattering, this is desirable as it should mean negligible voltage drop across a channel resulting the optimal ON-state conductance for a transistor. More exotic physics also becomes available for simple experimental exploration in the quantum world observable on these length scales, such

as the observation of the fractional a.c. Josephson effect in a hybrid semiconductor-superconductor InSb/Nb nanowire junction, a hallmark of topological matter such as a Majorana particle [60]

Diamond has been fabricated into vertical nanowires/nanograss/nanopilars by using colloids as an etch mask or patterning other plasma resistant materials locally on top of diamond. [61]. Electronic devices or applications have not been reported for such wires as the 3D processes required are significantly more difficult than standard planar processes which are used in other nanowire devices.

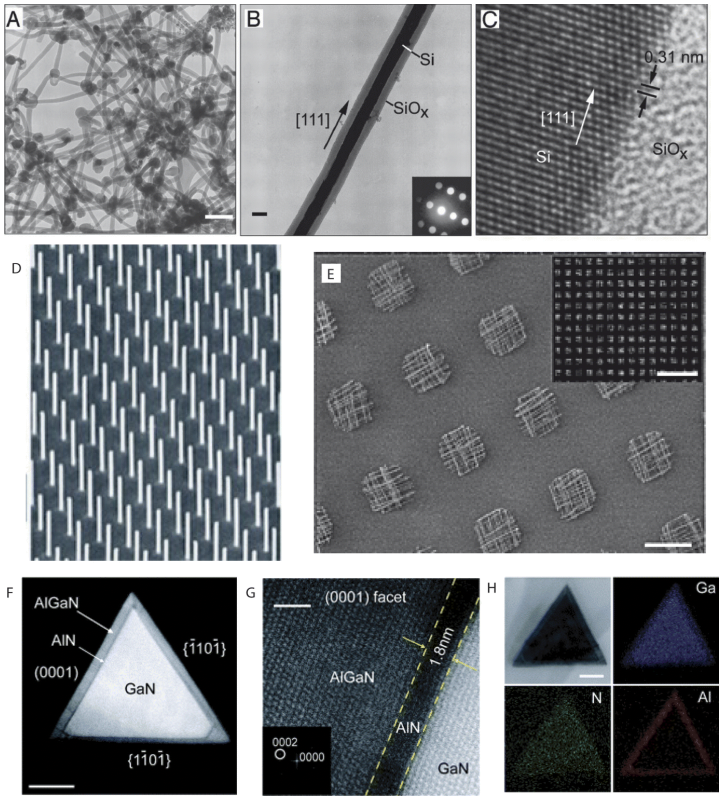

Figure 2.10: Overview of semiconductor nanowires and their applications. (A) TEM image of Si nanowires produced after ablation of a $Si_{0.9}Fe_{0.1}$ target. Scale bar: 100 nm. (B) Diffraction contrast TEM image of a Si nanowire. Crystalline material (the Si core) appears darker than amorphous material (SiO_x sheath) in this imaging mode. Scale bar: 10 nm. Inset: electron diffraction pattern recorded along the [211] zone axis perpendicular to the nanowire growth axis. (C) HRTEM image of the crystalline Si core and amorphous SiO_x sheath. The (111) planes (black arrows) (spacing 0.31 nm) are oriented perpendicular to the growth direction (white arrow). Reproduced with permission from [9](D) Tilted SEM image of a vertical InAs nanowire array grown on an InAs (111) B substrate. The spacing between nanowires is 0.5 μm. [10]. (E) SEM image of patterned crossed nanowire arrays. Scale bar: 10 μm. Inset: large area dark field optical microscopy image of the crossed arrays. Scale bar: 100 μm [11]. (F) High-angle annular dark field scanning transmission electron microscopy (HAADF-STEM) image of the cross section of a GaN/AlN/AlGaN nanowire. Scale bar: 50 nm. (G) Lattice-resolved HAADF-STEM image recorded at the (0001) facet of the nanowire. Dashed lines highlight the heterointerfaces between layers. Scale bar: 2 nm. (H) bright field STEM image and corresponding EDS elemental mapping of the same nanowire, indicating spatial distribution of Ga (blue), Al (red) and N (green), recorded on a GaN/AlN/AlGaN nanowire cross section. Scale bar: 50 nm. Taken from[12].

2.3.8 Diamond Transistors and Transistor Like Devices

A variety of devices such as MESFETs, MISFETs and even Bipolar Juncton transistors have been demonstarted using the hydrogen surface channel on diamond [62] [13]. These show high current densities, cut-off frequencies for current gain (fT) and power gain (fMAX), and reasonable output-power density at reasonable frequencies all however suffer from large reliance on ambient conditions on top of the usual diamond issues of small wafers of varying quality.

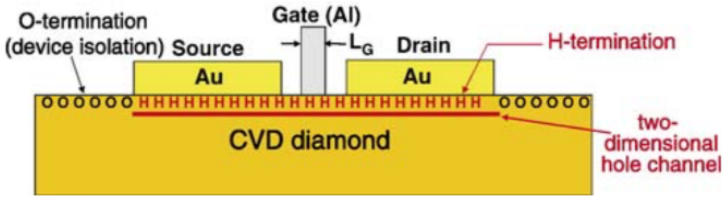

Figure 2.11: Schematic cross-section of H-terminated diamond FET.[13].

A device like Fig.2.11 must be oporated inside a vacuum if stability is desired. To avoid this different encapsulation processes such as SiO_2 or some mysterious proprietery polymers to stabilise the device [62]. Although progress continues to be made to make this kind of surface transfer doping based device, in any application where it can realistically displace Si or a material like AlGaAs it is unlikely to be viable. This is because one of diamonds unique selling points is stability, silicon and similar semiconductors can be engineered to be remarkably efficient and cheap. But the are all plagued (in some applications) by mobile dopant's, diamond does not suffer from this. Therefore traditional band gap engineering to substitutionally dope diamond is a large area of diamond research.

An inversion channel diamond MOSFET with normally-off characteristics has recently (at the time of writing this thesis) been proven [14]. Fig. 2.12 shows a schematic of the device. The MOSFETs exhibit a high drain current density compared with previously reported diamond JFETs (0.48mA/mm) and MESFETs (0.06mA/mm).

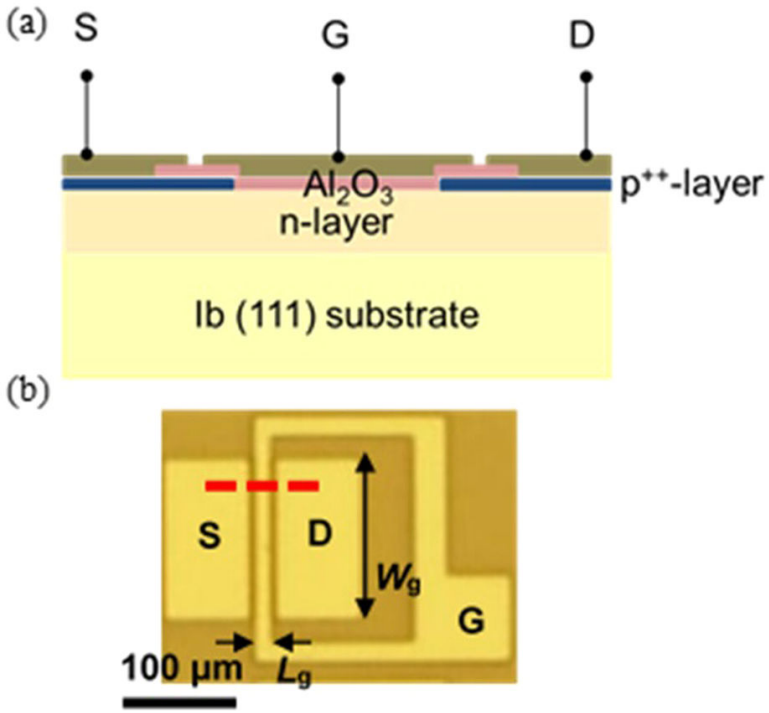

Figure 2.12: (a) Schematic cross-sectional structure and (b) top-view optical image of Al_2O_3/diamond MOSFET with n-type body. Schematic structure in (a) is cross-sectional view along red broken line in (b). S, D and G are source, drain and gate contacts, respectively. Taken from[14].

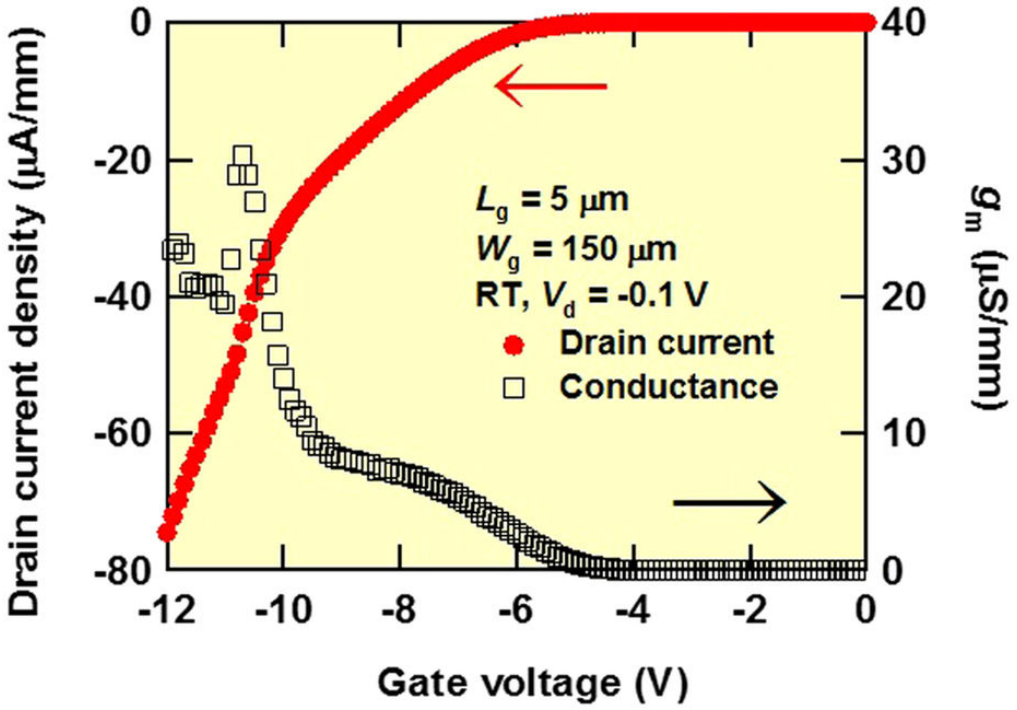

Figure 2.13: Applied V_g ranges from 0 to -12 V with a voltage step of -1V and V_{ds} is a constant value of -0.1V, for device in Fig. 2.12. Taken from[14].

As with most diamond devices there are multiple issues that need improving; substrate quality particularly in the n-type layer, interface quality between doped layers as well dielectrics and dielectric crystallinity need to be studied in more depth.

2.3.9 Diamond as a Superconductor

The electronic properties of bulk boron-doped diamond have been extensively studied for more than five decades. The interest in this system has even increased during the last ten years, with both theoretical and experimental results having demonstrated the existence of a superconducting state accompanied by a metal-insulator transition (MIT), at ever increasing temperatures. Most growers can now routinely make a single crystal sample with T_c=5 − 7 K, [35, 63, 64, 65]. The controversial record upper transition temperature for diamond of 25K [66] is generally thought to require further proof. Diamond is interesting as a superconductor as it is a very simple system, so trying to understand what is happening is easier then some of the more exotic high T_c materials and its unique physical properties make it ideal for making devices like MEMS[67] or high critical field superconducting interference devices[68].

2.3.10 Diamond and Biology

Diamond is an ideal material for biosensing; it is exceptionally biocompatible meaning a diamond bioFET could be used in physiological environments without significant biofouling [69]. A variety of functional groups can be easily attached and patterned over the diamond surface, allowing the use of orthogonal chemistry to affect the suppression of nonspecific binding. Diamond also possesses a wide potential window for electrochemical measurement (3V window where minimal gate-leakage current is observed).

2.4 Conclusion

This chapter has set the historical and technical background to this thesis. It describing the underlying chemistry and physics of diamond as well as some of the existing applications.

3

Experimental Methods and Process Engineering

3.1 Handling and Mounting Samples

Handling small samples requires patience and a Zen attitude. All movements and actions should be considered and controlled otherwise it is easy to spend hours on your knees looking for a small transparent sample. For some processes it is possible and desirable to mount a small sample on a carrier wafer. Various epoxies and oils can be used to attach the die to the carrier wafer. This approach has some advantages; The sample is now effectively large, easy to handle and potentially compatible with wafer scale processes. It has some disadvantages: the choice of bonding media must be compatible with all of the. This is particularly challenging if the process flow involves a mix of plasma and wet acid processes as well as requiring vacuum compatibility.

Choosing the appropriate tweezers for the sample and process is vital. Using the smallest tweezers that can comfortably hold the sample prevents some issues, namely there is often residue on the corners of the sample after spinning resist which can cause the samples to stick to tweezers in unpredictable ways. When drying a sample holding the sample down on a clean wipe and blowing with the highest flow of an inert gas (normally N_2) is vital to ensure no residues are left behind.

3.2 Cleaning Samples

Diamond is a very resilient material. This means that for films thicker then a fewμm we can clean them quite aggressively. A mixture of boiling acid and oxidising agent can be used to remove both organic and metallic contamination. This also has been shown to functionlise the surface with various oxygen moieties[70]. For processes where the surface chemistry must not be too greatly changed, sonicating in strong solvents such as butyl-acetate, acetone and IPA will remove grease, dust and a number of other contaminants. Cleaning samples is of vital importance; a speck of dust on a 4mm chip can cause resist to flow in weird and wonderful ways, resulting in varying film thickness and uncontrollable results.

3.3 Knowing your Carbon Allotrope

There are many techniques that can be used to identify diamond thus ensuring that your partner hasn't purchased a cubic zirconium crystal or that your sensor is not mostly graphite.

3.3.1 Raman

Raman spectroscopy is a powerful technique for quickly recognising diamond, as it has clear and distinct features. Raman spectroscopy named after Sir C. V. Raman works when incident radiation inelastically scatters off phonons or other exitons in the material system under interrogation. The monochromatic light (now usually from a laser source although the original work by Raman in the 30s used sun light) excites a state within the system to a virtual state before the now inelastically scattered light escapes.

The zero phonon line (ZPL) manifests as a sharp peak at 1332 cm^{-1}, and graphitic carbon content and crystal stress can also be analysed by looking for the sp2 carbon, Raman active modes and peak shifts in the ZPL respectively. This makes Raman spectroscopy is an easy way to identify diamond and in the aforementioned ways qualitatively compare different samples.

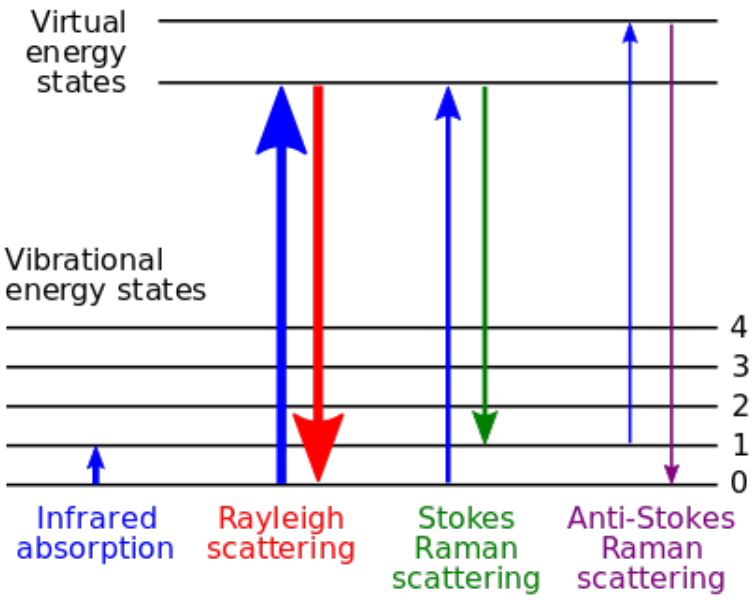

Figure 3.1: Raman scattering processes. Taken from [15]

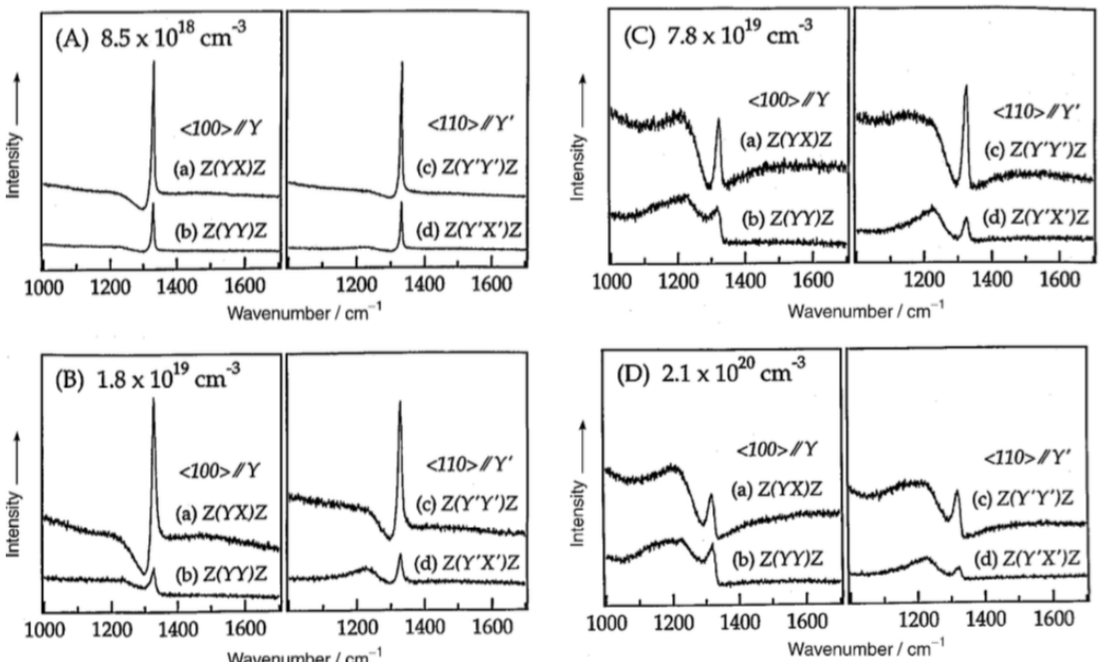

Figure 3.2: Polarized Raman spectra of 100 facet for B-doped CVD diamond single crystals with different boron concentrations (A) 8.5x10$^{18}cm^3$, (B) 1.8x10$^{19}cm^3$, (C) 7.8x10$^{19}cm^3$, and (D) 2.11x10$^{20}cm^3$. The electric vector of the incident laser is parallel to $(a), (b)100, and (c), (d)110$, respectively. The incident laser was the 514.5 nm line of an Ar ion laser. Taken From[16]

3.3.2 Secondary Ion Mass Spectormetry

SIMS is fundamentally a very simple and powerful technique. Primary ions of low energy (in the case of diamond 10-15keV) heavy particles such as $Ar^{+} or O^{+}$ are used to sputter the solid in question. Statistically, the ejected particles are most likely to come from the first 1-3 atomic layers, making the technique very surface sensitive. The secondary ions that escape can be collected and categorised as a function of their mass, giving a lot of information about the composition of the surface as you etch through a small area.

SIMS in diamond is slightly more difficult as light atoms and strong bonds (diamond is hard) make for a challenging process. Add to this very thin impurity layers and effects such as SIMS' induced ion mixing and the whole experiment can become very difficult. It is, however, possible [71] and can be used to measure doping concentrations and film thickness.

3.3.3 Low Energy Electron Diffraction

LEED (Low Energy Electron diffraction) can be used to probe the surface reconstruction of a single crystal material. By shining electrons within the range 20 - 200 eV upon the sample a backscattered electron diffraction pattern is produced. Only elastically scattered electrons contribute to the diffraction pattern and the pattern itself is the Fourier transform of the real space lattice of the crystal.

The bare diamond surface has two dangling bonds at each surface carbon atom. These can form a variety of bonds with a range of atoms, or the surface may reconstruct via dimerisation to form a Π surface. As shown in Fig.2.7 this results in a (2x1) symmetry in the LEED pattern [72]

The sharpness and intensity of the pattern observed during a LEED measurement says something about the quality of the crystal at the surface as well as possibly giving insight into what chemical species are there (if there is a known and unique surface reconstruction for some given element). It does not, however, give definitive information about the surface chemistry, as many different moieties can raise the same reconstruction. Accordingly, it is now generally believed that the 1x1 reconstruction involves the dihydride structure (when the sample has not been annealed above 1000K) [73].

3.4 Lithography

By spin coating polymers that are sensitive to either electrons or photons of a certain energy it is possible to pattern a substrate with either a positive or negative resist. This process happens when the resist is selectively exposed to such radiation and various chemical processes lead to either scission of long polymeric chains or polymerisation. In the case of a positive resist the exposed areas can be removed after exposure by immersion in a solvent. The parameters of the exposure (focus, time, power/charge per unit area) and of the development (strength of developing solution, time in solution and temperature of solution) will affect the angle of the side walls (aspect ratio) as well as film properties such as stress. Both exposure and development parameters can effect the final shape achieved after lithography.

Obtaining uniform continuous films of polymers on small samples can be challenging. One major problem is the dreaded edge bead. This manifests as a build up of polymer gathered in a corner due to the surface tension at the corners/edges and the forces that push the fluid polymer flat and out towards the edges. At the intersection of two edges the problem is particularly pronounced. This is a particular issue for photolithography where the substrate to be patterned is to be placed in hard contact with a mask. Edge beads cause several problems: firstly, a large edge bead can greatly reduce the usable area of a substrate; this is mostly due to the greatly increased thickness requiring different exposure parameters, and is true for any type of lithography. Secondly, in multi-layer devices made with photolithography where alignment is sensitive or fine the edge bead can cause the sample to move relative to the mask as you bring the sample up to the plane of the mask.

The edge bead can be minimised. For any given resist, substrate material and substrate geometry there are several important steps to optimising the resist. Assuming a square or symmetrical substrate, the sample must be placed as near as possible to perfectly central. If this is not the case, the off-axis spinning will mean one edge bead is significantly large then the others. The spin coater has a variety of pucks for use with different substrates, and the choice of puck is vital. I generally use the goose-neck puck (a puck with a small goose necked vacuum hole), as I find if the resist is dispensed in the correct way it gives the best results. By painting an excess of resist (using a clean pipette) across the substrate and the puck a good even film can be achieved. Although

the fluid dynamics are complicated I think that some sort of wicking-type process helps overcome the large surface tension experienced on the edges/corners of the samples. The negative aspect of this puck is that the vacuum hole is small relative to the chip dimensions and for thinner samples there can be some bowing during spinning which can lead to a uniform area of resist where the vacuum hole is and then a gradient out to the edge.

After mounting the sample carefully there are two parts to the spin process that must be optimised. First, we must flick off excess resist and then we must smooth out the remaining polymer to produce a uniform film. The flick stage of the spin can be approached in a number of ways, with really gloopy (high viscosity) resists such as the AZ series photoresists an initial very fast spin, relaxing down to a lower smooth stage can be succeful, athough this is unusual. Normally, a quick acceleration to around half of the the final spin speed for a second or two is appropriate. With small samples, spinning at high RPMs, sometimes out of the range listed in data sheets can allow better uniformity of the resist over a large area and significantly smaller edge beads. Spinning for too long or too fast with some resist can lead to streaking and poor film quality.

3.4.1 Photolithograhphy

3.4.1.1 Resists, Exposure and Development

After much process engineering the following processes have been settled upon and used extensively throughout this thesis. For liftoff, LOR10B with S1818 on top. Coating one layer at a time, spin at 1krpm for 0.2 s and then 4.5krpm for 45s, bake at 190C and 115C for 10 and 1 mins respectively. Expose with 23mW of UV. Both are positive resits. As a rule of thumb liftoff is possible for a film up to 1/3 of the resist height. The resist height will vary depending on the substrate size and geometry. Develop for 30s after pattern clears in MF-26A. For a $3.6mm^2$ piece, 200nm of material can be lifted off from a 1.2μm resist stack. Development time is 90s.

SPR220-7, Spin at 9999rpm and bake at 100C. For a thicker SPR220 film spin a second layer and bake at slightly High T. SPR220-7 is also a positive resist. These resist are like treacle; this process was developed to work on a Bosch style deep etch where the SPR220 works as the etch mask. It is useful as CMOS compatible machines

normally ban metals as they can contaminate the process. Our usual mask materials when working with diamond are not CMOS compatible.

3.4.2 E-beam Lithography

Electron beam lithography relies on the chemistry that happens when some materials are exposed to electrons. Some negative resists will polymerise, forming stable long chain materials; others will undergo some kind of scission making them less stable. Accordingly, by drawing a beam of electrons across such materials very small patterns can be made. Electrons can be accelerated across an electric field, this allows them to be very high energy. This allows them to beat the diffraction limited limit of visible light seeing or drawing smaller features.

Due to the proximity effect the electron dose require will depend on the geometry and writing strategy, how the Raith 150-two e-beam lithography machine feels on a given day and subtle differences in process. Differences between susbstrates can mean charging issues vary from not important to very important; the time between exposure and spinning can make small differences, as can humidity and temperature in the room.

3.4.2.1 Resists

2 layers of PMMA 950 A4 baked 180C for 2mins. This is a by-layer for lift off can be formed by repeating this process twice. This should have minimum undercut. Doses required depend on structure and it often feels like a lot depends on how the machine feels. This resist stack is perfect for lift-off style processes, allowing lift off of films up to 70nm.

Hydrogen silsesquioxane (HSQ) is a negative e-beam resist. That means the parts of the pattern that are exposed will remain. It can be further diluted in MiBK to get different thickness films; 6% for 80nm. 4% for 40nm 2% for 15nm. 0.5% for 7nm. Develop in MF-319. This developer has a small amount of surfactant, which lowers the surface tension as drying. This helps to keep high aspect ratio patterns standing.

3.4.2.2 Write field Alignment and Design/Writing Strategies

To achieve alignment to small features it is necessary to place alignment marks close to the features. During write field aligment the SEM takes images of some marks or

features and then compares the positions to those of the ideal positioning in the design file. Accordingly, the machine can then calculate the scaling shift and rotation required for a given write field.

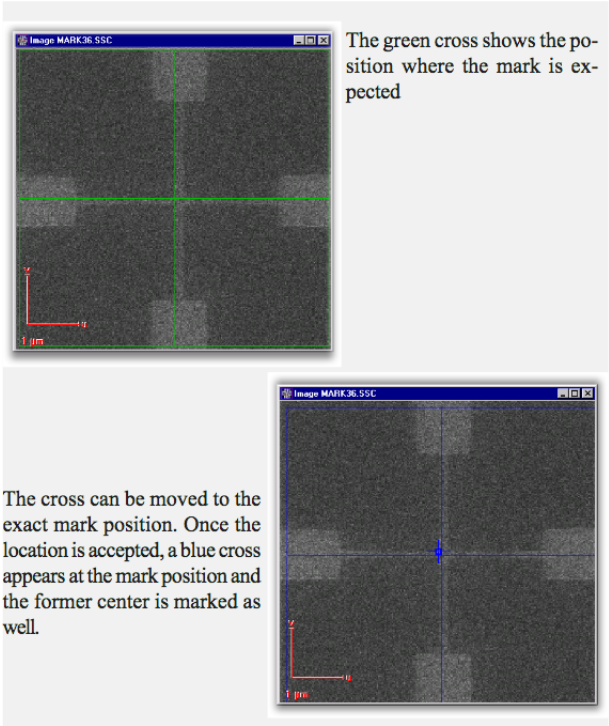

Figure 3.3: To set local coordinate system manual alignment to a feature like this standard one is required. Taken from[17]

As a rule of thumb passed for which I know works but am not sure of the origin or even the reasoning the minimum thickness for an alignment mark in nm = 2600/(Z-14). For gold Z= 79 so the minimum thickness required would be 40nm.

Within a write field the beam will raster in a snake pattern unless told to do otherwise. The mask design should consider this.

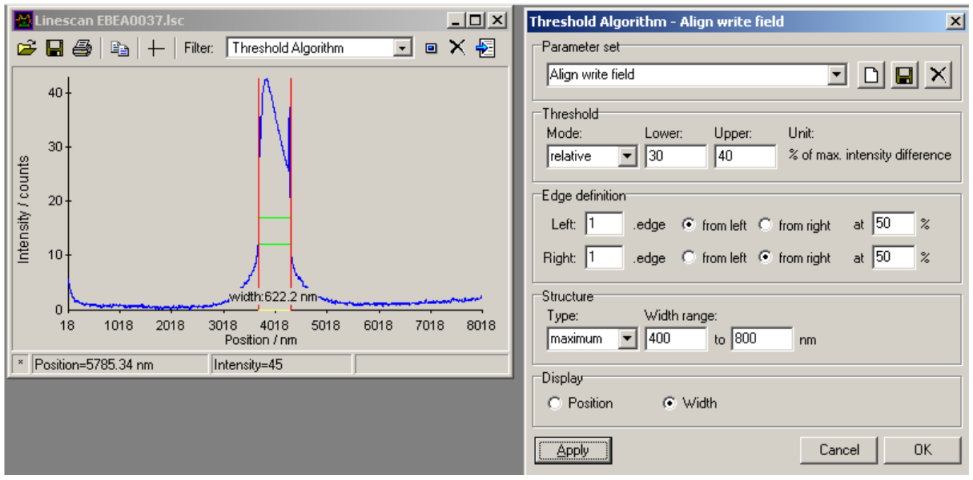

Figure 3.4: Automated alignment using computerised image analysis, edge detection and then mapping the alignment marks current position to that of a reference map, allow many alignment marks to be used without constant supervision. Taken from [17]

3.5 Reactive Ion Etching

For a lot of applications patterning or defining different areas of a substrate is essential. Often this involves making a 3D topography from a planar material via some sort of etching process. Wet chemical etching is not practical for diamond, due to the high temperatures and dangerous environments required to achieve it. Therefore a lot of work has been done to optimise and understand the reactive ion etching processes that can be used. In normal reactive ion etching (RIE) a plasma is produced by an RF electric field ionising some precursor gas. This Plasma produces both chemically reactive free radicals and energetic ions, both of these can radically transform a material. In inductively coupled plasma RIE (ICP RIE) two RF power generators are used, as in Fig.3.5b. This allows greater control of the ion energy and, separately, ion density.

Due to the hard and chemically resistant nature of diamond, RIE of diamond is not a trivial process and as a result traditionally requires hard metallic masks to provide sufficient etch selectivity for deep etches. Using metallic masks with oxygen plasma often results in the sputtering of metal onto the diamond surface, creating nano-scale etching masks that cause diamond nano-′whiskers′ to form on the etched surface of diamond. This micro-masking can be used on purpose to form nano-grass or pillars [74].

Paper	Ar	O_2	$Other$	$Pr.(mT)$	CP	$PP(W)/Bias$	$Etch$	S	$Ra(nm)$	$Mask$	$DiamondType$
			$(sccm)$		(W)		$Rate$				
$M.Karlsson2001$	8	7	–	2.5	500	140	$190nm/min$	0.3	–	$Photo-resist$	CVD
$Y.Ando2002$	$CF_4 : O_2 =$			$15to30$	$100to280$	0	9.5μm/h	–	< 0.4	Al	$(B)HPHTIb100, 111$
	$0to12.5\%$										
$D.S.Hwang2004$	30	90	–	$15to50$	$700to1000$	$0to200*$	40μm/h	50	–	Al	$SCIb100$
$H.W.Choi2005$	10	30	–	5	$250to1000*$	0	$228nm/min$	4.5	< 3	$SPR220$	IIa
$J.Enlund2005$	8	7	–	2.5	600	$100to180(V)$	$200nm/min$	–	3	$Nano495PMMA$	$B-HPHT, SC-CVD100$
$C.L.Lee2006$	15	40	–	$5to30*$	$100to800$	$0to300*$	0.22μm/min	–	1.2	$SPR220$	$Natural, HPHT$
$C.L.Lee2007$	15	40	–	5	400	40	0.04μm/min	–	3	$SPR220$	CVD
$C.F.Wang2007$	–	40	$CF_4 : 1$	50	300	$700(V)$	5.8μm/h	–	–	Al/Ti	$Ib, HPHT$
$T.Yamada2007$	$CF_4/(CF_4 + O_2)$			15	1000	100	$5.5nm/s$	10	1	SiO_2	$Ib(100)$
	$= 2to100\%$										
$H.Uetsuka2008$	$CF_4/(CF_4 + O_2)$			4.5	1000	100/	$18.8, 30\mu$m/h	$12/188, 67$	–	Al/SiO_2	$(B)SCIb100$
	$= 2to100\%$										
						$100, 200$					
$C.L.Lee2008$	25	–	$Cl_2 : 40$	5	400	300	$1nm/s$	0.06	0.19	$SPR220$	$IIa, HPHT, CVD$
$M.P.Hiscocks2008$	–	20	$CF_3 : 0.5$	75	200	0	$70nm/min$	–	–	SiO_2	$SCIb100$
$Hausmann2010$	–	30	–	10	700	100	$200nm/min$	–	8	Au	$SCIIa, HPHTIb$

Table 3.1: Summarised ICP RIE recipes from a review of the literature which aim to fabricate smooth and/or high aspect ratio diamond structures. Ar and O_2 are in sccm. In the Diamond Type column, (B) denotes both intrinsic and boron doped diamond were investigated. Pr. is pressure in mTorr. PP, platern power. S, selectivity. Ra is average roughness. $'$-$'$ denotes no data was available in the paper source. $*$indicates particularly influential experiments.

(a) Surface Technology Systems ICP DRIE

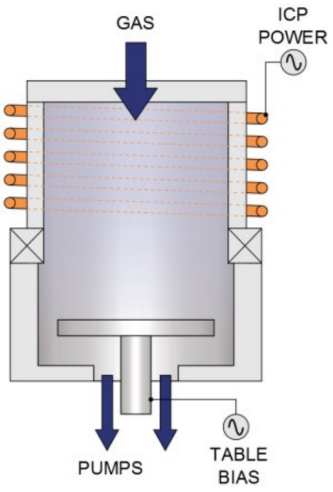

(b) Schematic from Oxford Intruments showing ICP RIE.

Using photolithography hard metal masks can be patterned to define features as small as $1\mu m$. This hard mask will protect the diamond underneath from the RIE processes. After a thorough literature review Table.3.1 it is clear that a variety of parameters are possible depending on the what sort of feature or pattern is required as well as the quality of the diamond to start with and the type/shape/condition of the etcher used to etch.

3.6 Metallisation

3.6.1 Evaporation

Evaporation is a word used to describe the phase change between liquid and gas. Most metal evaporation first requires a melt of metal which is then followed by evaporation. Sublimation (direct from solid to gas) is usually avoided.

3.6.2 Thermal Evaporation

Fig.3.7 shows a molybdenum boat, into which evaporant can be put. When current is passed through the boat, Joule heating will heat the boat, which is in thermal contact with the evaporant. The evaporant will melt and then evaporate. Key to good thermal

Figure 3.6: Edwards A306 Belljar Evaporator in LCN cleanroom

Figure 3.7: An example of a resitive evaporation boat

evaporation is patience; rushing to too high an evaporation rate (high current) will flash the material, both using a lot of the material you want to evaporate and not allowing a controlled crystal growth on the substrate. Ideally, a stable evaporation rate should be reached before opening the shutters to the substrate; this allows the crystal to grow with consistent incident ion energy and will result in a more homogeneous crystal.

3.6.3 Electron Beam Evaporation

Figure 3.8: Edwards A500 FL500 Electron Beam Evaporator, 4 pocket Temescal Electron Beam gun, 2 thermal sources. Metals include Ti, Au, Mo, Pt

My work has so far only required Ohmic contacts. To achieve a good Ohmic contact on diamond over a wide potential window and down to low temperatures (<2K) a few things must occur. The sample must have high doping levels (particularily for for low temperature work or all the carries will freeze out and the sample will become more and more resistive), the closer to two metals interfacing the better. As the diamond doping level reduces, a larger barrier hieght should be expected at the interface. Forming a carbide by deposition of a reactive metal such as titanium, helps. as some amount of diffusion is posible in diamond and carbide forming metals will change the stochiometry at the interace. As titanium is so reactive it then must be covered with another metal. It is usual in diamond if the aim is to make a device that will last a long time to do a tri

layer metal stack with titanium at the bottom covered by a platinum diffusion barrier which in turn is covered in a thick gold layer onto which one can wire bond [75]. The electron beam allows for higher temperatures then thermal evaporator, which allows the evaporation of materials such as platinum and titanium.

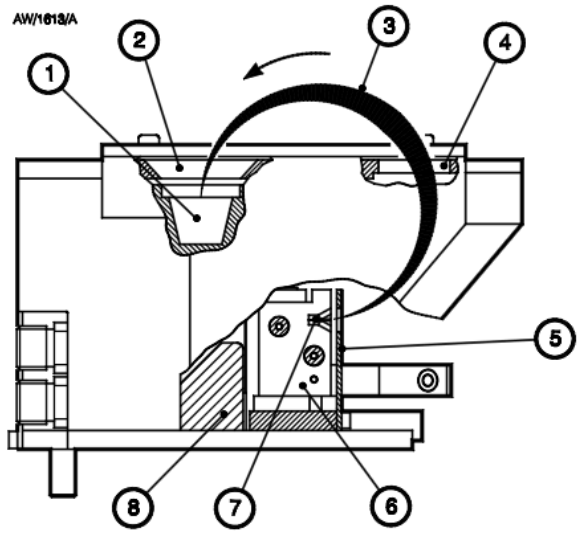

1. Crucible hearth
2. Aperture in top shield
3. Electron beam
4. Aperture in top shield
5. Anode plate
6. Emitter assembly
7. Filament
8. Permanent magnet

Figure 3.9: Principle of opertation for e-beam Evaporator. Taken from [18].

When the Source is operated, high voltage electrical supplies (provided by the EB3 3 kW Power Supply) heat a tungsten filament (7) until it is incandescent; the filament then spontaneously and randomly emits electrons. The anode plate (5) then collects the electrons and forms them into a beam (3) which is accelerated through the high voltage potential of 5 kV. Magnetic fields created by a permanent magnet (8) and the pole pieces and pole piece extensions deflect the beam through 270 until it impacts on the evaporant in the crucible n hearth (1), which is at electrical ground potential. If the electron beam contains sufficient energy, the evaporant in the crucible is evaporated. For the beam to reach the crucible, it passes through two apertures (2, 4) in the top shield on the source which focus the beam this is shown in Fig.3.9, [18].

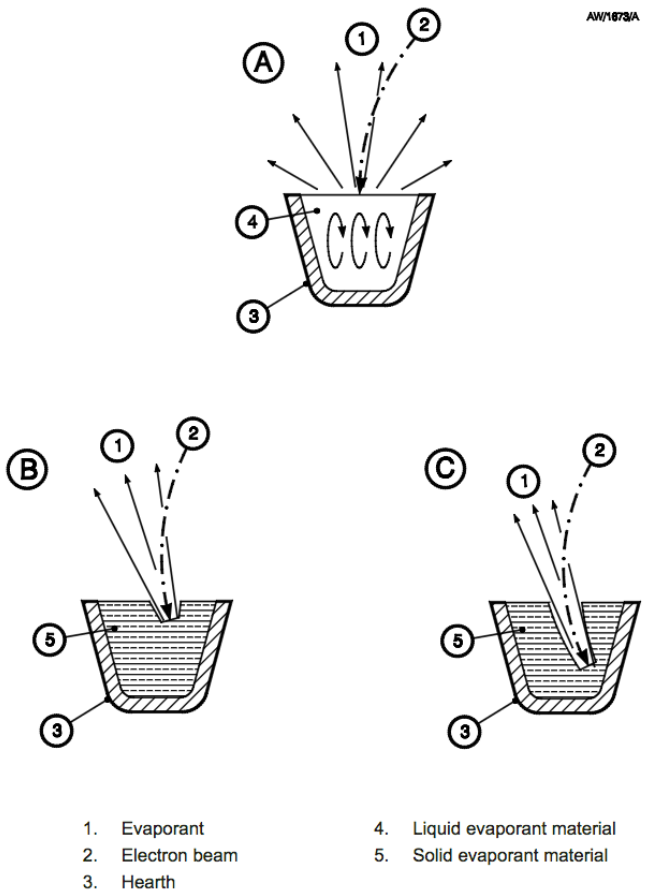

Figure 3.10: An appropriate raster pattern ensures a smooth even melt[18].

By choosing a material-specific raster pattern a smooth even melt can be achieved. This is important both in terms of maintaining the hearth and material within it and getting an even coverage of evaporant over a wide area.

The thickness of the evaporated metals are monitored by quartz crystal micro-balances during deposition. Afterwards, polarimetry or ellipsometry can be used to qualify that measurement against a total thickness and the technicians can then work out tooling factors and keep an eye on the machine performance. This is a correction between the amount of material that reaches the micro-balance and the amount that reaches the sample. This is usually different due to geometrical issues with the evaporator.

3.7 Tools for Electrical Characterisation

3.7.1 ACMS - Alternating Current Magnetic Susceptibility

The quantum design physical properties measurement system (PPMS) is a turnkey muti-use tool based around a cryogenic dilution refrigerator. With the normal helium-4 insert it can reach a base temperature of 1.8K and generate magnetic fields up to 14T. The PPMS can be used in a number of configurations to perform many different kinds of measurement. In this instant it is used for Alternating Current Magnetic Susceptibility (ACMS).

ACMS is one of the measurement options available. Magnetic susceptibility is interesting as it says a lot about how the magnetic moments within a sample are behaving. In DC magnometry the sample is magnetized by a constant magnetic field, and the magnetic moment of the sample is measured. The resulting moments are measured by a set of inductively coupled pick op coils. In ACMS a small AC field is applied to a sample, either with or without a larger DC field, and the resulting AC moment is measured. The induced sample moment is time-dependent. AC measurements yield information about magnetization dynamics which are not obtained in DC measurements, where the sample moment is constant during the measurement time. This sort of AC measurement gives information about the slope of M(H) (the magnietisation as a funtcion of the magnetic feild strength) and not the absolute value, according small shifts can be detected when the absolute moment is large [19].

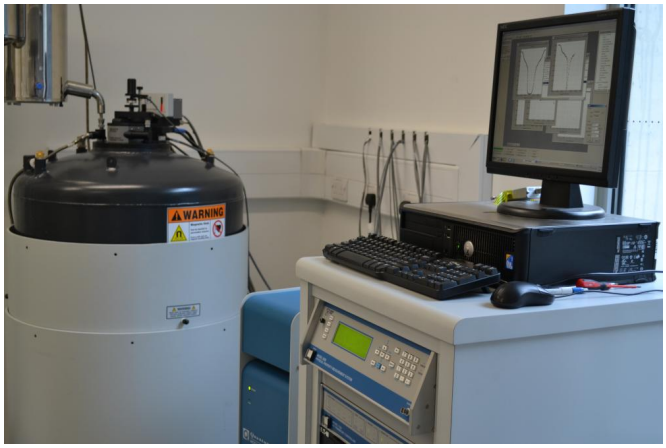

Figure 3.11: Quantum Design PPMS

ACMS is a powerful non-destructive tool for investigating superconductive materials. As a material undergoes a phase change to a superconducting state the material must ultimately change to being a perfect diamagnet with magnetic susceptibility χ' = -1, the onset of a non zero χ' is taken as the upper superconducting transition temperature.

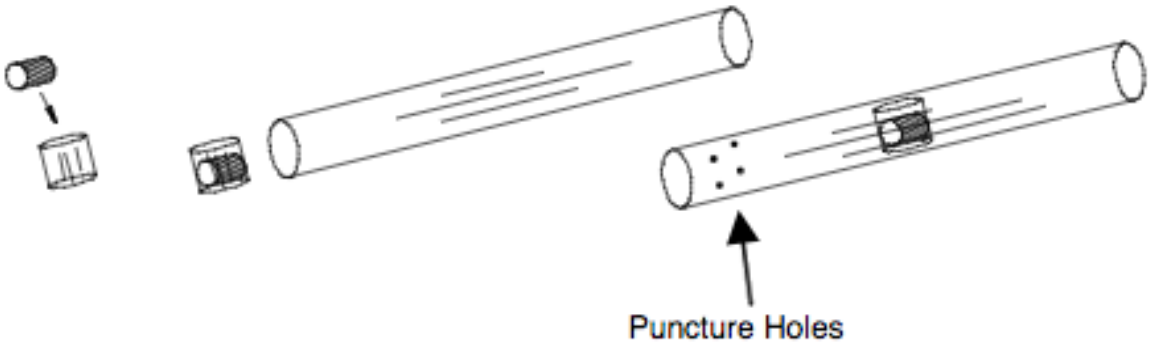

Figure 3.12: Straw mounting for ACMS in PPMS, the sample is mounted in a little pouch to stop vibration causing the sample to move. Further, holes are put in the straw to allow helium coolants to flow in and trapped air or moisture to exand. Taken from [19]

The sample can be mounted in a number of ways, but usually a straw (common drinking straw) provides a low background signal, cheap and easy way to proceed. The sample is prepared as in Fig.3.12 and then lowered into the fridge. The sample space

is then cooled and measurements can begin.

3.7.2 Angle Resolved X-Ray Photoemission Spectroscopy

ARPES (Angle Resolved X-Ray Photoemission Spectroscopy) is an extremely powerful technique for accessing the electronic structure of materials resolved in energy and in momentum space. By using ARPES we can probe the electronic properties of a solid state system within the whole Brillouin zone (BZ). Each ARPES measurement corresponds to the electron binding energy (E_B) and its dispersion as a function of $\vec{k}_{||} = \vec{k}_x + \vec{k}_y$, $\vec{k}_{||}$ is the momentum vector parallel to the surface, $\vec{k}_x and \vec{k}_y$ are the momentum components in the x and y directions respectively. These vectors define reciprocal or k-space. In addition, given the fact that the $\vec{k}_z$ depends on the photon energy ($h\nu$) used for the data acquisitions [76], by varying $h\nu$ we can map the evolution of electronic structures along the $\vec{k}_z$ direction of the bulk BZ.

The electronic properties of bulk boron-doped diamond have been extensively studied for more than five decades. The interest in this system has increased even further during the last ten years, with both theoretical and experimental results having demonstrated the existence of a superconducting state at temperature T_c=7 K, accompanied by a metal-insulator transition (MIT) [35, 63, 64, 65]. So far, photoemission has proven to be a powerful tool in characterizing the electronic properties of B-doped diamond. In particular ARPES measurements with high photon energies ($>$ 170 eV), where sensitivity is restricted to the bulk states only [35, 77], has been demonstrated to access the momentum-resolved electronic dispersion of B-doped diamond, mostly focusing on revealing the metallic character of these samples, and importantly, their putative superconductivity. Such superconductivity has been associated with boron-induced metallicity [35, 78, 79, 80]. In particular, it has been shown that near the Γ point of the BZ, strong phonon modes can couple with the hole bands, driving the formation of a superconducting state. Whilst this picture is often complicated by the presence of a boron impurity band, which challenges the understanding of the origin of superconductivity [78, 79, 81], strong boron doping is nonetheless necessary for turning diamond into a superconductor.

3.7.3 Transmission Line Model

In a transistor or similar device, understanding the nature of a contact system is crucial for understanding the whole system and how the contacts will affect the devices behaviour.

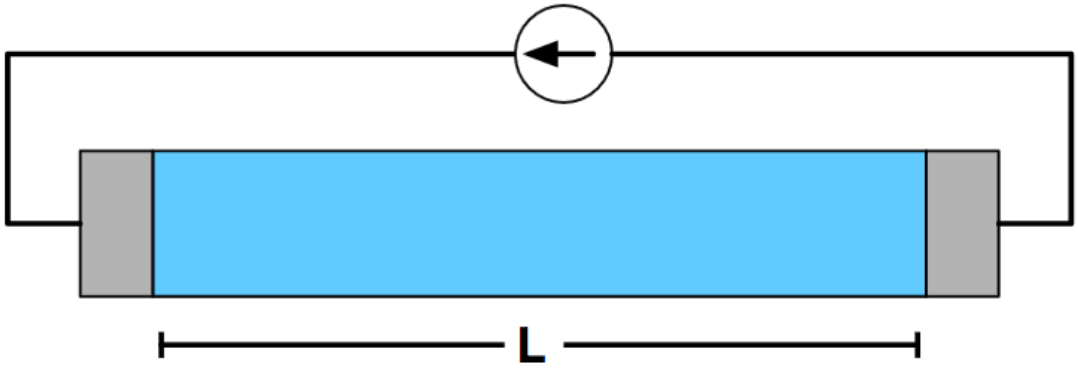

Figure 3.13: Two terminal resistor in cross section. Taken from [20]

To Inject current into a simple wire two contacts are required. In Fig.3.13 the contacts are the grey areas at the ends of the channel. Each contact has an area A_C

$$R_T = 2R_m + 2R_C + R_{semi} \tag{3.1}$$

where R_M is the resistance due to the contact metal, R_C, is associated with the metal/semiconductor interface, and R_{semi} is the usual semiconductor resistance. R_M is in most cases much larger than R_C and so can be ignored.

$$\begin{aligned} R_{semi} &= R_S L/W \\ R_T &= R_s/WL + 2R_C \end{aligned} \tag{3.2}$$

Eq.3.2 has the same form as the equation of a straight line, so as shown in Fig. 3.15 by measuring a few resistors which are identical other then having different lengths (as shown in Fig.3.14) at the y intercept (of a plot of their resistances vs their channel length), which is where the channel length would be zero we get a number proportional to the contact resistance R_C. The slope of this graph is also proportional to Sheet resistance R_S.

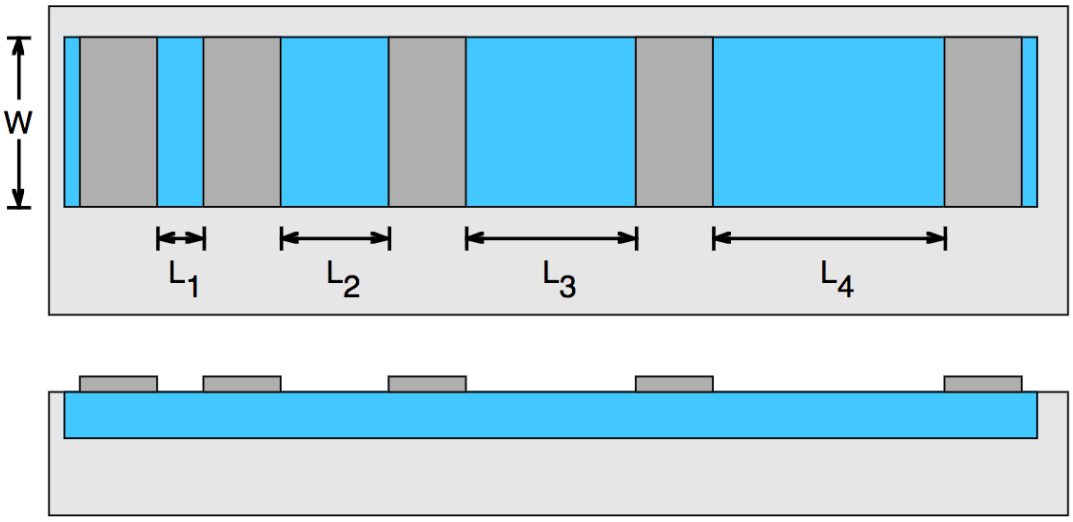

Figure 3.14: A typical arrangement for a TLM test pattern. There is a single rectangular region (blue in the figure) that has the same doping (i.e. same sheet resistance) as the contact areas of the devices. An array of contacts (darker gray in the figure), with various spacings, is formed over the doped region [20]

Instead of measuring lots of single resistors the resistance between each pair of contacts in some device that looks like Fig.3.14 can be used to construct the Transmission Line Model (TLM) graph Fig. 3.15. From the graph the parameters R_S, R_C, ρ_C can be calculated [20].

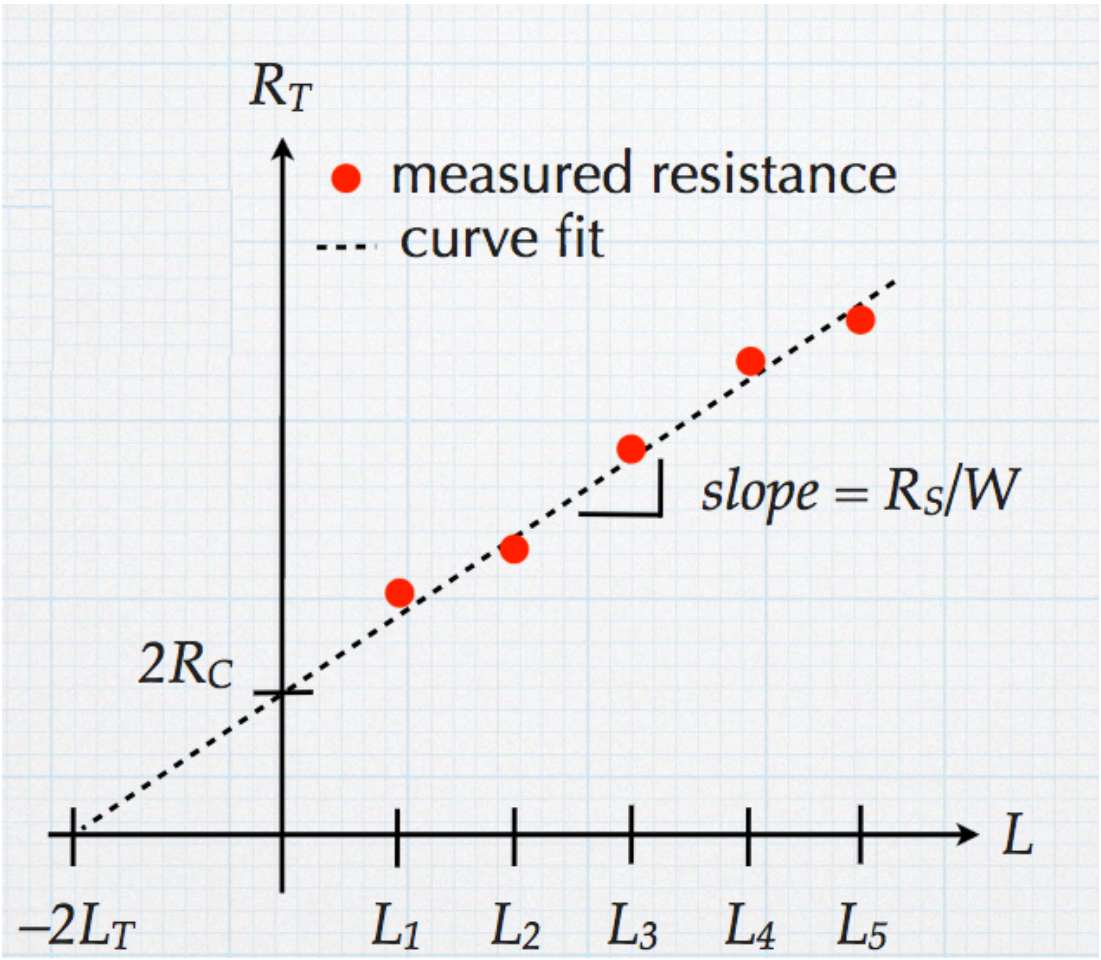

Figure 3.15: From a plot of total resistance vs resister length we can derive key carachteristic numbers for the contact. Taken from [20]

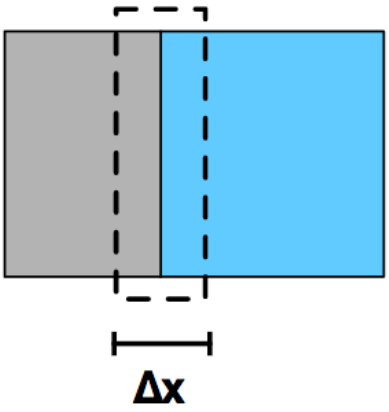

Figure 3.16: Small Region Near contact. Taken from [20]

As the contact resistance depends on the size of the contact it is not that useful as a metric for comparison between materials or devices. Using the contact resistivity is better. This can be derived as follows. Consider a small region in on the edge of a contact (Fig.3.16).

$$\begin{aligned} R_C &= \rho' \Delta x / A_C \\ \lim_{\Delta x \to 0} (\rho') &= R_C A_C \end{aligned} \tag{3.3}$$

So R_C will units of [Ω].[L^2]. Typical values for semiconductors will be in the range $10^{-3} to 10^{-8}$ Ωcm^2 [20].

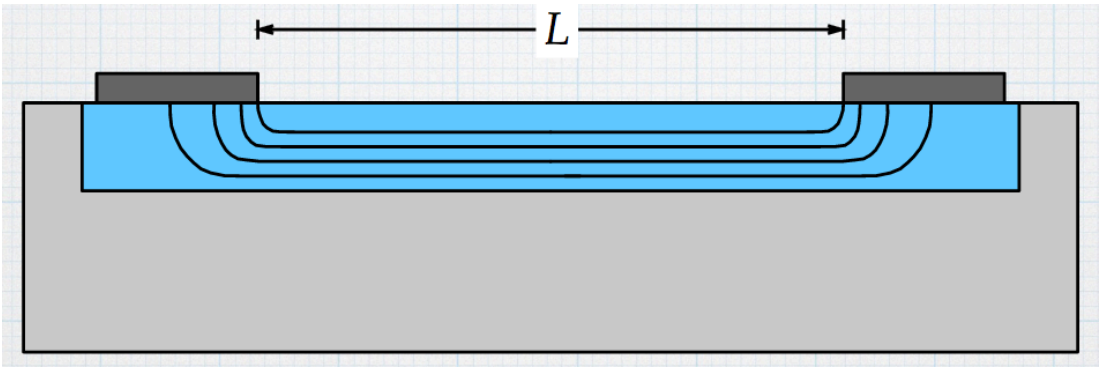

Figure 3.17: Lines of constant current. Current flow in device bulk is uniform but the filed lines and tranport behavior are more complicated near the contact edges. Taken from [20]

The contact geometry shown in Fig.3.13 is however not practical for most devices and a planar geometry, as shown in Fig.3.17, is used. In the main body of the device the current flow and EM field lines are uniform. However, around the contacts things are more complicated and current crowding is seen. This makes it difficult to understand the effective physical length and width of the contact. The current crowding drops of following an exponential decay (Fig. 3.18) over a length L_T, the transfer length, which can be interpreted as the active contact length.

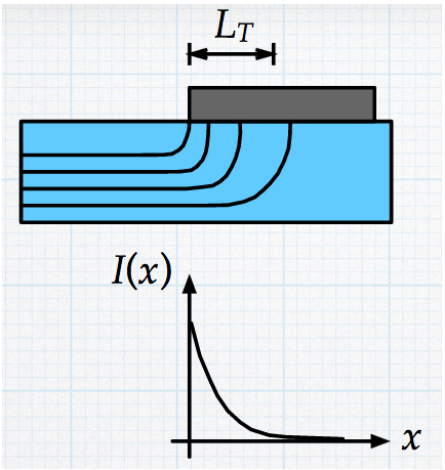

Figure 3.18: The majority of current is injected around the inside edge. This drops off as youmove to the far edge away from the channel. Taken from [20].

$$\begin{aligned} R_T &= \sqrt{\rho_C / R_S} \\ R_C &= \rho_C / L_T W \\ &= R_S L_T / W \end{aligned} \tag{3.4}$$

$$\begin{aligned} R_T &= R_{semi} + 2R_C \\ &= R_S L/W + 2R_S L_T/W \\ &= R_S/W(L + 2L_T) \end{aligned} \tag{3.5}$$

So Eq.3.5 tells us that the x intercept will be $-2L_T$. Thus we can measure all of the variables required to extract the contact resistance.

3.7.4 Hall Effect

The Hall effect was observed by Edwin Herbert Hall during his PhD and published in his seminal work of 1879 'On the new action of magnetism on a permanent electric current'. This observation has been of profound in the development of modern theory and practice.

In an ideal Hall effect system a current density (j) flows while experiencing a magnetic field (B) perpendicular to the plane defined by current. Due to the Lorentz force mobile charge carriers will be bent to one side of the channel and an electric field that is perpendicular to j and B will be developed, this is often called the Hall voltage. The hall voltage can be measured by passing current through an appropriate material that is exposed to a magnetic field perpendicular to the plane. The Van der Pauw geometries and the Hall bar geometries provide a number of current sources and drains as well as voltage probes to measure the hall voltages that develop. The ratio of the Hall Voltage with the product of j and B is the Hall coefficient. From this same experiment it is also apparent that the ratio of the voltage dropped ,or parallel electric field, to the current density will reveal the resistivity of the sample. From these data we can derive the carrier concentrations and Hall Mobilities.

3.7.4.1 Van Der Pauw Method

The Van Der Pauw method for measuring the Hall effect has several advantages the simple geometry allows for quick fabrication and analysis of material. As shown in Fig. 3.19, only four contacts are required and the simple symmetrical geometry means that it is not necessary to know the exact spacing between each contact. This ease of measurement is balanced by the fact that errors can easily creep in due to error in contact size and placement.

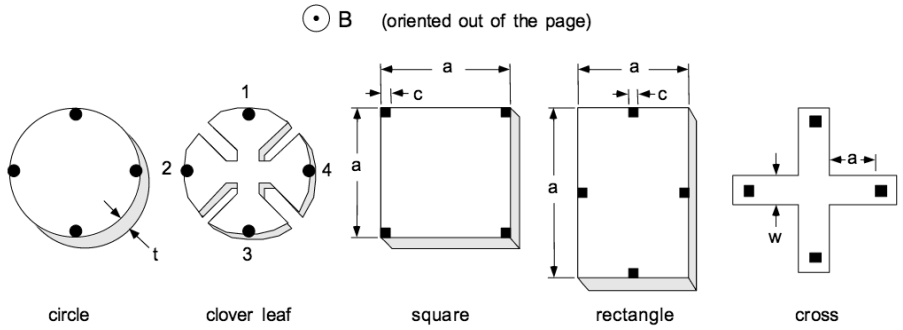

Figure 3.19: Common Van Der Pauw geometries from the Lake Shore 7500 Series Hall System User's Manual

3.7.4.2 Hall Bar Method

By defining a so called Hall bar such as Fig. 3.20, errors dues to stray fields and asymmetries in contacts can be reduced as the channel and probe dimensions are carefully defined.

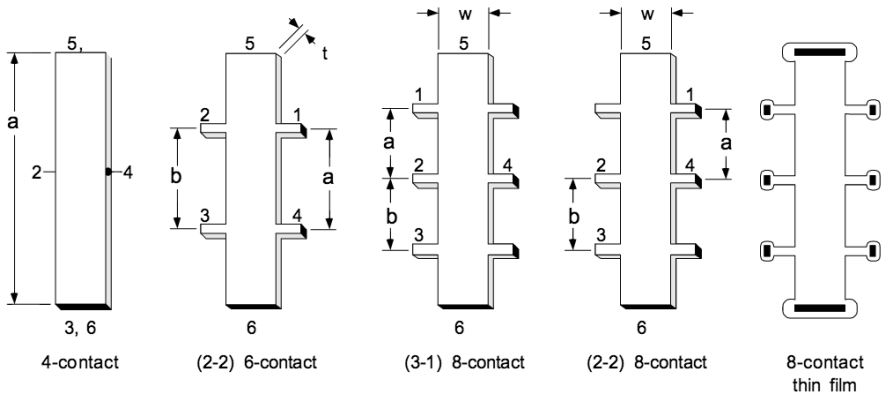

Figure 3.20: Common Hall bar geometries from the Lake Shore 7500 Series Hall System User's Manual. Sample thickness, t, of a thin film sample = diffusion depth or layer thickness. Contacts are black, numbered according to the standard to mount in Lake Shore sample holders

3.8 Conclusion

This chapter described the experimental techniques used in the results chapters and gave some processing and handling information gleaned from many hours of experimental work.

4

RESULTS: boron Doped Diamond Growth

4.1 Introduction

Fig.4.1 shows the high thermal conductivity[82], high electronic carrier mobilities[23] of diamond which coupled with, high breakdown field strength[83] and other superlative optical, chemical, materials properties[84] make diamond a potentially disruptive technology in a broad range of applications from power electronics to bio-chemical sensors. To make semiconductor devices it is necessary to be able to do a certain amount of band gap engineering, controlling doping levels and preferably having a range of available dopants. This is difficult in diamond.

At low doping concentrations boron induces an acceptor state 0.37eV bellow the conduction band; this provides the most promising route towards viable electronic devices in diamond as other dopants such as phosphorous or nitrogen give much deeper donor states 0.7 and 1.6 ev respectively [**?**] .

Growing boron doped diamond of varying quality by CVD is now commonplace in many laboratories [85] [78]. The basic principle is to introduce some boron precursor into the hydrogen plasma during growth. However, due to subtle differences in growth equipment and, more importantly, large differences in the diamond seeds used to grow epilayers on, it is impossible to compare the properties of existing bulk thick boron doped diamond layers to the nanometrically thin boron doped diamond layers grown to be delta-doped diamond for high power high frequency applications[7]. It is desirable

to be able to make direct comparisons to help understand why the expected carrier mobilities and and concentrations are not seen in the delta layers, as well as to glean insight into boron doping diamond, for example, what changes as a thin film becomes a thick semi-infinite one.

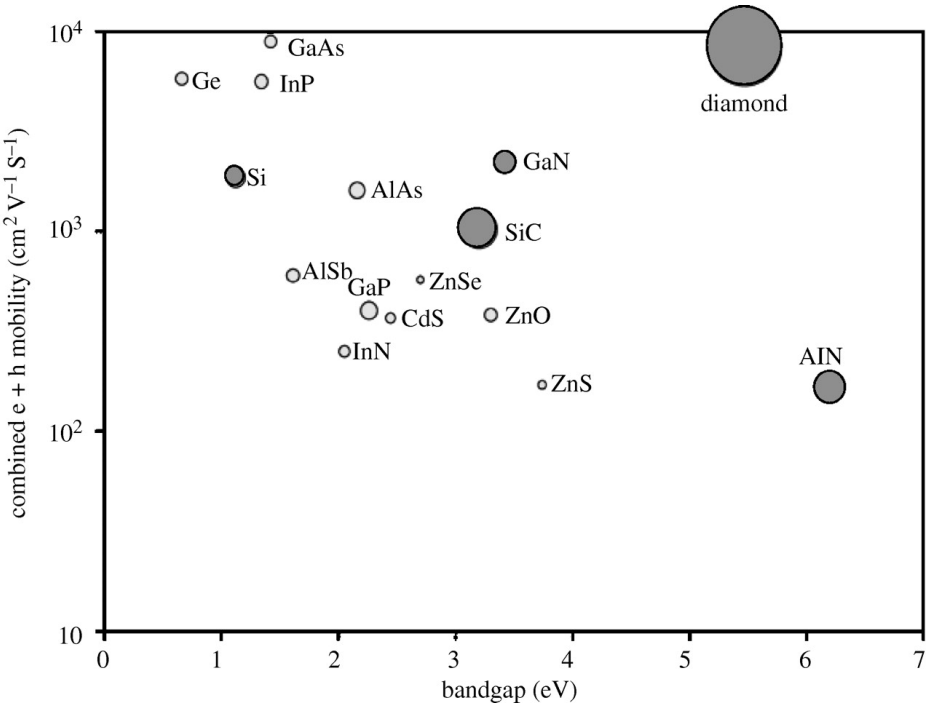

Figure 4.1: Comparison of diamond's combined carrier mobility, bandgap and thermal conductivity with other semiconductors (area of circle is proportional to the material's thermal conductivity). Adapted From[21].

In this thesis a reductive approach is taken to try and understand the fundamental issues and properties of boron doped diamond (BDD). To this end we require comparable thin and thick films of BDD, where thin means the technological limit for spatial confinement of a metallic epilayer and thick means semi-infinite as far as a any technique we wish to use is concerned. This chapter will cover the growth of a thick heavily boron doped diamond film and the characterisation techniques used to qualify the growth and compare it to a 'delta doped' layer grown by external collaborators, and more generally to the state of the art for single crystal boron doped diamond. More complicated and powerful analysis methods such as angle resolved photo-emission will then be used in later chapters to compare and contrast the ways in which a semi-infinite bulk material

behaves, compared to a thin film that approaches various quantum length scales.

4.2 Experiment Details: Growth Of Thick Heavily Doped Single Crystal Diamond

The growth of the delta layer is covered in Balmer et al [7]. Although the details are trade secrets and not discussed in detail, it is known that fast gas switching (automated well designed specialist valves and gas manifolds as seen in Metal-Organic Chemical Vapour Deposition systems) and high quality substrates are important. To grow a thick film that could be reasonably compared it was essential to start on a substrate which had the same processing as the delta layer substrates. This was a (100) low impurity, high quality, intrinsic chemical vapor deposition (CVD) buffer layer grown on top of a chemical mechanical polished, high pressure high temperature (HPHT) substrate from the same batch of substrates on which the delta layers were grown. The thick boron doped layer was grown in an Astex - AX6500 MEPCVD reactor using trimethylboron, TMB $[B(C_2H_5)_3]$ as a boron precursor source. Samples were placed in the reactor and the chamber was pumped on overnight to achieve base pressures in the order of 10^{-6}mbar. By creating a hydrogen plasma with a microwave generator it is possible to grow diamond in a metastable quasi-epitaxial manner. It has been postulated that the polishing process does a lot of damage to the crystal lattice in the first 10μm or so bellow the surface. Several groups are working on pre CVD growth treatments to help with this[22], in which the first 4-10μm are removed by plasma etching. Substrates are chosen after careful selection by measuring surface roughness using AFM and comparative crystal stress looking for birefringence when viewed between cross polarisers.

The thick heavily doped films were grown in Cardiff by the author, but the lab there was not set up for single crystal growth. The methodology was governed by two limiting factors: firstly limited substrates, there were 8 substrates to develop a recipe on and secondly by a lack of a perfect experimental set up. A major problem was thermometry, (thermometry is a problem for all diamond growers), normally for single crystal growth a disappearing filament thermometer is used. A disappearing filament thermometer works by having a filament with a known black body spectrum in front of the line of sight of the sample on the stage. Current is passed through a metallic spiral joule heating causes the spiral to glow. As the sample is heated it will start to

Growth #	1	2	3	4	5	6
TMB (sccm)	200	200	200	200	200	200
CH_4 (sccm)	25	16	16	16	16	20
H_2 (sccm)	500	16	184	100	100	5
Power (kW)	4	3.5	1.6	1.6	1.9	1.9
Pressure (Torr)	80	100	130	140	5	150
Temp (C)	800	?	700	990	1100	1000
Time (min)	120	60	120	120	120	120
Sheet Resistance (kOhm)	100	20	45	11	0.02	0.1

Table 4.1: Growth paramaters for growing Heavily boron Doped Diamond

radiate light, the peak wavelength of the light will be proportional to the temperature of the sample, when the temperature of the sample matches that of the the spiral the spiral will disappear from the view of the experimenter. This was not possible for these growths, this meant using a dual wavelength pyrometer with a larger spot size then the sample. This combined with assessment by eye of the colour of the diamond as it heated up. We then optically assessed each growth, looking at the colour across the substrate. An estimate of the sheet resistance was taken by probing with a multimeter and then used a microscope to look for growth defects which would indicate that the alpha parameter was off and that growth was for example preferentially occurring along the 111 crystallographic plane.

Taking an example of 6% methane in a feed gas, the B/C ratio in gas phase was calculated using following procedure: the number of boron atoms (twice the B_2H_6 concentration in ppm) divided by the number parts of carbon (which will be 6/100 for 6% of CH4 flow). So depending on the B_2 H_6 flow (sccm)out of the total flow (sccm) in the reactor, the amount of B_2H_6(ppm) in the feed gas can be determined.

For conversion of standard cubic centimeters per minute (sccm) to parts per million (ppm), suppose total flow of gas is 400 sccm which is distributed into 106 parts, so if 0.6 sccm of diborane (B2H6) which is diluted in hydgrogen to 10% is used, then only 0.06% of B_2H_6 is only going into the feed gas hence from unitary method we have 400 sccm = 106 (1 million parts), 1 sccm = 106/400 ppm (parts per million). Therefore, 0.06 sccm of B_2H_6= (106/400)x0.06 ppm = 150 ppm.))

Growth 5 would ultimately be the best growth and of high enough quality to do a

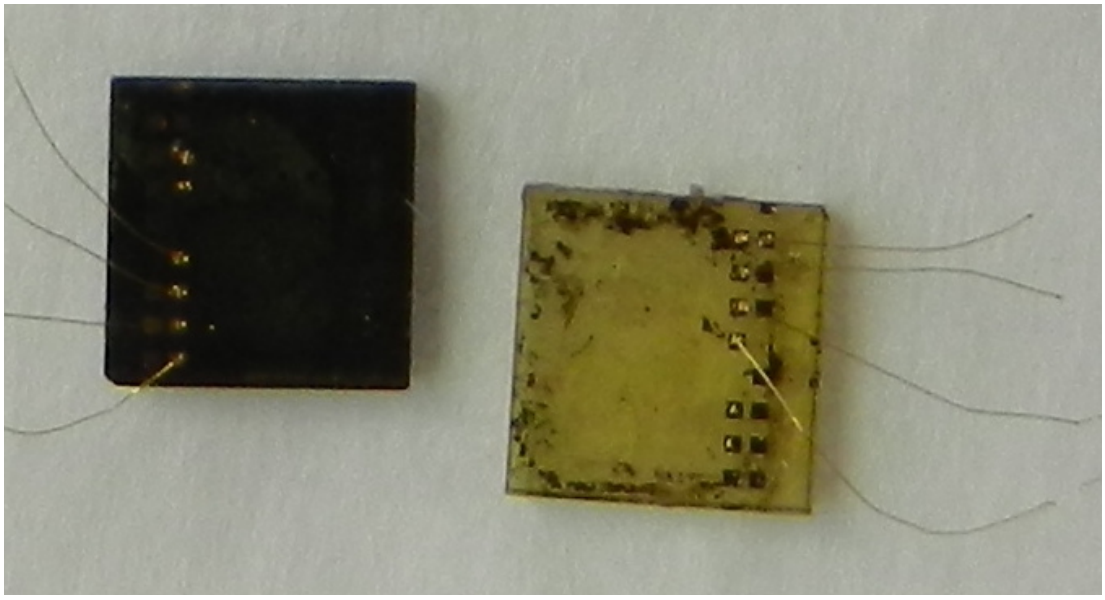

Figure 4.2: Optical picture showing the colour difference between the thick film (left) and thin film (right). Boron concentraton is shown to be in the same order of magnitude, the differenc being the right sample has a delta layer a few nm thick and the left sample is bulk doped for several micometers.

lot of novel science with. It would be code named Sup1. It was grown for 120 minutes at 150 Torr with the gas phase being approximately 60%tmb and 5% methane, 1.9kW of microwave power was used to generate the plasma. The temperature was measured with a Williamson dual wavelength pyrometer, the stable temperature was measured to be approximately 1000C. Under these growth conditions it is expected that growth rates would vary between 1-10μm an hour [86]. The uniform deep blue colour Fig. 4.2 shows that the film is thick, diamond becomes more blue as the boron incorporation increases. In Fig. 4.2 the crud around the edges of the sample on the right is underneath the sample and comes from carbon tape which has been used to attach the sample to a microscope.

Under an optical microscope as shown in Fig. 4.3 and 4.4 the quality of the diamond surface can be clearly seen. Although there are twins and other growth defects the surface as a whole shows only nm scale roughness. The growth defects are interesting in that they appear to be atomically flat, with growth along crystallographic planes. From this it is possible to see the miscut angle of the substrate.

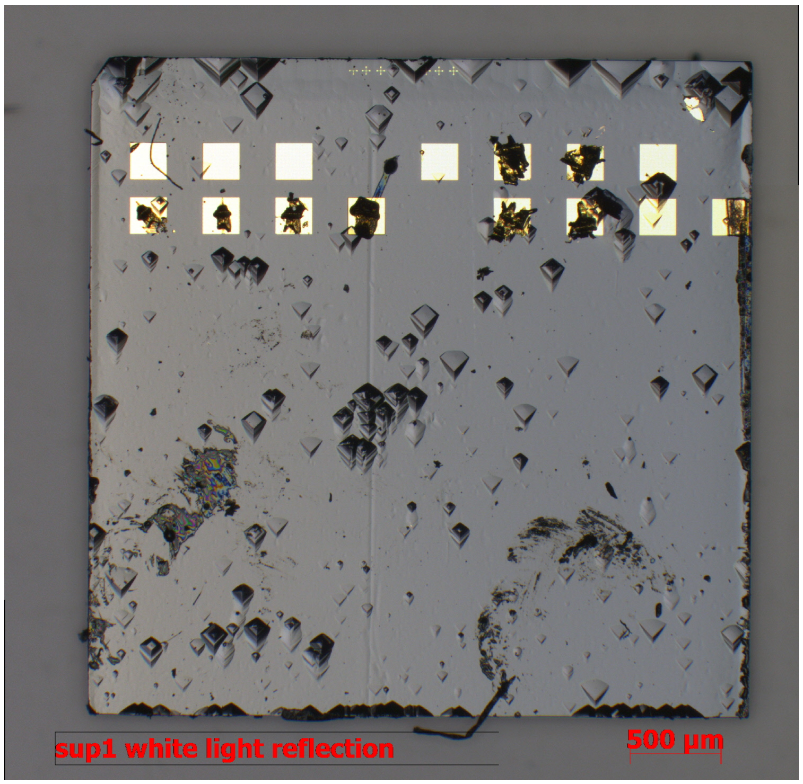

Figure 4.3: Mirograph of thick BDD film, showing flat looking areas as well as other features, for a thick film this looks like a low defect denisty.

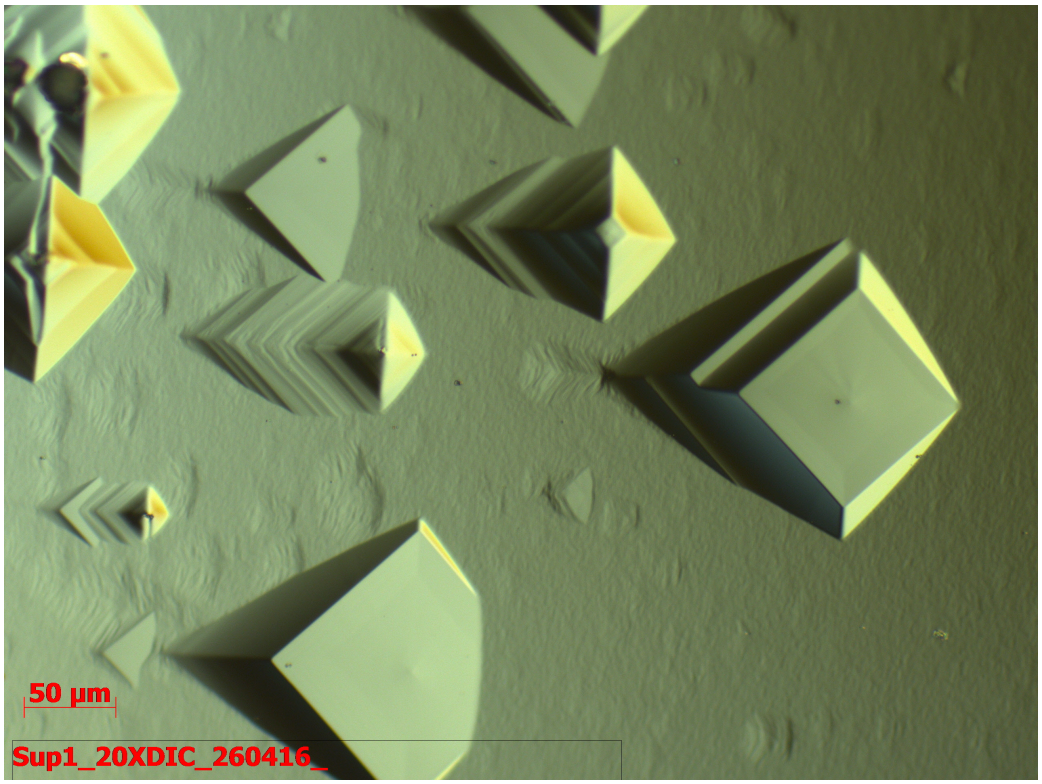

Figure 4.4: Image taken on microscope with cross polarisors. This shows very flat growth zones as well as what could be nm scale thickness variations in the thick BDD film

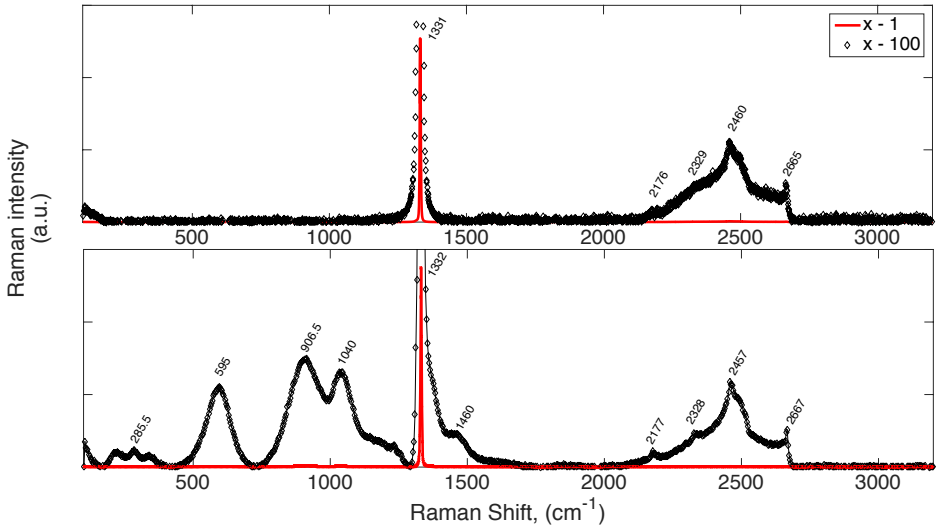

Figure 4.5: Raman spectrum from 532nm excitation of (top) delta doped diamond and (bottom), thick boron doped epi layer.

4.3 Characterisation of boron Doped Diamond Growth

SIMS and Raman spectroscopy can be used together to give information on the quality f teh diamond crystal and the absolute thickness and doping densities of the the diamond films. Raman Spectra were taken on a Renishaw system with a 532nm laser the diamond zero phonon line (ZPL) is a sharp peak at 1332 cm^{-1}, this intense feature is an indicator of high quality single crystal diamond with little graphitic diamond content.

To quantitatively measure both the level of dopant present in the diamond as well as the thickness of both the nominally thin and thick boron doped diamond samples SIMS measurements were carried out at Loughborough Surface Analysis Ltd by Alison Chew with assistance from the author.

The samples were coated with a gold layer to minimise potential sample charging.

The samples were analysed using O^+ primary ion bombardment and positive secondary ion detection to optimise the sensitivity to boron and nitrogen. High mass

resolution conditions were used to allow the ^{14}N signal to be separated from interferences such as $^{12}CH_2$ and ^{13}CH. The data were quantified using reference samples of boron in diamond and nitrogen in diamond. The depth scales were determined by measuring the sputtered crater depths using a Dektak 6M. ^{18}O is used to get the best sensitivity to N in C. When ^{18}O is used it is reasonable to hope to measure down to 1^{16} atom cm^{-3} nitrogen, but if ^{16}O is used then it is much higher. For the boron layers the extra sensitivity was not required. If a mass resolution of 250 is used then that means adjacent masses can be resolved, so ^{12}C can be differentiated from ^{13}C or ^{11}B from ^{12}C. But, when looking for N in C an interference from ^{12}C + H^2 and ^{13}C +H can be assumed in the 14N signal. They are all nominally mass 14 but in fact ^{12}C H^2 is 14.01565, ^{13}C is 14.01118 and N is 14.00307, so in this case higher mass resolution is used to separate these species out.

Primary ion species	O^{2+}
Primary ion energy	10keV and 15keV
Primary ion current	200nA to 1μA
Raster size	75μm and 125μm
Secondary ions	Positive
Transfer lens	150μm
Analysed area	60μm
Contrast aperture	No 2 and No.3
Mass resolution	250 and 3000

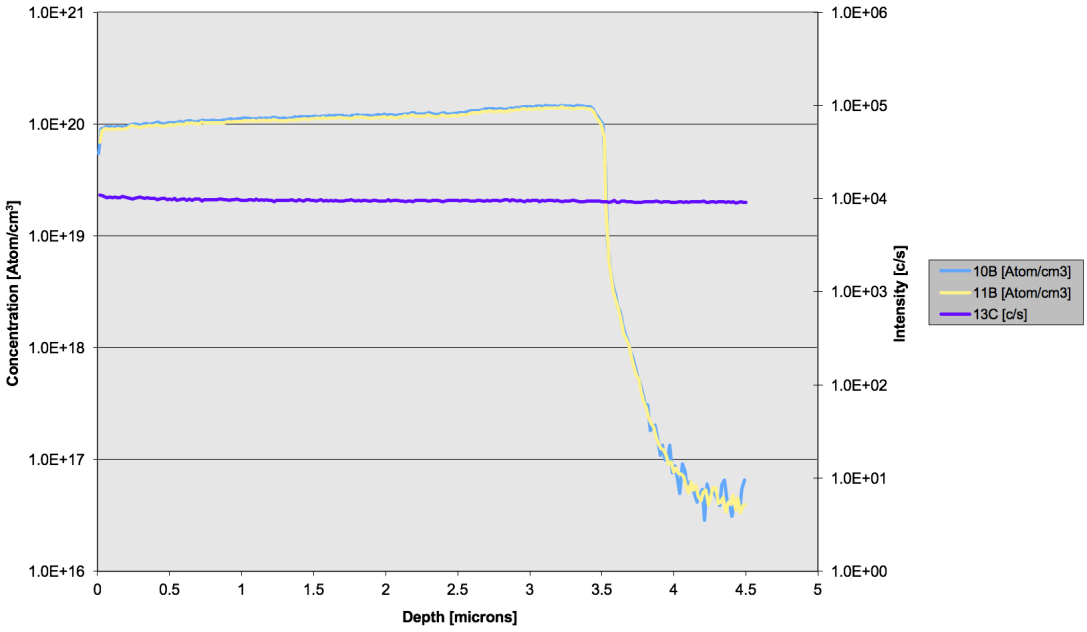

Figure 4.6: SIMS for thick boron doped epilayer, showing a semi-infintie heaily boron doped epilayer

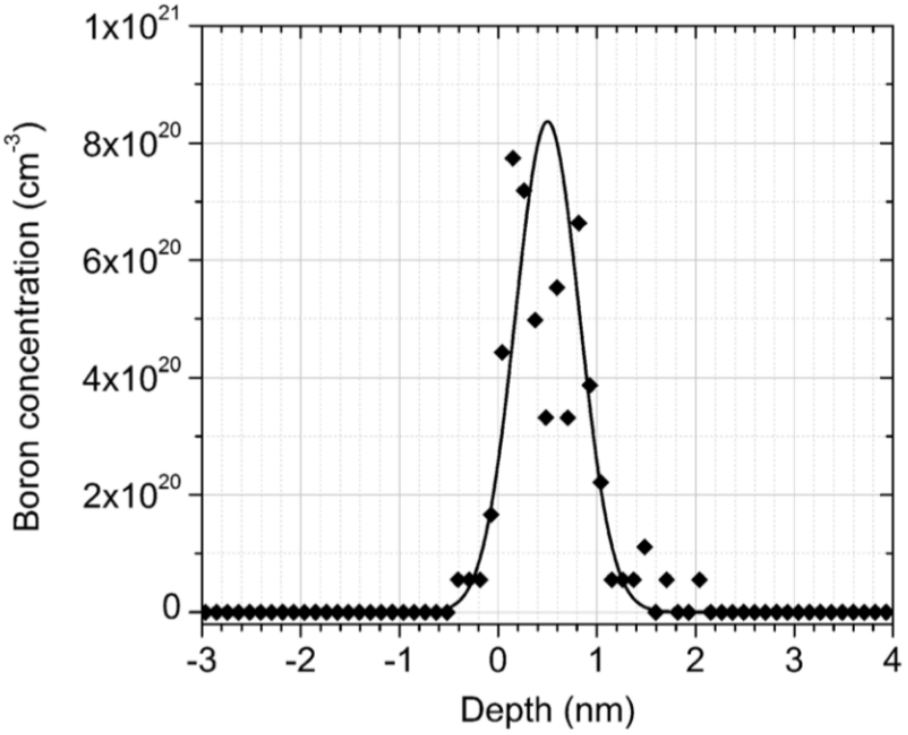

Figure 4.7: A plot of the boron profile of an example delta layer measured by ERDA showing a full width at half maximum of 1 nm. Solid line represents a Gaussian fit to the measured data, the boron from depth < 0 nm is a measurement artifact. This measuremnt was taken on a sample frown at the same time and with the same processing and supply chain as the delta layer sample use throughout this work. Taken from [7].

Diamond as heavily doped as Fig.4.6 and Fig.4.7 should be show superconductivty [78][79]. However nano-metrically thin epilayers such as Fig.4.7 have not been shown to undergo a superconducting transition, this means that at least above normal helium temperatures there is some significant process that suppresses superconductivity in a near 2D thin boron doped diamond film.

ACMS is a powerful non-destructive tool for investigating superconductive materials, as a material undergoes a phase change to a superconducting state the material must ultimately change to being a perfect diamagnet $\chi' = -1$, the onset of a non zero χ' is taken as the upper superconducting transition temperature. The measurement is taken in a quantum design physical properties measurement system (PPMS) applying a 3567Hz AC field of 13Oe. The samples were cooled to 2K in zero field and then measurements were taken as the sample warmed up.

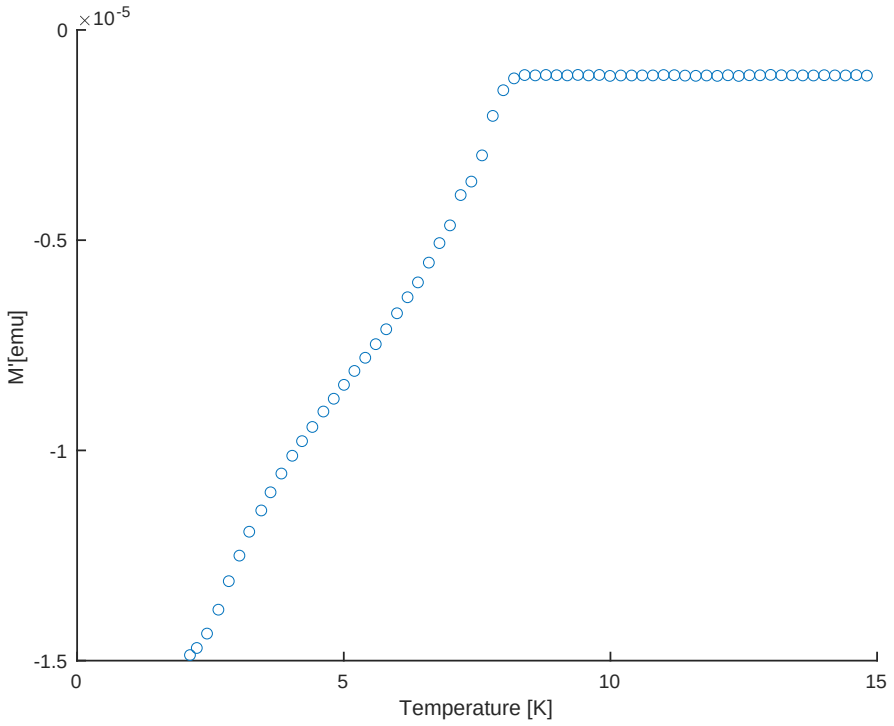

Figure 4.8: ACMS Spectrum for thick highly boron doped diamond showing a large phase change around 8K. This sort of change towards a negative magnetic susceptibility is indicative of a transition from a normal state to a superconducting one.

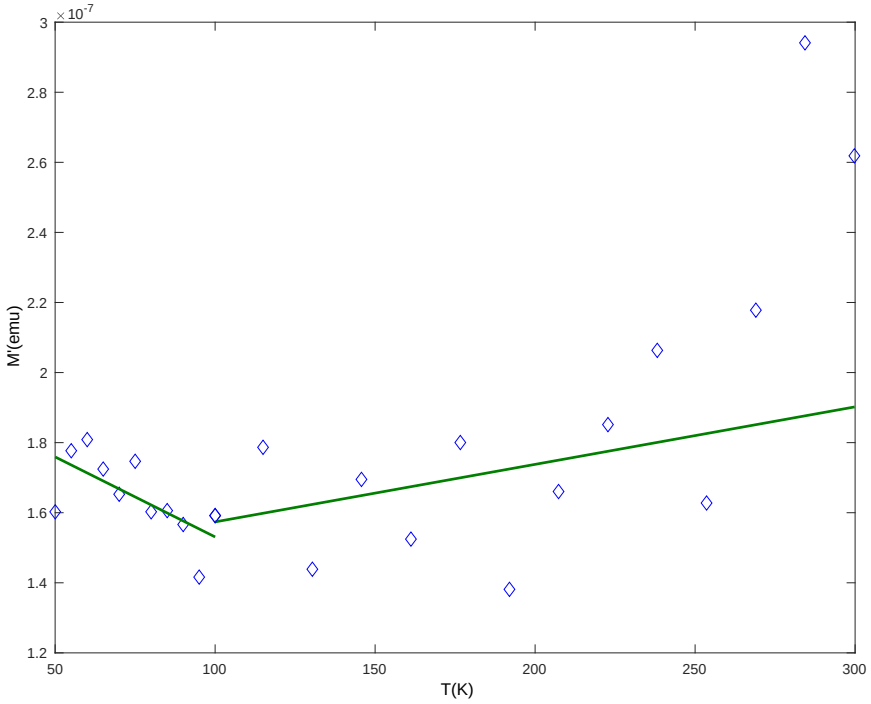

Figure 4.9: ACMS Spectrum for thick highly boron doped diamond showing an inflection and reduction in noise around 100K, some papers use small changes like this to suggest superconductivity. This thesis does not make that claim, however it is probably indicitive of some change in ordering. Understand this observation is beyond the scope of this work.

4.4 Discussion

In Fig. 4.5 it is clear that both samples show a large narrow 1332 cm^{-1} peak as well as the second order diamond peaks between 2070-2700 cm^{-1} [87] which indicates both samples are high quality diamond. The thick layer also shows several features typical of heavily doped diamond the shoulder at 1460cm^{-1}, the features between 450-1300 and the Fano line shape of the ZPL. The Fano lineshape is an assymmetry casued by interference effects between the phonon spectra and the electron-hole pair excitation spectra and is indicitave of BDD that is degenteraly doped and should show superconductivity at sufficiently low temperatures [88] [89]. The delta layer does not show these Raman features. This is attributed to the significant thickness difference between the doped regions and the sampling volume of the Raman process. The 532nm laser excites down through at least 13μm of material. The SIMS measurements show that the doping levels are around the level of the Mott transition in diamond [7] and that the thick sample is around $3\mu m$ thick and the thin $'$delta doped$'$ sample is metallic for just over 1nm. In Fig. 4.8 it is clear that the sample undergoes a large phase change around 8.4K, this on set of a non zero susceptibility is indicative of a transition to a superconducting state. [90]. This would place this sample with the best singlecrystal diamond samples in terms of superconducting transition [66]. There are other features visible in the real part of the susceptibility Fig. 4.9 but interpreting them is extremely difficult. More studies are required to fully understand these figures.

4.5 Conclusions

A recipe for growing thick heavily boron doped films of very high quality was developed. Using a range of characterisation methods the quality and thickness and doping concentration of the film was determined and compared to a nanometric thick film. Comparable boron concentrations were measured but with the film thickness's differing by several orders of magnitude. These high quality films were then subjected to non invasive tests that suggest a superconducting transition for the thick film at approximately 8K, a high temperature. The thin film does not show this behaviour at temperatures reachable by most dilution refrigerators. This suggest that although the doping levels are measurably comparable there is some difference in the physics of how

the two systems behave at low temperatures. These boron doped diamond epilayers are shown to be of as high a quality as any CVD synthetic diamond available.

5

RESULTS: Angle-resolved Photoemission. Probing the Electronic Differences Between Thin and Thick Boron Doped Diamond Films with x-rays

5.1 Introduction

Angle Resolved Photo-emission, ARPES with soft x-rays is a very sensitive probe of the first few atomic layers of a crystalline structures. ARPES is a surface science technique capable of giving considerable information about the electronic structure of a material. Extensive synchrotron-based x-ray experiments are presented, combining data taken at 4 different synchrotrons over 5 different beam times. It is shown that boron doped diamond maintains bulk-like electronic properties even when the doping distribution ($10^{20}B/cm^3$ peak doping level) is reduced to a few nanometres FWHM. Experimentally measured electronic band structures of unprecedented resolution across a wide incident photon energy range are presented.

Accordingly, we confirm that certain fundamental crystal properties of diamond hold true to our samples and investigate if there are any emergent quantum effects present when the doping is confined to a near atomic layer.

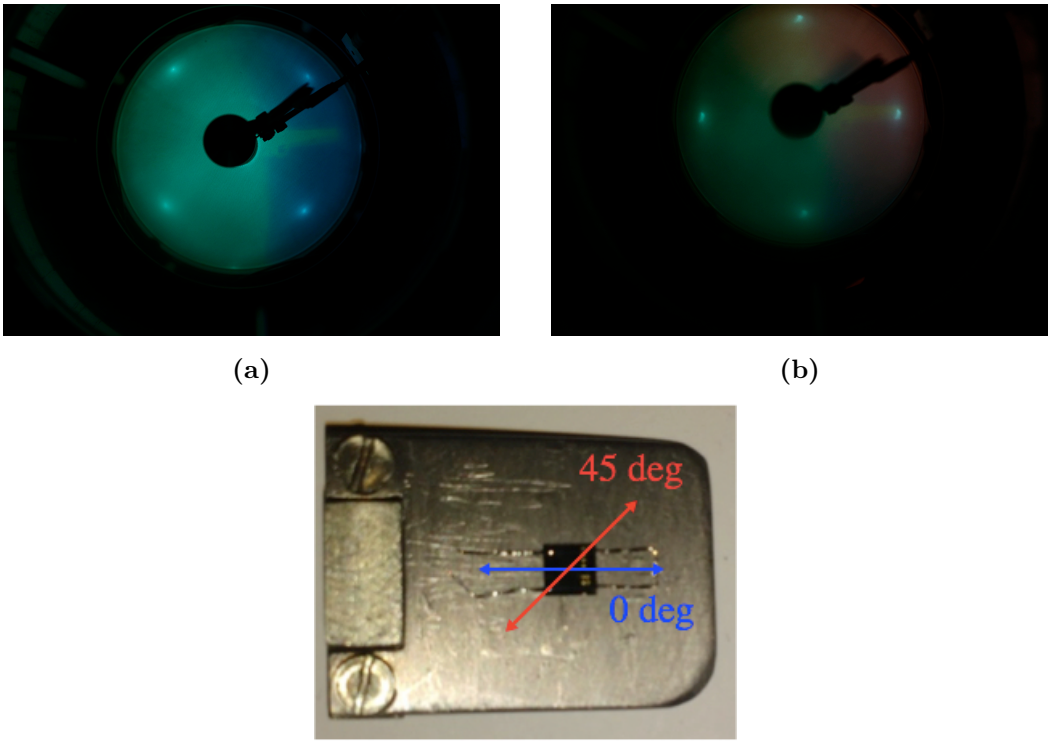

(a) (b)

(c)

Figure 5.1: (a) LEED for sample Sup1 (b) LEED for sample S07 (c) relative orientation in real space to probe along the same symmetry axis in k-space

5.2 Using Angle Resolved Photoemision Spectroscopy to Probe Diamond's Band Structure

In Fig. 5.2 the electronic structure of the thick film of boron-doped diamond is shown. This is the same sample as described in the previous chapter of this thesis. The ARPES measurement has been performed at a photon energy $h\nu = 170$ eV along the direction of the BZ indicated by the green line in the inset of Fig. 5.2. The crystalographic direction for each sample is checked using low-energy electron diffraction (LEED). The sharp 1x1 LEED pattern in Figures 6.1a, 6.1b tell us that we have a clean high crystalline quality diamond surface. As we kept the anneal temperature bellow 1000K the bare diamond surface should not have been exposed and the surface reconstruction is probably due to hydrogen forming dihydride moieties[73]. The rotation in the LEED pattern suggests that the edges of the element6 substrate are 45 degrees rotated from the Russian sample

S07 shown in Fig. 5.1b.

The $\vec{k}_z$ position of the data acquisition could then be determined following Ref. [76]. Our determination of the $\vec{k}_z$ position shows a departure from Ref. [77], for which ARPES measurements for a similar system and at a similar photon energy were performed. In Ref. [77], the authors claim to measure exactly from a cut through the Γ point of the bulk BZ, however according to our measurements it is not clear the exact photon energy for which this condition is realized, because of uncertainties arising from the strongly varying matrix elements in this system. Moreover, from the trend observed in the data of Fig. 5.3, it seems that the electronic dispersion reaches its minimum value of binding energy (upward in our energy scale) below $h\nu = 155$ eV. However, apart from these differences observed between our work and Ref. [77], the agreement with the data of Ref. [77] is overall good.

The bulk boron-doped diamond electronic structure reported in Fig. 5.2 reveals three bands. The band dispersions are indicated by the schematic bands labeled as 'A', 'B' and 'C' (red, yellow and green curves respectively), overlaid on the experimental data. 'A' crosses the Fermi level (E_F) and is therefore responsible for the metallic character of the sample. Such a metallic character is in agreement with our preliminary transport measurements and with Ref. [7]. The electronic structure of Fig. 5.2 is also in agreement with the soft-X-Ray ARPES measurements and theoretical calculations reported in Ref. [35]. Two additional horizontal bands, 'H1' and 'H2', are visible at higher values of binding energy. These bands are an artifact caused by the fact that at the edges of the BZ the electronic states have an exceptionally high intensity and such intensity spills into the whole BZ, resulting in seemingly dispersionless horizontal features in the ARPES image.

Additional information about the electronic structure of the samples can be found by collecting ARPES data at different values of photon energy, which in other words, means collecting ARPES data at different values of $\vec{k}_z$. Mapping the electronic structure of diamond along $\vec{k}_z$ is of interest for understanding the dispersion along this direction and it additionally reveals the electronic dimensionality of the system: If the electronic structure of a material varies with $\vec{k}_z$, then the system must be electronically 3D and conversely, if the system is seen to be dispersionless with $\vec{k}_z$, then it must be electronically 2D. Varying $\vec{k}_z$ (by varying the photon energy) is therefore a straightfor-

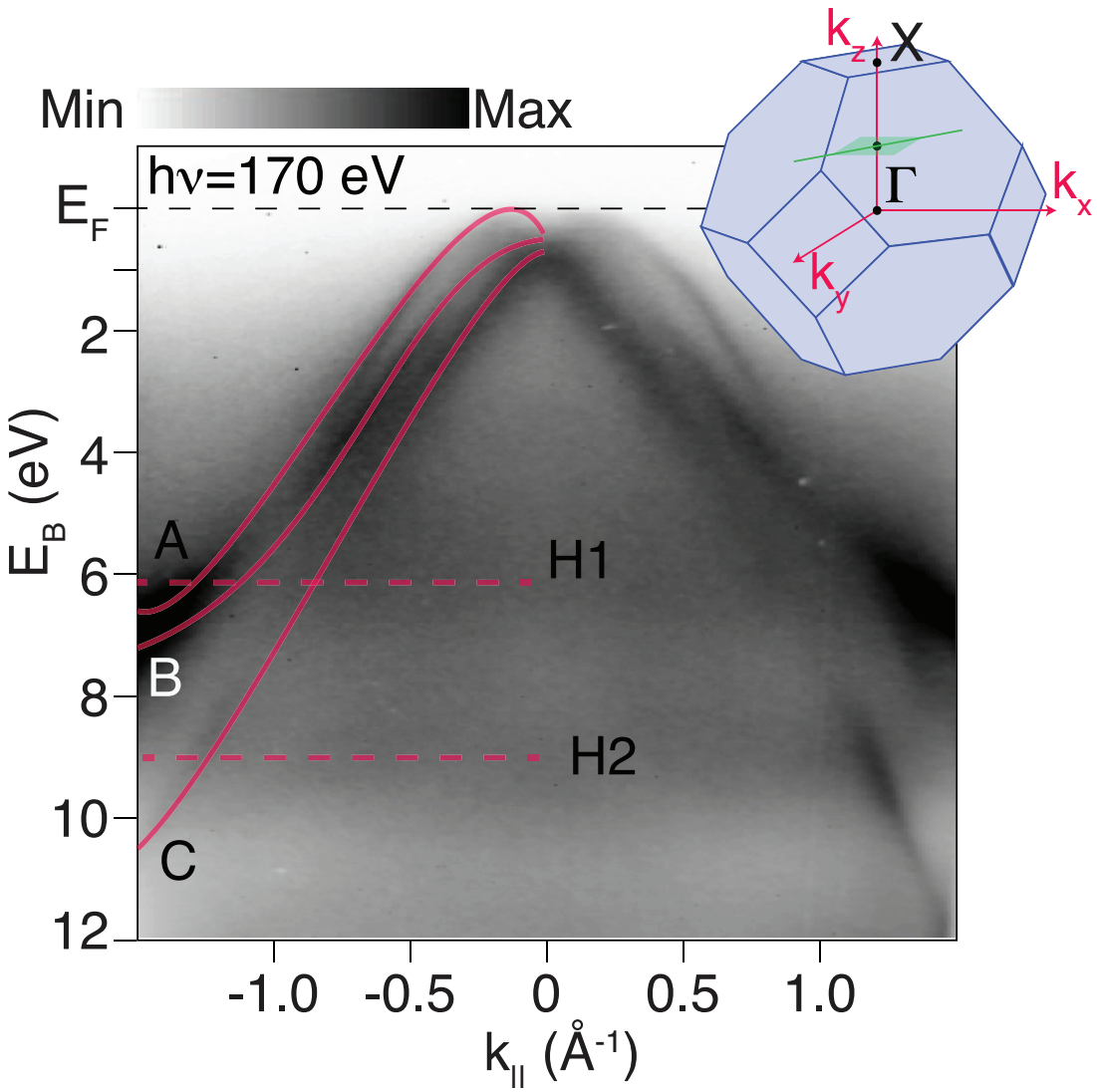

Figure 5.2: ARPES measurement collected at a photon energy of 170 eV for a thick (> 1μm) boron-doped diamond film showing the binding energy (E_B) dispersion as function of $\vec{k}_{||}$; the measurement corresponds to the band structure of boron-doped diamond acquired along the green line shown in the inset representing the BZ of diamond. Three bands (labeled as A, B and C) disperse close to the Fermi level (E_F), with 'A' crossing E_F, hence contributing to the metallic character of the sample. Additional horizontal bands (H1 and H2, see horizontal guide depicted by the dashed lines) are detected: These bands are an artefact coming from the edges of the Brillouin zone, where the electronic states have exceptionally high intensity and therefore such intensity can scatter across to the Brillouin zone center.

ward probe of the dimensionality of the electronic structure and has been successfully used to study a wide variety of materials [76, 91, 92, 93].

ARPES measurements for photon energies $155 - 170$ eV for a thick boron doped diamond sample are shown in Fig. 5.3a. For this analysis, we chose the photon energy range from 155 eV to 170 eV (which in $\vec{k}_z$ is from approximately 6.4 Å^{-1} to 6.7 Å^{-1}), since at lower values of photon energy (from approximately 40 eV to 150 eV) the intensity of the ARPES spectra is exceptionally weak (data not shown here). Using photon energies from 155 eV to 170 eV we observe a strong change in the spectral weight around the band's center. At 155 eV, the intensity of the band around $\vec{k}_{||} = 0$ is completely suppressed and smeared out with the background signal (see Fig. 5.3a); on increasing the photon energy the intensity gradually recovers and is fully revealed at 170 eV. We believe that the observed suppression of the spectral intensity is a consequence of selection rules: transitions from an initial to a final state are dictated by the availability of the final states and matrix elements, which determine the probability with which these transition can happen [92, 94, 95, 96]. This is also suggested by the fact that the different bands are not equally intense at one photon energy and that when the photon energy is changed we can fully recover the band's intensity [95].

In order to understand the dimensionality of the electronic structure we can extract the spectral intensity along $\vec{k}_{||}$ at a certain value of binding energy from each of the ARPES data of Fig. 5.3a (indicated by the horizontal green lines), which are all acquired at different $h\nu$ (and therefore $\vec{k}_z$). This allows us to build intensity 'maps' at certain binding energy values, representing how $\vec{k}_{||}$ varies with photon energy. Such maps are plotted in Fig. 5.3b for two chosen values of binding energy ($E_B = 1.6$ eV and $E_B = 2.0$ eV; we chose these values of binding energy because here the bands appear more intense, allowing for a better estimate of their positions). In these maps, 2D electronic band structures would appear as horizontal, dispersionless features whereas 3D electronic bands would disperse with photon energy. In Fig. 5.3b, within the photon energy range used, we could not observe any significant dispersion of the electronic bands of thick boron-doped diamond. Thus, even though the sample is a bulk system, its electronic bands seems to be electronically 2D. Summarizing; the electronic structure measurements of thick boron-doped diamond confirm the metallic character of the sample with bands crossing the Fermi level (Fig. 5.2 and Fig. 5.3), and our analysis indicates 2D electronic behavior, even though the sample is a bulk system.

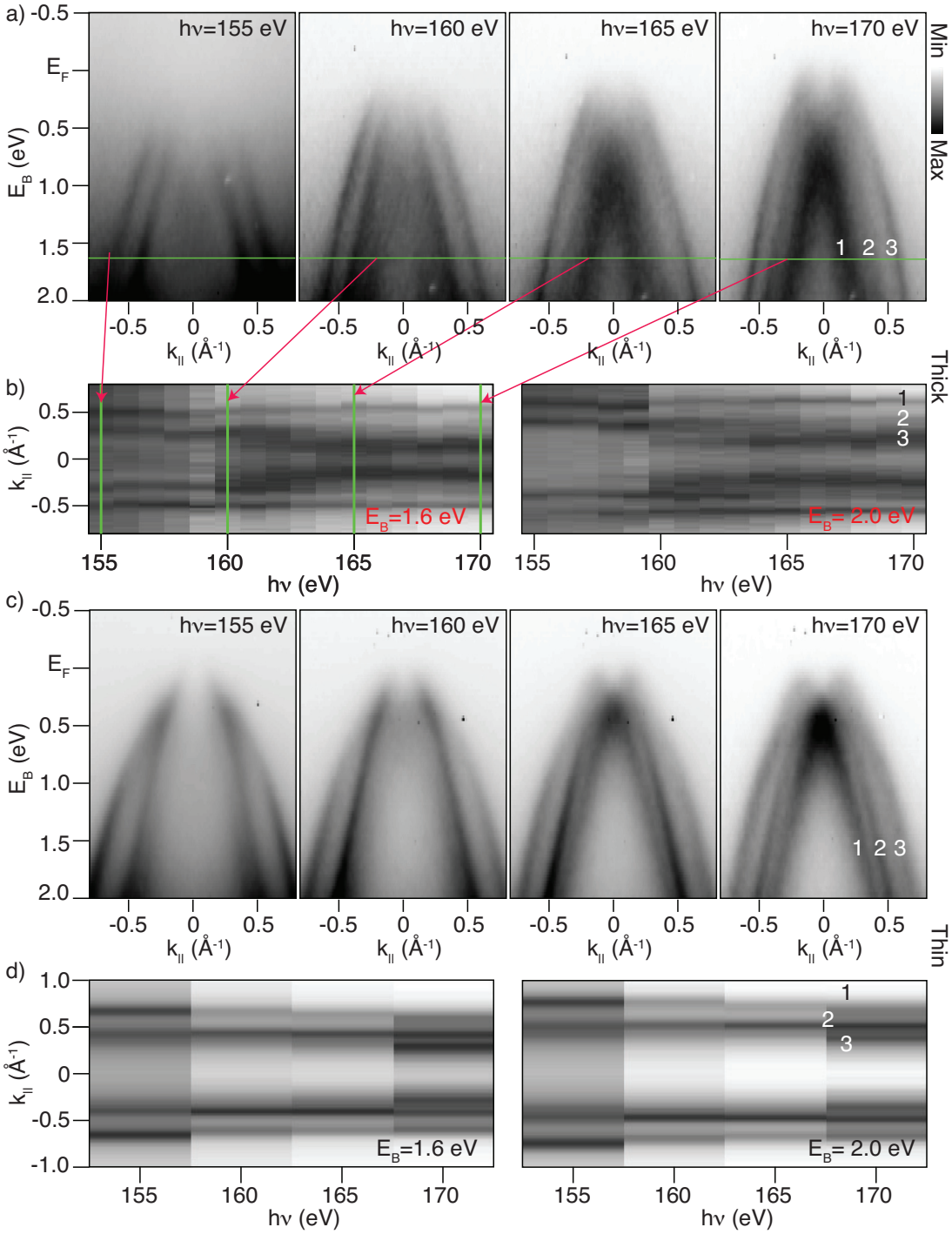

Figure 5.3: ARPES data and dimensional analysis for bulk and thin films of boron-doped diamond. a) ARPES measurements for thick and c) thin film ($\approx$ 2 nm) diamond acquired at different photon energies ($h\nu$) and through normal emission. Intensity map for b) thick and d) thin samples, showing momentum distribution curves as function of photon energy. Horizontal dispersions can be interpreted as 2D electronic states. The markers connected by lines are the band positions extracted from fitting the bands. The measurements have been carried out along the (001) crystallographic direction.

Whilst there is a large volume of experimental and theoretical work on bulk boron-doped diamond, focussing on the detection and understanding of the elusive electron pairing mechanism responsible for bulk superconductivity [78, 79], very little is known about the electronic structure of thin film boron-doped diamond. In Fig. 5.3c-d we introduce this missing piece of information, presenting ARPES measurements for thin film boron-doped diamond.

The ARPES measurements for thin boron-doped diamond, at first glance, appear qualitatively similar to the thick film data. Within the photon energy range shown (155 eV to 170 eV) we observe also a similar suppression of the spectral intensity, with a similar recovery fully happening at photon energy 170 eV. From the ARPES data of Fig. 5.3c, it is also clear that the thin film diamond has the remarkable advantage over the thick samples of an increased sample quality: although the quality of the thick system is good, as confirmed by the sharp and distinct features present in the ARPES data, the crystal quality of the thin systems is even better, as demonstrated by the lower background intensity in the ARPES measurements of Fig. 5.3c. The lower level of the background intensity for the thin samples compared to the bulk counterpart indicates a less significant contribution from electron-impurity scattering, which is ultimately responsible for broadening the measured band structure, contributes to an increased background signal in ARPES measurements and, crucially, supresses superconductivity.

It is also clear that the thin samples are very similar to the thick samples in terms of the dimensionality of the electronic bands. As confirmed by the $\vec{k}_{||}$ *vs* photon energy analysis in Fig. 5.3d, three bands can be observed, and all three show a 2D electronic behavior, exactly as it has been shown for the bulk system in Fig. 5.3b. The strong analogies between bulk and thin film boron-doped diamonds have been also quantitatively represented in Fig. 5.3b and Fig. 5.3d, where the bands are illustrated together with their fits (markers plus lines; red for band 'A', yellow for band 'B' and green for band 'C') [1]. From the fit results, the three bands observed in Fig. 5.3 show a maximum dispersion in momentum of $\Delta k_{||} \approx 0.05\text{Å}^{-1}$ at $E_B = 2.0$ eV, a small deviation value for the photon energy range considered for this analysis. Therefore, within this uncertainty ($\Delta k_{||}$), a 2D electronic character can be assigned to both samples, irrespective of their physical dimensions, meaning that the observed states are localized at the surface.

[1] The bands are fitted using Lorentzian curves convoluted to a Gaussian. The Gaussian accounts for the finite experimental resolutions of the instrument

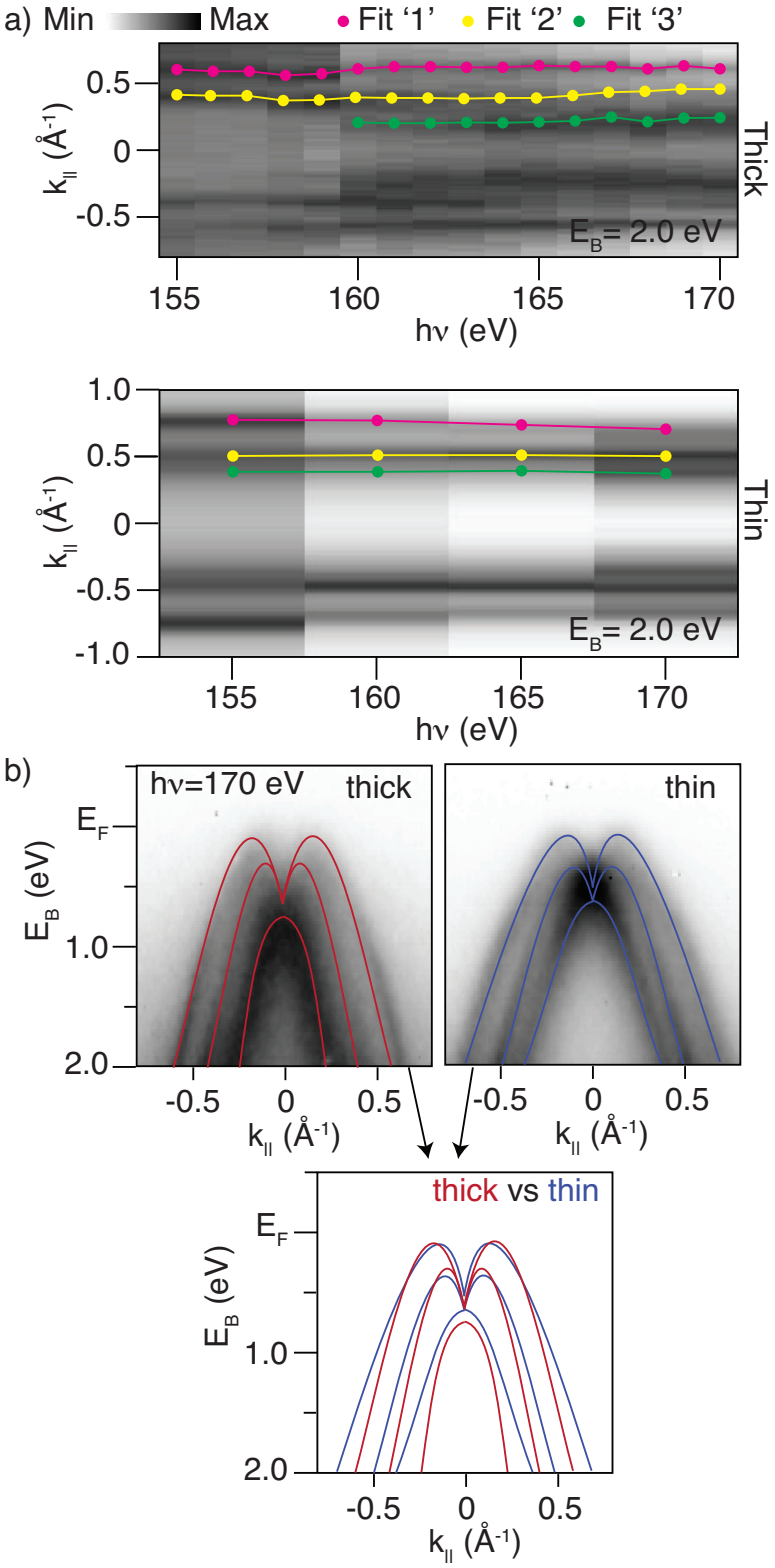

Figure 5.4: ARPES measurements for thick and thin film samples at photon energy 170 eV, with red and blue schematics respectively overlaid to the data to track the electronic dispersion. The dispersions are obtained by zooming in the dataset shown in Fig. 5.3. By comparing the dispersions, the bands show differences in the values of their effective masses: the thin sample supports higher effective masses than the thick samples (the electronic dispersion looks wider in momentum space). We believe this to be caused by electron correlations, playing a bigger role as the effective physical dimension is reduced.

We have also conducted ARPES measurements of thin and thick boron-doped diamond at low photon energy (from 35 eV to 40 eV, see Fig. 5.5). As was the case for high photon energy data acquisitions, final state effects and matrix elements are favourable also in this energy range and allow for the detection of ARPES data with high band-intensity/background-intensity ratio. We present low photon energy ARPES measurements in Fig. 5.5, only for the thin boron-doped diamond sample; ARPES measurements for the thick films show a similar behavior but with a slightly higher background intensity.

We could observe 2D electronic structures (see Fig. 5.4) whilst within the high photon energy range, low photon energy acquisitions reveal additional 3D electronic bands, as demonstrated by the $\vec{k}_{||}$ *vs.* $h\nu$ plot of Fig. 5.5b, which shows bands dispersing significantly with photon energy. The fact that low photon energies reveal the 3D, bulk-like nature of these samples and high photon energies do not, is another manifestation of the unusual cross section of these materials. Whilst highly unusual, a similar situation has been reported for other highly doped systems, namely phosphorus δ-doped silicon, for which low photon energies were necessary to access the electronic structure of a buried layer [92, 97]. It is also very surprising that ≈ 2 nm films show bulk-like 3D electronic bands at all, as we observe in Fig. 5.5b, and that the bandstructure is strikingly similar to the thick film counterpart. However, B-doped diamonds grown on intrinsic diamonds are not expected to behave as metal/insulator interfacial heterostructures for which the wavefunction of the metallic state is essentially confined entirely within the metal layer. In our systems, the B-doped diamond epilayer and the intrinsic diamond substrate share several crystallographic properties, and only differ in their B concentrations. Therefore, the wavefunctions in the doped region can be expected to extend some distance into the underlying intrinsic diamond, leading to a less abrupt confinement. The lengthscale of the confinement potential is defined by the screening length, which depends on the (strongly varying) carrier density and for this system can be expected to extend into the bulk several nanometers.

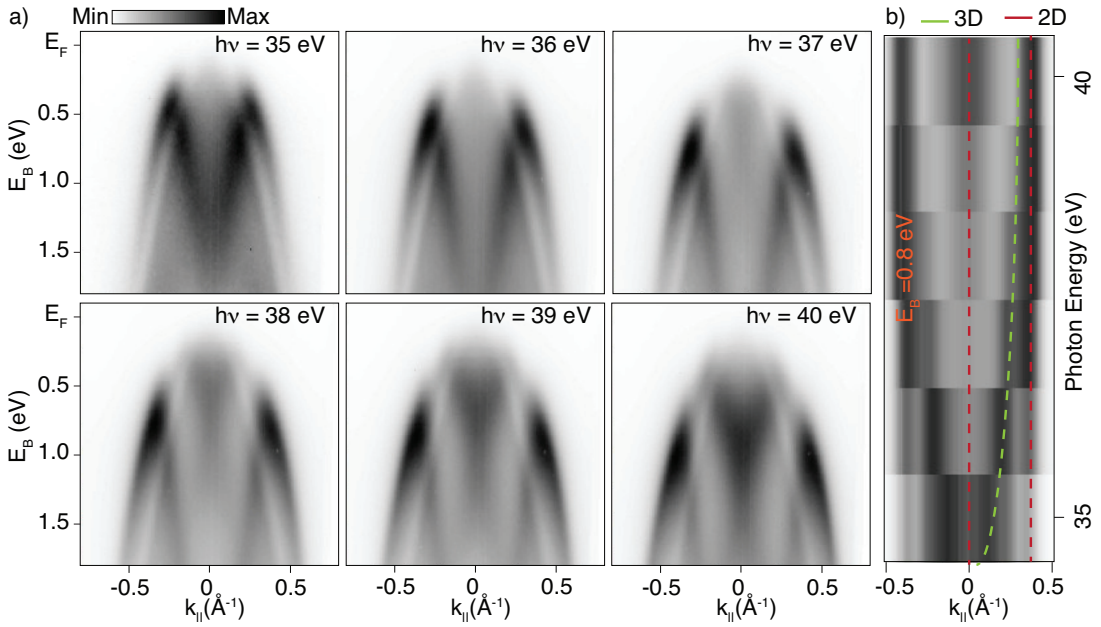

Figure 5.5: ARPES spectra acquired at low photon energies. a) ARPES data acquired for thin film boron-doped diamond from photon energy 35 eV to 40 eV. b) The bands which disperse with photon energy (guide for the eye: green line) are evidence of a 3D electronic behavior, the non-dispersing (guide for the eye: red lines) indicate 2D behavior.

5.3 Conclusions

So far, we have demonstrated that samples of thin and thick boron-doped diamond are electronically very similar, despite the enormous difference in thickness. For both thicknesses, the bands observed in the ARPES measurements seem to have the same electronic dimensionality, they have a similar dispersion in energy and momentum space, and both samples show a metallic character.

Although there are obvious similarities for the two systems, a closer inspection of the ARPES data also shows significant differences in the systems' effective masses. In Fig. 5.4b the red schematic indicates the dispersion of the thick boron-doped diamond, whilst the blue schematic indicates the dispersion of the thin one. From the thick to the thin sample, a renormalization of the electronic structure can be observed, corresponding to an increased value for the hole effective mass. In other words, the electronic structure of thin film diamond appears significantly wider than that of thick samples for the same values of binding energy.

The differences in the effective masses observed between thin and thick B-doped diamond can be attributed to electron-electron interactions. Indeed, electron correlations are expected to play a much more significant role in thin films than in thick films [98]. In particular, for metallic systems, electron-electron correlations have been demonstrated to induce a bandwidth narrowing and to increase the effective mass of the electrons/holes when the dimensionality of the sample is reduced [98, 99, 100]. This picture finds full agreement with our data, where both a bandwidth narrowing and an increase of the hole effective mass is observed (see Fig. 5.4b). In addition, electron-electron interactions are expected to be significant in stabilizing the electronic structures of superconductors and of materials which exhibit a MIT, and both of these effects have been documented for boron-doped diamond [35, 63, 64, 65]. For systems displaying these properties, in general, as the number of the effective dimensions decreases, even weak interactions break the quasiparticles into collective excitations and we believe this is exactly the case for boron-doped diamond [98, 101]. In these terms, thin film boron-doped diamond would constitute a perfect playground for exploring the role of correlation effects and exotic physical phenomena such as superconductivity at unusually high temperatures [102].

6

RESULTS: Characterisation of Nanometric Diamond Delta Doping with Boron

6.1 Introduction

Diamond is desired as a material for high voltage, high frequency, high power active and passive electronic devices because of its superlative materials properties [23], including high electronic carrier mobilities[83] high breakdown field strength[103], high thermal diffusivity[82], matrix for quantum devices, and diverse other optical, chemical, materials properties[84]. However, a major barrier to exploiting diamond for active electronic applications has been the lack of dopants with a sufficiently low thermal activation energy barrier to create an adequate concentration of electronic carriers at room temperature. While there are many known defect and impurity states in the wide bandgap (5.45 eV) of diamond, several of which can act as donors or acceptors of electronic charge, only boron [23] (creating an acceptor state) and phosphorous (creating a donor state)[104] have been demonstrated as reliable dopants. Boron, the most commonly used diamond dopant, has the smallest activation energy of 0.37 eV at low doping concentrations ($< 10^{17} cm^{-3}$). This value still means that only a fraction of the boron present is activated at room temperature, leading to relatively low concentrations of free carriers. Increasing the boron concentration reduces this activation energy, and at ca. $5 \times 10^{20} cm^{-3}$ the metal to insulator transition point occurs[63] and a fully activated

impurity band is formed via the quantum tunnelling of holes between neighbouring boron acceptor states[31]. Unfortunately, as the activation energy of holes decreases so does carrier mobility, not only because of the increased impurity scattering but also due to the onset of a low mobility, hopping-like conduction. The resulting material is one that has subunity carrier mobility and typical sheet carrier densities in excess of that which are readily controlled by a typical field effect transistor (FET)[105]. In this work we characterise boron doped diamond samples which show high Hall mobility and derived sheet carrier concentration by introducing nanometre-thick boron delta doped layers in to intrinsic or p-, type material (p- here defined as a boron concentration of less than $10^{17} cm^{-3}$) epitaxially grown diamond films with high mobility. A well known solution to creating BOTH high mobility AND high carrier concentrations for electronic materials in two dimensions is nanometric delta-doped layers[7]: nanometer thick, heavily doped layers (boron in our case) adjacent to high mobility intrinsic or p- material where a fraction of the carriers created by the heavily ionized dopant layer reside in the adjacent high mobility layer. Similar two-dimensional carrier conductivity has been observed on hydrogen terminated diamond surfaces with negative electron affinity. These surfaces create a subsurface two-dimensional hole gas[106] by electron transfer to adsorbates, but since they display stability issues, they will not be covered in more detail in this thesis. The success of delta doping requires the epitaxial growth of very thin (1 to 2 nm) heavily doped delta layer (preferably above the insulator to metal transition, ca. $5 \times 10^{20} cm^{-3}$ for boron in diamond)[63] and abrupt interfaces between the delta layer and the high mobility intrinsic or p-layer[107]. In addition, the interfaces must be atomically smooth to minimize carrier scattering. Recent reports from three experimental studies provide an in-depth discussion of their observations and implications. Balmer et al.[7] interpret measurements on uncapped, surface boron doped delta layers with a two carrier type model, but present no data showing the expected enhanced mobilities and sheet carrier concentrations. They also point out that mobilities measured by the Hall effect will overestimate the channel mobility in a working device. Scharpf et al.[108] demonstrate a boron doped solution gated field effect transistor based on an uncapped surface delta layer, with adequate sheet carrier density, but a channel mobility of 0.1 cm^2/Vs which they attribute to poor lateral homogeneity and interrupted morphology of the delta layers. Chicot et al.[109] present results on buried boron doped delta layers of varying thicknesses ranging from<2nm to

35nm which were capped with 30nm to 65 nm of undoped diamond. They also summarize the published literature reports of mobilities and sheet carrier concentrations along with their results (Ref.[109], Table IV), which are reproduced below. All of their measured carrier mobilities were in the range of 1 cm^2/Vs to 4.4 cm^2/Vs which is typical of bulk diamond doped above the metal insulator transition of $5 \times 10^{20} cm^{-3}$. The desired values in delta doped layers are greater than 100 cm^2/Vs for mobility, and $> 10^{13} cm^{-2}$ for sheet carrier concentrations. In this chapter, significant progress in growth and characteristics of diamond nanometric thick delta doping with boron is shown, demonstrating both enhanced room temperature Hall effect mobilities and carrier concentrations over the previous experimental reports. The adopted approach employs: ultra-smooth diamond substrates ($\frac{R_a}{S_a} < 0.3$ nm) (R_a is the arithmetic average of surface profile along a line, and S_a is the average over an area), a custom built microwave plasma assisted chemical vapor deposition (CVD) reactor with laminar flow and fast gas switching[110], very slow growth rates, smooth epitaxial films, and chemically gettering residual boron in the reactor when growing intrinsic/lightly doped material by adding H_2S to form gaseous boron sulfur compounds[111].

6.2 Experimental

The single crystal diamond substrates used in these experiments were type IIa (no nitrogen detectable by IR absorption spectroscopy) obtained from New Diamond Technology (St. Petersburg Russia) and the Technological Institute for Superhard and Novel Carbon Materials (Troitsk, Moscow, Russia). Their size was either 3×3×0.5 mm or 3.5×3.5×0.5 mm with major polished faces nominally (100). The samples displayed little or no birefringence when viewed between crossed polarizers. These samples were repolished mechanically to a surface roughness, R_a, of 0.3 nm or less, typically 0.1 nm over areas of 80×80μm for S_a, and lines of over 1mm for R_a, and then etched in an inductively coupled reactive ion etcher (Oxford Instruments, Plasmalab 80) to remove polishing damage in the top ca. 4-5 μm[112]. The CVD reactor was custom designed[110] specifically for the delta doping growths with nearly laminar flow and rapid switching of the reactant gas mixtures to achieve abrupt interfaces. Typical growth conditions employed a flow of 900 sccm hydrogen (Pd diffusion cell purified), 1.4 sccm methane (ultra-pure, 99.999%), 6 to 17 sccm of 0.1% B_2H_6 diluted in hydrogen,

and 6 to 14 sccm of 0.1% H_2S diluted in hydrogen. Typical growth rates were determined by SIMS-SP, to be between 30 and 90 nm/hour. The total gas pressure was 30 to 50 Torr and the microwave power was 1.5 kW. Transmission electron microscope (TEM) images were recorded aligned to the diamond [110] axis. TEM sample preparation was performed in a Helios FEI FIB. To keep the surface layer undamaged, it was coated with platinum. TEM investigation was carried out on 300 kV FEI titan. SIMS-SP was performed in an IONTOF TOF.SIMS-5 using Cs ions (1keV) for sputtering, and Bi ions (25 keV) for probing. It was found out that for smooth (root mean square deviation $R_a < 1$ nm) surfaces the use of 1 keV energy sputtering ions allows a depth resolution of 1.2 - 2 nm for the investigated structures. Room temperature Hall measurements were carried out in van der Pauw geometry after an acid cleaning process (boiling in conc. sulfuric and nitric acids with added KNO_3) known to leave oxygen moieties on the diamond surface to minimize any contribution from a hydrogen surface conductive channel. At Institute for Physics of Microstructures of the Russian Academy of Sciences (IPM), indium Ohmic contacts were deposited at 180 degrees Celsius, not only on the surface but also to the end pads. This provided satisfactory electrical contacts to the delta layer with stable characteristics without additional annealing and allows the Hall measurements with small errors. At UCL, Ohmic contacts were made with silver epoxy annealed at 70 C. Measurements were made in a Lakeshore 7500 series Hall effect probe system with a stabilized current source. Measurements were performed in magnetic fields of up to 1 T with both polarities. UCL then fabricated Hall bars on the reverse of the crystals. Photolithography was carried out using a Karl Suss MJB3 Mask Aligner. The sample was masked with 500nm of Al and etched in a STS ICP dRIE in an oxygen and argon plasma. Ti/Pt/Au contacts were then patterned to allow the devices to be electronically addressed. This would enable a measure of the concentration of bulk impurities and not irreversibly damage the delta layer side which was wanted for other surface science experiments. Measurements we made on the same Lakeshore Hall effect system.

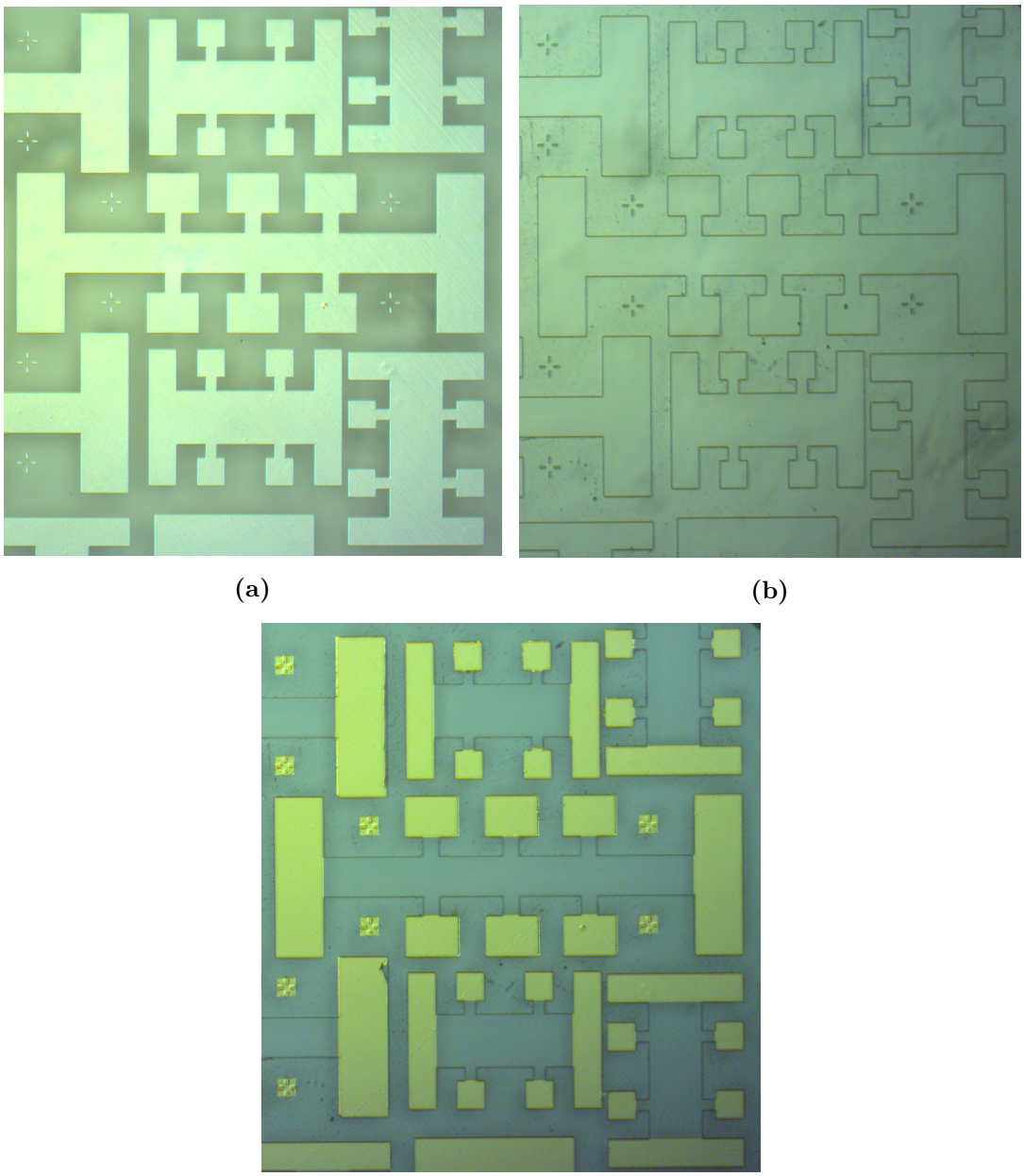

Figure 6.1: sample S16 is (a) masked with 500nm of Al (b) mesa is etched in RIE and then Al mask removed. (c) After photo lithography, Ti/Pt/Au is e-beam evaporated and the lift-off process leaves well aligned second layer of contacts.

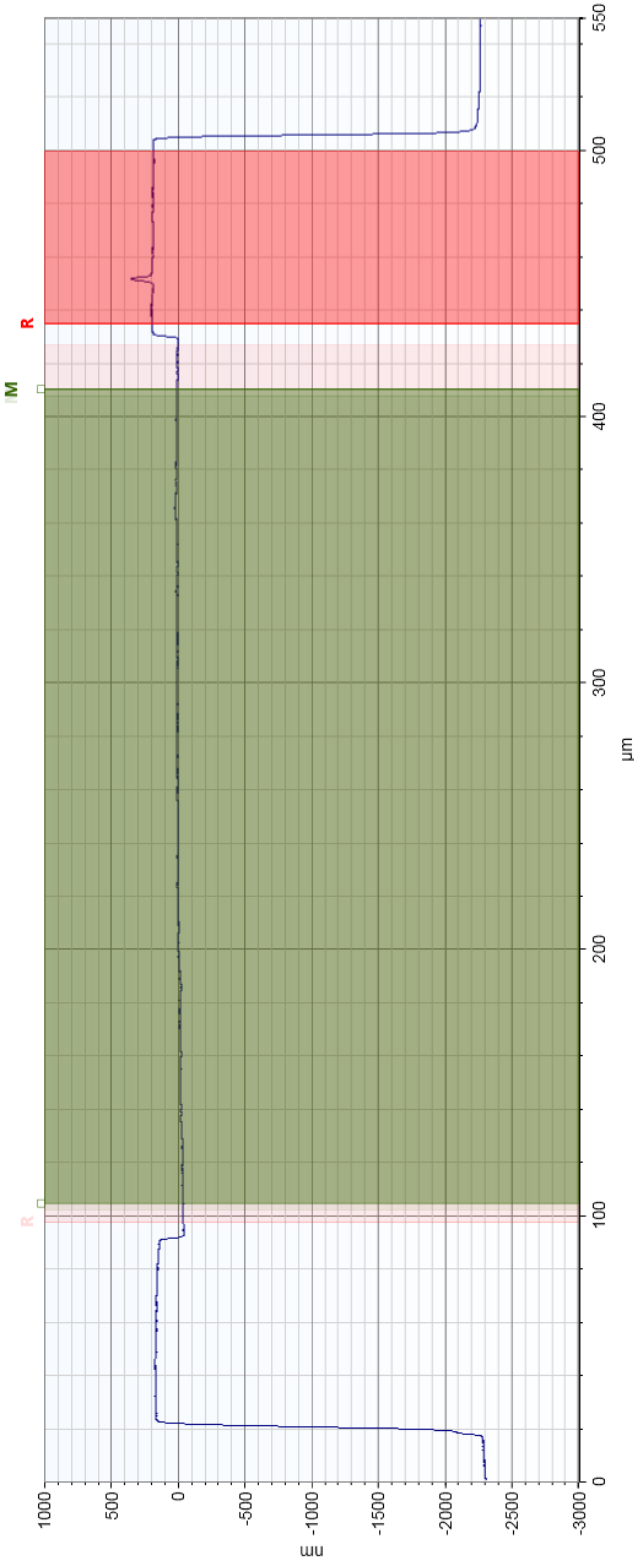

Figure 6.2: Profile from bottom of mesa (-2300nm) to top of contact (195nm, higlighted in red on right hand side. Device is symmetrical along this cut so left to right is the same as right to left) down to the channel (highlighted green and at 0nm), up to the next contact and then down to the mesa floor. This confirms a metal stack of 195nm and an etch depth of 2.3μm. The highlighted areas M and B are the regions over which an average is taken to comaper relative heights.

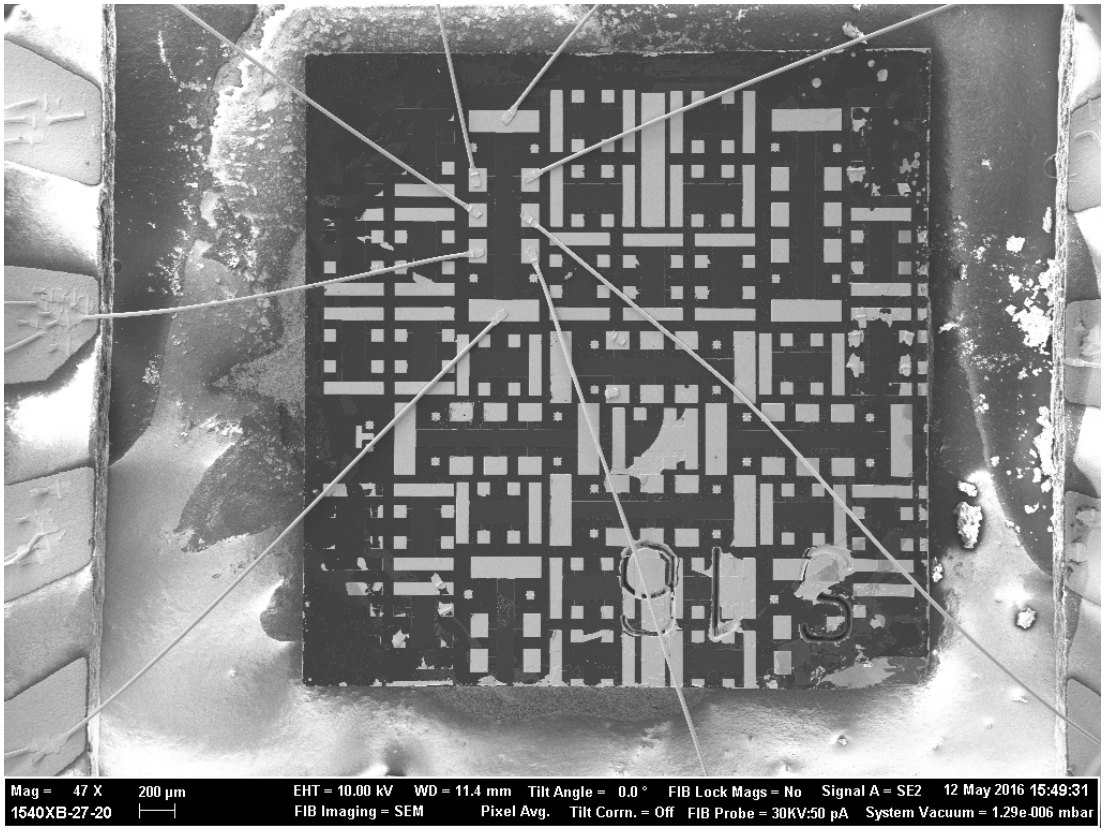

Figure 6.3: Packaged and wire bonded Hall bar on sample S16. Lift off has failed in a few areas.

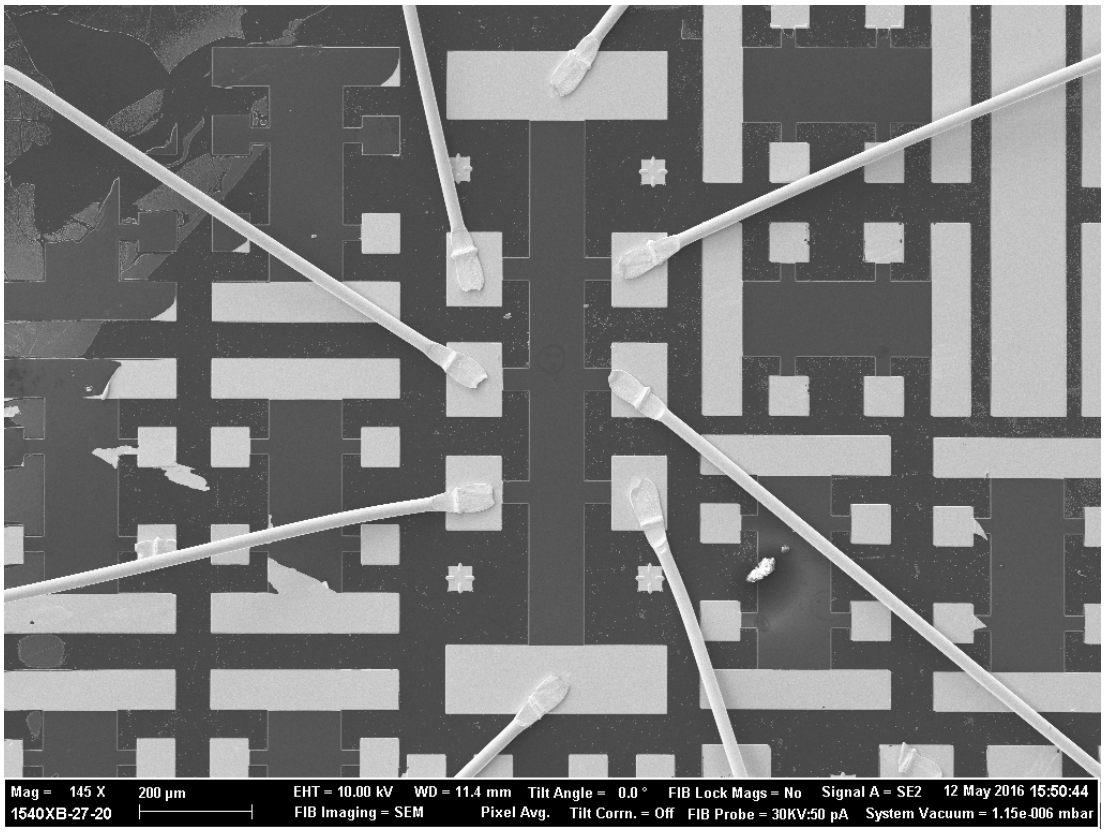

Figure 6.4: wire bonded Hall bar on sample S16.

6.3 Results

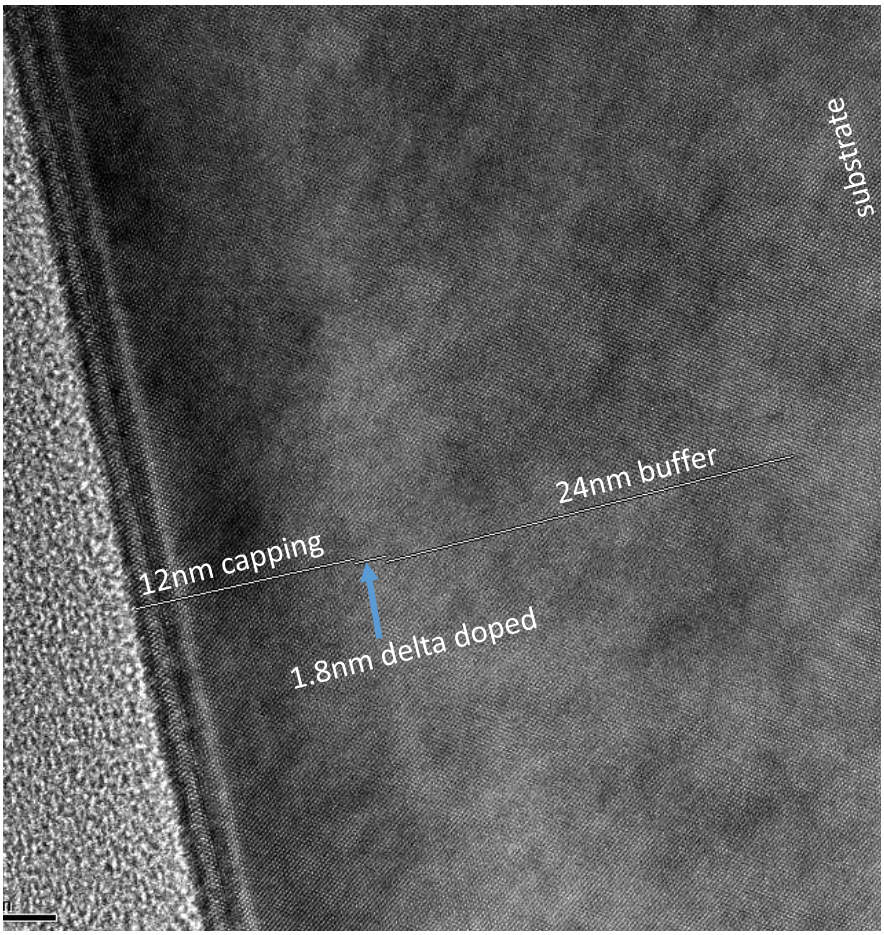

Figure 6.5: Transmission electron micrograph image of a focused ion beam thinned section of a sample with a single *'delta layer'* sandwiched between intrinsic/lightly doped buffer and capping layers on a single crystal substrate. The electron beam was normal to the [110] crystallographic direction and the epitaxial growth direction was normal to the (001) crystallographic plane. The annotation of the layer positions is solely based on the expected growth rates (see text for explanation).[22]

Examination of focused ion beam (FIB) thinned portions of one of our delta doped samples by electron diffraction and transmission electron microscopy (TEM) confirms the [001] direction of our epitaxial growth, as shown in Fig.6.5. It should be noted that due to the epitaxial relationship, similarity in atomic numbers of C (12) and B (13), maximum boron concentration of less than 0.1%, and lack of significant structural

defects, the interfaces between the buffer layer, substrate, delta layer, and cap layer are not visible in the figure. Shown in the figure are the positions expected for the epitaxial layers based on the expected growth rates of each layer. At lower magnifications (not shown) some additional contrast does appear in the delta doped area, probably due to strain. The ultimate test of the success of delta doping has to be in electrical measurements. We report here our initial room temperature measurements of carrier concentrations and mobilities by the Hall effect (van der Pauw configuration) on the whole samples containing single delta layers of thickness between 1.8 and 2.8 nm and capped with a buffer layer. The results of measurements of the room temperature Hall effect mobilities and carrier concentrations using the van der Pauw geometry of our initial set of samples by 2 participating laboratories is reported in Table.6.1. Also reported in this table are the published measurements of several previous experimental efforts. The most notable thing is that the carrier mobilities of the samples grown in this work exceed those of all the previous reports on similar samples by over an order of magnitude (the non-italicised entries in Table.6.1), and the related resistances are also over an order of magnitude lower. The italicised entries are for data which may be compromised by contributions dominated by the bulk, lightly doped regions of the sample and not because of conduction adjacent to the delta doped layer as discussed later.

source	sample label	P_s (cm^{-2})	mobility at $T = 300$ K (cm^2/Vs)	resistance (Ω/sq)
UCL	*S16*	5.00×10^{11}	*750*	*16455*
UCL	S19	1.00×10^{12}	90	33131
UCL	S18	4.00×10^{12}	10	182310
IPM	S09	6.50×10^{11}	240	40000
IPM	S21	6.50×10^{13}	16	6600
IPM	S23	1.00×10^{13}	99	6000
IPM	E35-14	1.30×10^{13}	120	4000
IPM	S24	6.40×10^{13}	92	1100
IPM	S12	5.10×10^{13}	17	7000
IPM	S12-1	6.00×10^{13}	18	5300
Ref. [22]	*1*	1.40×10^{13}	*54.6*	
Ref. [22]	2	1.60×10^{14}	3.3	158000
Ref. [22]	3	4.40×10^{15}	2.9	
Ref. [22]	4	2.30×10^{15}	4.4	
Ref. [16]	5	3.20×10^{14}	3.3	15000
Ref. [16]	6	3.20×10^{13}	1	
Ref. [16]	7	1.40×10^{14}	3.8	50000
Ref. [16]	8	1.80×10^{14}	3.1	
Ref. [16]	9	6.0×10^{14}	3.7	
Ref. [16]	10	2.20×10^{13}	0.6	
Ref. [14]	*348*	3.70×10^{12}	*35.4*	
Ref. [14]	*366*	1.00×10^{16}	*3.8*	
Ref. [14]	*385*	1.20×10^{11}	*679.8*	
Ref. [14]	*459*	4.30×10^{8}	*438.1*	*126000*
Ref. [23]	*A*	1.40×10^{15}		
Ref. [23]	*B*	8.00×10^{12}	*9.8*	
Ref. [23]	*C*	1.20×10^{13}	*13.3*	
Ref. [15]	S	2.40×10^{13}	0.1	

Table 6.1: Sheet carrier concentrations, room temperature mobilities, and resistance of the samples grown for this work and measured at UCL and IPM. Additional measurements reported in the literature are also presented. Entries shown in italics are not directly relevant as the conduction is likely dominated by the bulk p-buffer and cap regions based on the thermal activation energy measurement as discussed in the referenced papers.[22]

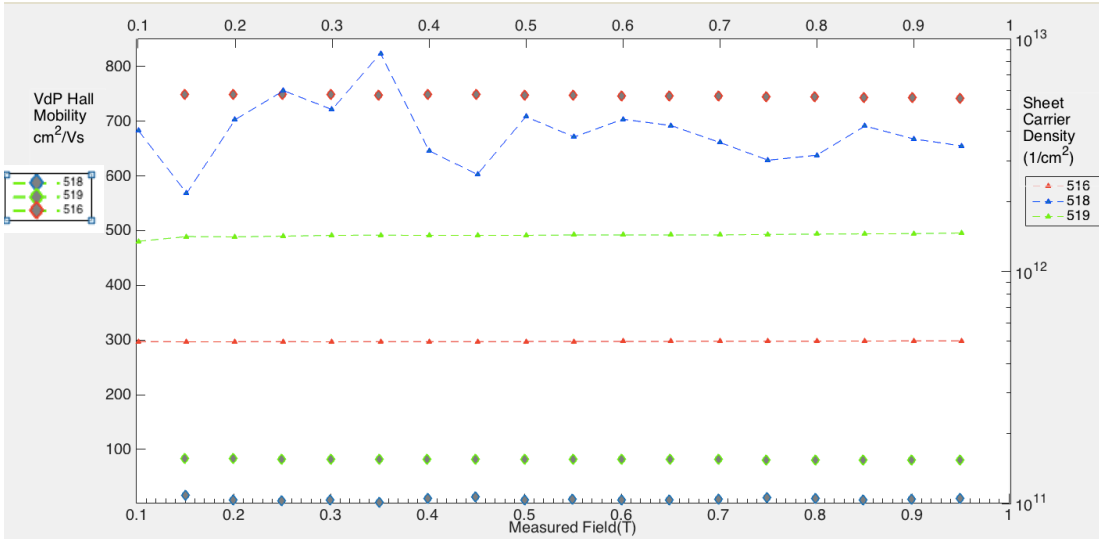

Figure 6.6: Hall mobility derived from Hall effect measurements on top of sample S16 measured using VdP geometry. The sheet carrier denisty is on ploted on the right scale with the points at each field strength connected by the dotted line. Hall mobility is plotted to the right, in single unconnected points. The colour for each sample is consistant for mobility and carrier concentration.

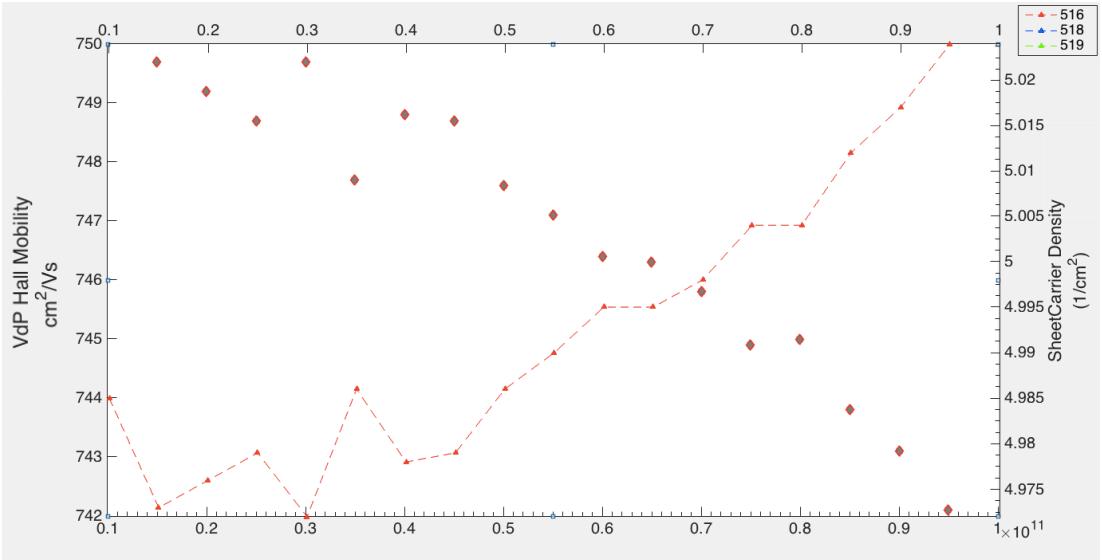

Figure 6.7: Hall mobility derived from Hall effect measurements on top of sample S16 measured using VdP geometry.

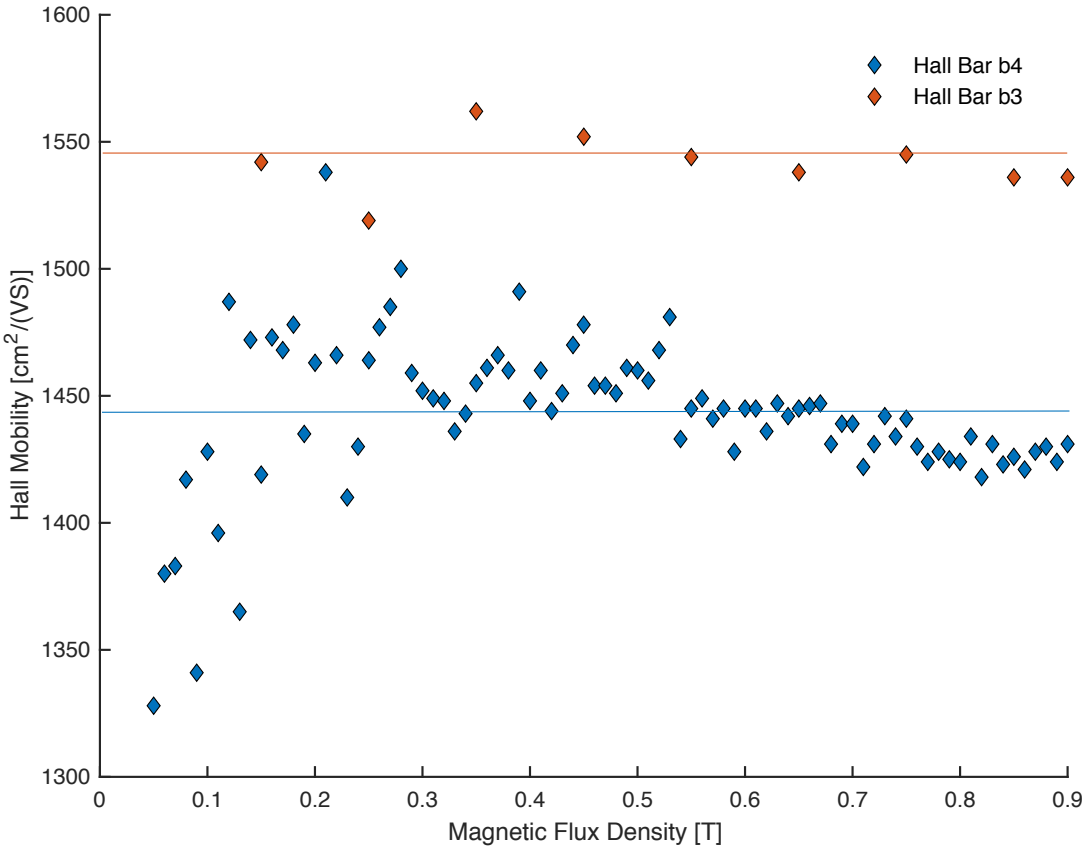

Figure 6.8: Hall mobility derived from Hall effect measurements on sample S16 measured on two different Hall bars (Each chip had 10-20 devices on it. The two devices measured here were Hall Bar b3 and b4). Devices fabricated on bulk unintentialy doped substrate. Lines are a guide for the eye towards averaged non-zero field Hall mobility.

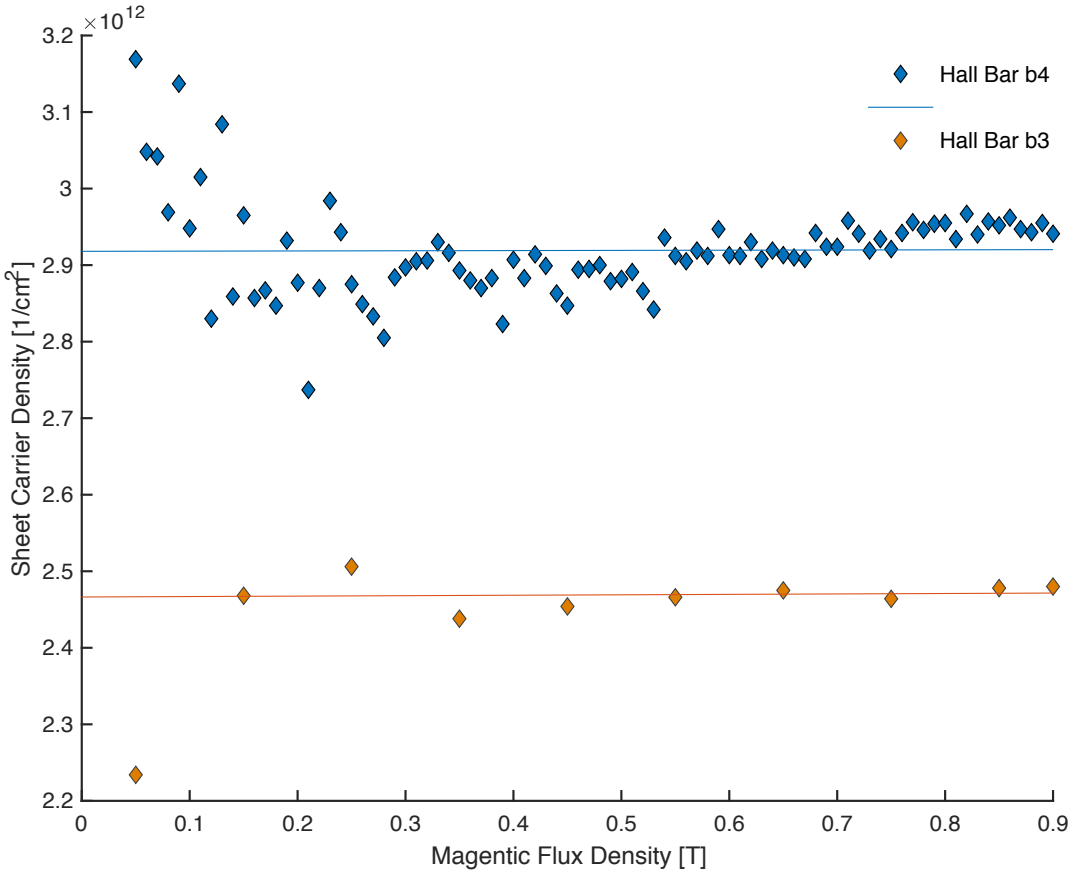

Figure 6.9: Carrier density derived from Hall effect measurements on sample S16 measured on two different Hall bars. Devices fabricated on bulk unintentialy doped substrate. Lines are a guide for the eye towards averaged non-zero field Hall mobility.

6.4 Conclusions

There are many parallel electrical conduction paths possible in a sample with a capped single delta layer. These consist of conduction on the surface, in the bulk p-doped capping layer, in the heavily doped delta layer, in the p- layers on either side and adjacent to the delta layer, in the bulk p- doped buffer layer, and in the diamond substrate. Surface conduction is easily prevented by oxidation of the diamond surface, but all other paths cannot be ignored. Conduction in the heavily doped delta layer is characterized by low mobilities and high carrier concentrations, typically $3cm^2$/Vs to $5cm^2$/Vs and 1020 cm^{-3}. Conduction in the CVD grown bulk p-doped layers should exhibit high mobilities, greater than 1000 cm^2/Vs, but low carrier concentrations. Conduction in the diamond substrate may vary depending on the unintentional doping of the HPHT substrate with B and N. Measurements on three substrates suggests that the background boron level is not negligible. For Hall effect measurements with room temperature sheet carrier concentrations near 10^{12} cm^{-2}, the dominant conduction path is likely via the high mobility bulk p- buffer and capping layers, while for carrier concentrations above 10^{14} cm^{-2}, the dominant contribution is from conduction in the low mobility, heavily doped delta layer. Hence, the region of Table.6.1 relevant to the enhanced mobility and carrier concentration is the non-italicised entries between $10^{12}cm^{-2}$ and $10^{14}cm^{-2}$ sheet carrier concentrations. Note that almost all our initial Hall effect measurements exceed the previously reported values by over an order of magnitude.

The Hall effect measurements presented here are encouraging indicators of the success of this approach to growth of effective delta doped layers. Yet there is still much work to be done to clearly demonstrate the enhancement necessary for functioning active electronic devices. As pointed out by previous researchers, the Hall effect mobilities overestimate the actual channel mobilities in a device[7]. We are in the process of fabricating and testing Hall-bar structures to more precisely determine the local properties on a scale similar to a device structures. Measuring the temperature dependence (activation energy) of the carrier concentrations will assist in identifying the conduction paths measured by the Hall effect. We are also fabricating and testing various field effect transistor structures to determine actual channel mobilities, conductivity, and gate pinch off. We view the successes presented here as just an initial step toward enabling a class of active electronic devices based on the superlative properties of diamond. The

great care in polish and quality control (selecting samples carefully after the polishing step befor epi-layer growth) is probably key to the samples quality. Another key factor is the quality of the HPHT substrate. This is a a brand new material produced in Russia and has been shown to be very low stress and defect density, this most like makes the propagation of errors that can dominate crystal growth less problematic.

7

RESULTS: NanoWires

7.1 Introduction

At the date of writing, the consensus within the diamond community is that delta-doping of diamond has been has been a failure. The limitations of MEPCVD and difficulties in doping diamond in general have meant that the enhancements to electronic transport through the reduction of one of the key dopant distribution length scales has failed to materialise. Diamond has, however, continued to prove itself an interesting material. For observing other quantum mechanically predicted phenomena. Its high Debye temperature [113], in particular, makes it a good candidate for observing such quantum phenomena without having to be at cryogenic temperatures [114] [115]. Pursuing a reductionist agenda, an attempt is made to physically and electronically confine the carriers further both to make the ultimate classical devices and in the hope of seeing quantised transport phenomena. This will push the technological limits to produce amongst the smallest electrically addressable diamond devices to date.

There are many reasons to do as Feynmann suggested and look for room down at the bottom. Not only does making smaller devices allow us to squeeze a higher density of devices in a given area, but it allows us to build devices that utilise totally different physics to operate. ′nanowire′ is a broad term that is used to define a wide variety of systems. At least one physical dimension for the system will be measured on the order of nanometres. This usually means a nanowire's length to width ratio can be huge. This very high surface area to volume ratio makes them potentially very sensitive to changes in surface chemistry/physics [116]. Nanowires can be made from a metal, a

semiconductor, an insulator or even an organic compound. Each of these material systems will produce very different nanowires. Even within any given material system a nanowire may be very different depending on whether the fabrication is bottom-up or top-down. As a new unmeasured type of nanowire will be fabricated here it is unknown exactly which superlative qualities or uses they will find in the future. The motivation will be to first fabricate a lateral boron doped diamond nanowire and then to electrically interrogate it. It may be assumed that these nanowires will be extremely robust, both physically and electromagnetically, which should enable new fast transistors and resilient sensors. The length scales for these devices, mixed with diamonds unique physical structure could, also lead to the observation of quantum effects even at room temperature [114].

The cornerstone of the process developed herein is the use of hydrogen silsesquioxane (HSQ). This is a negative resist when exposed to an electron beam (from a programmable electron beam lithography system (EBL). HSQ will cross link after exposure forming a non-stoichiometric silicon oxide film. This is useful as the selectivity of SiO to diamond in an oxygen RIE plasma is good. The resist also allows for very high resolution, single pixel lines (a single pass of the EBL, as it rasters around the patter, this is essentially the resolution limit for any EBL). The HSQ is diluted in MiBK, which is a solvent. It comes in 6

Although this work was conceived at UCL the first serious fabrication attempts were attempted by the author with the assistance of collaborators at Yale University. Unfortunately this was unsuccessful. The work is documented below as, although the alignment method proved to be unsuccessful, it would be a more industrially scalable approach then the ultimately successful route taken in the UCL cleanroom. The initial approach was to mount the diamond die on a patterned Si wafer (shown in Fig.7.2) the only subsequent difference in processing was in how the EBL machine aligned on and between layers. The core of the solution found in the LCN clean room was to put alignment marks on the chip itself and to change the design to allow more misalignment tolerances.

7.2 Fabrication of Nano Structured Diamond

7.2.1 Yale Approach

To prevent charging issues whilst exposing the first layer of the device (the HSQ mask) the diamond sample was grounded by careful placement of conductive copper tape on corners. This allowed for a uniform pressure to be applied, keeping the sample flat. On the second layer (metallisation for contact pads and vias), when the substrate is no longer conductive due to the RIE ecthing to define the mesa shaped devices, a thin layer (<10nm) of Au was evaporated onto the PMMA stack. This acts as a Faraday cage, stopping a build up of charge from causing the electron beam to be distorted. At Yale samples were ultimately mounted onto the carrier wafer using a two part epoxy. This was chosen as the diamond chip needed to stay perfectly fixed for a multiple layer process to stand a chance of working. After Exposure the carrier wafer and diamond would be developed in strong developer, dried (critical point drying was tried but saw only a minor improvement in our achievable pitch) then etched in a 02 plasma, dipped in HF rinsed, cleaned, coated in PMMA by-layer, exposed in EBPG (raith branded 100keV EBL at yale), developed again, metallised and then finally a lift off process as shown in process flow Fig.7.1.

At Yale I was unable to see etched alignment marks on the delta doped diamond as the E-Beam was fixed at 100kV and the contrast between shallow etched areas and the conductive channels was insufficient. The contrast between any etched in feature and the substrate is proportional to the energy of the incident radiation. At 100keV the alignment marks in the diamond are not distinguishable from the diamond substrate. This meant a different alignment procedure would be necessary. Metal alignment marks could not be placed on the diamond as the clean room manager did not want metals in the DRIE.

By using alignment marks on the carrier wafer it was hoped to achieve alignment on the order of 100nm. This approach was also perused as it would be very industrially scalable allowing for multiple samples to be placed on a single carrier wafer which would be able to fit into an existing fab process flow.

The first step of the process was to understand the doses of electrons required to get good definition of the mask, Fig.7.3 shows such a dose test. The proximity effect resulted in each structure requiring different doses to come out as designed. Working

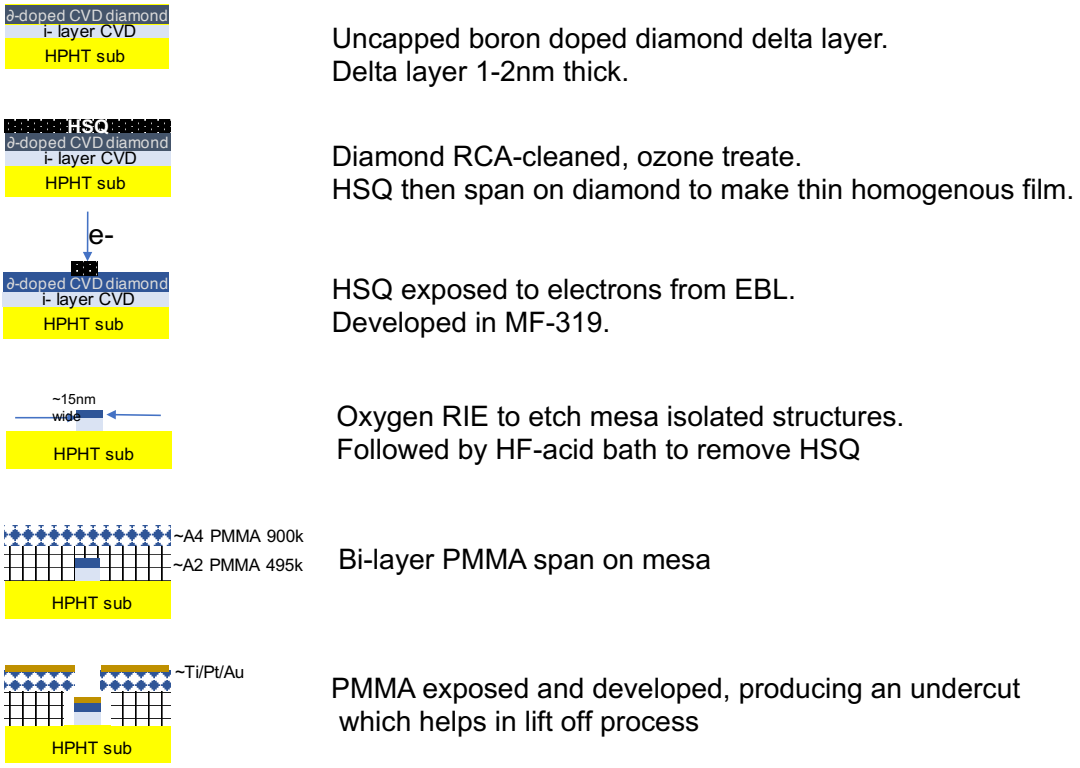

Figure 7.1: General process flow for fabricating lateral nanowires in single crystal diamond.

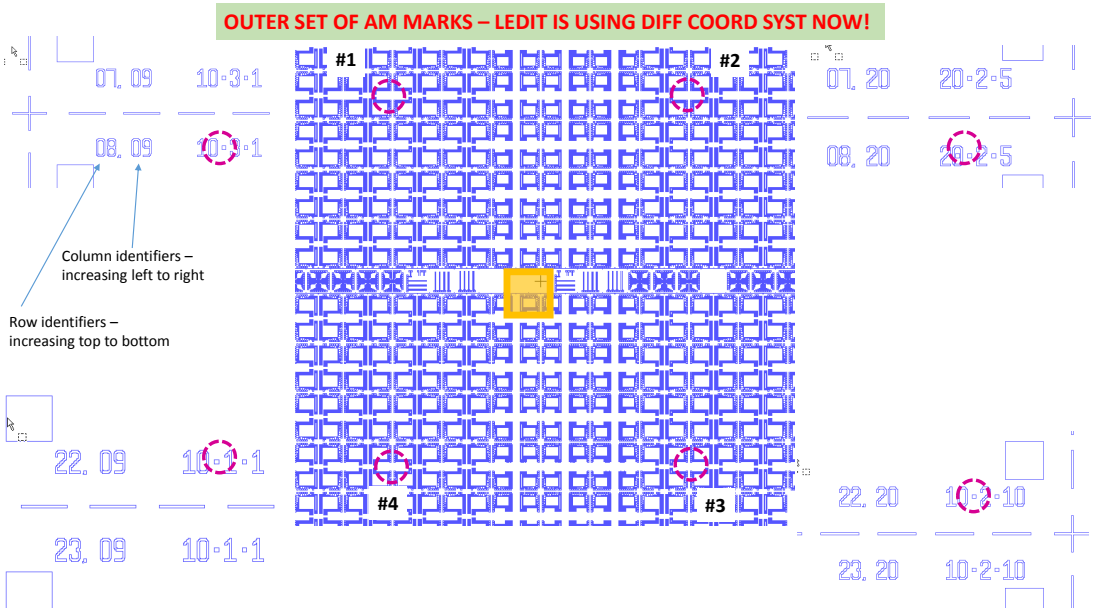

Figure 7.2: LEDIT (mask design software) screen capture for the carrier wafer used for off-chip alignment at yale. The position for the diamond is represent by the yellow square. The circled features are pints used to automatically align writefields and subsequent layers.

out the optimal dose was time consuming as the doses required were so high. This led to long write times.

The next step was to etch the diamond and HSQ mask in a fairly diffuse O_2 plasma. 200 W rf power and 200W ICP power, with a pressure of 20 mT and a flow of 40 sccm. After 1 min in this plasma 40nm of diamond had been removed with an unmeasurable amount of HSQ being etched. This selectivity is remarkable. After the etch the samples were soaked in 49% HF for 15 minutes to remove the HSQ mask. In between each step the chip was profiled as can be seen in Fig. 7.5. Unfortunately the profilometer used at Yale was very old and did not output data so only camera images of the screen are reproducible, hence the poor quality of Fig. 7.5. It does however show a very high selectivity and ultimate etch dept of 40nm for the mesa.

The next step was to spin on the by-layer PMMA and expose the metallisation pattern.

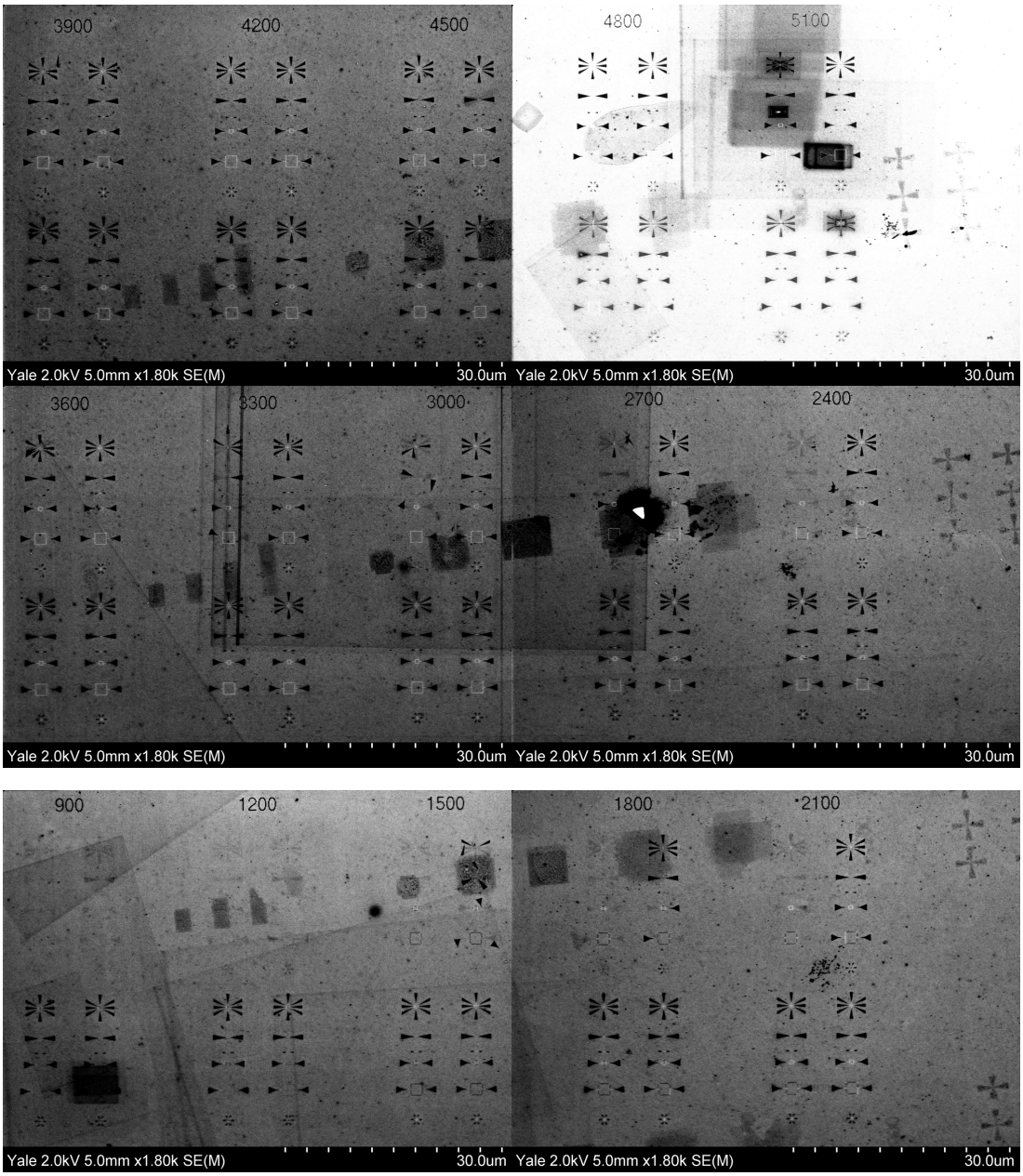

Figure 7.3: 4% HSQ, dose test. Numbers 900 - 5100 represent factors by which the dose for each pattern is increased. Exposed using 100keV, Vistec EBPG 5000+, imaged on Hitatchi SEM

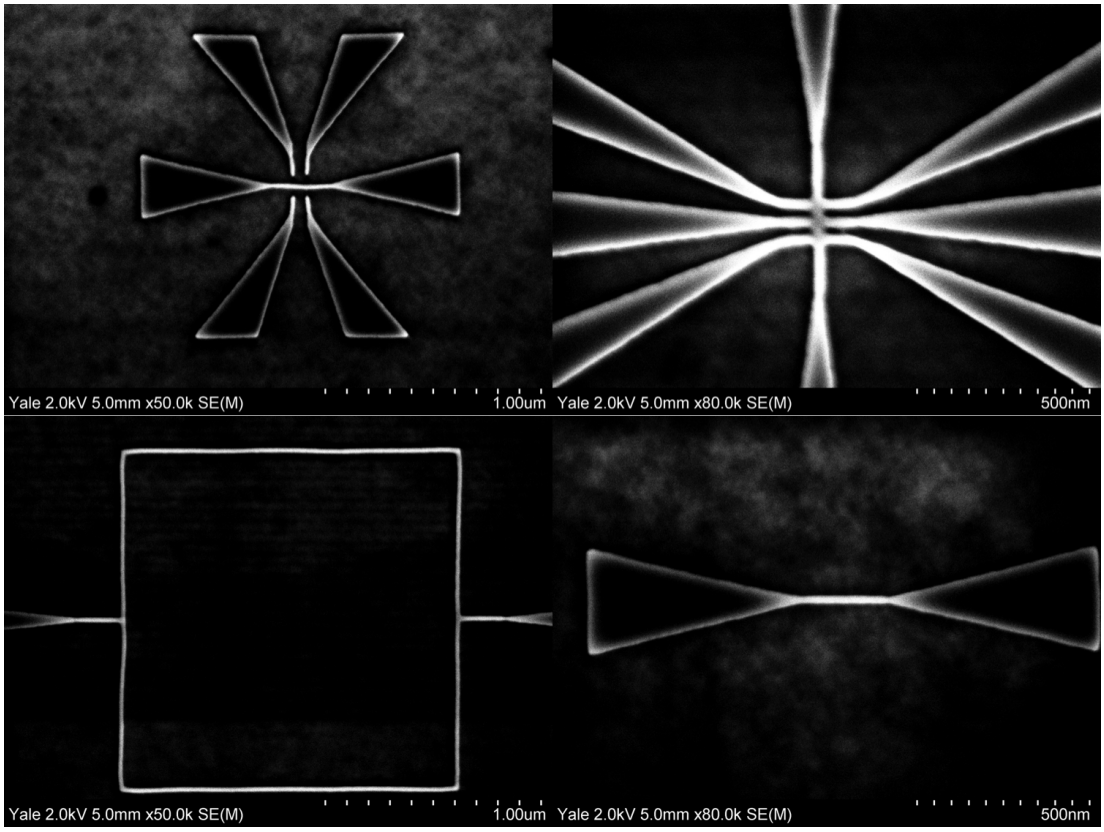

Figure 7.4: 4% HSQ Optimal doses are clear as there is a lack of scum in corners, the pitch between features is small and the wires are straight. Moving from top left to bottom left in a clockwise fassion: Double Gated nanowire,9-terminal nano-Hall bar, Single Pixel ring, and nano-wire exposed using 100KV, Vistec EBPG 5000+, imaged on Hitatchi SEM

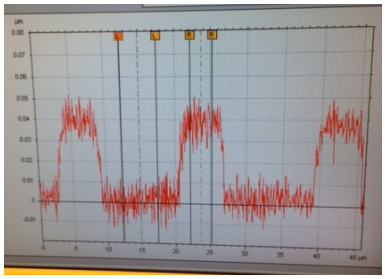

(a) 40nm HSQ.

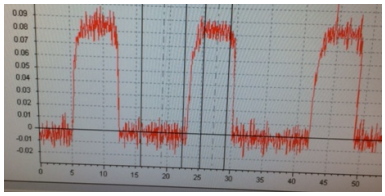

(b) 80nm total, (HSQ + Etch).

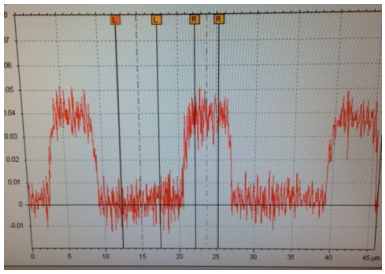

(c) HSQ Removed, 40nm Mesa Etch nanostructure

Figure 7.5: Profiling the Mesa etch on delta doped single crystal diamond. Unfortunately the profilometer used at Yale was very old and did not output data so only camera images of the screen are reproducible, hence the poor quality. It does however show a very high selectivity and ultimate etch dept of 40nm for the mesa. The labels at the right show the noted down profiles.

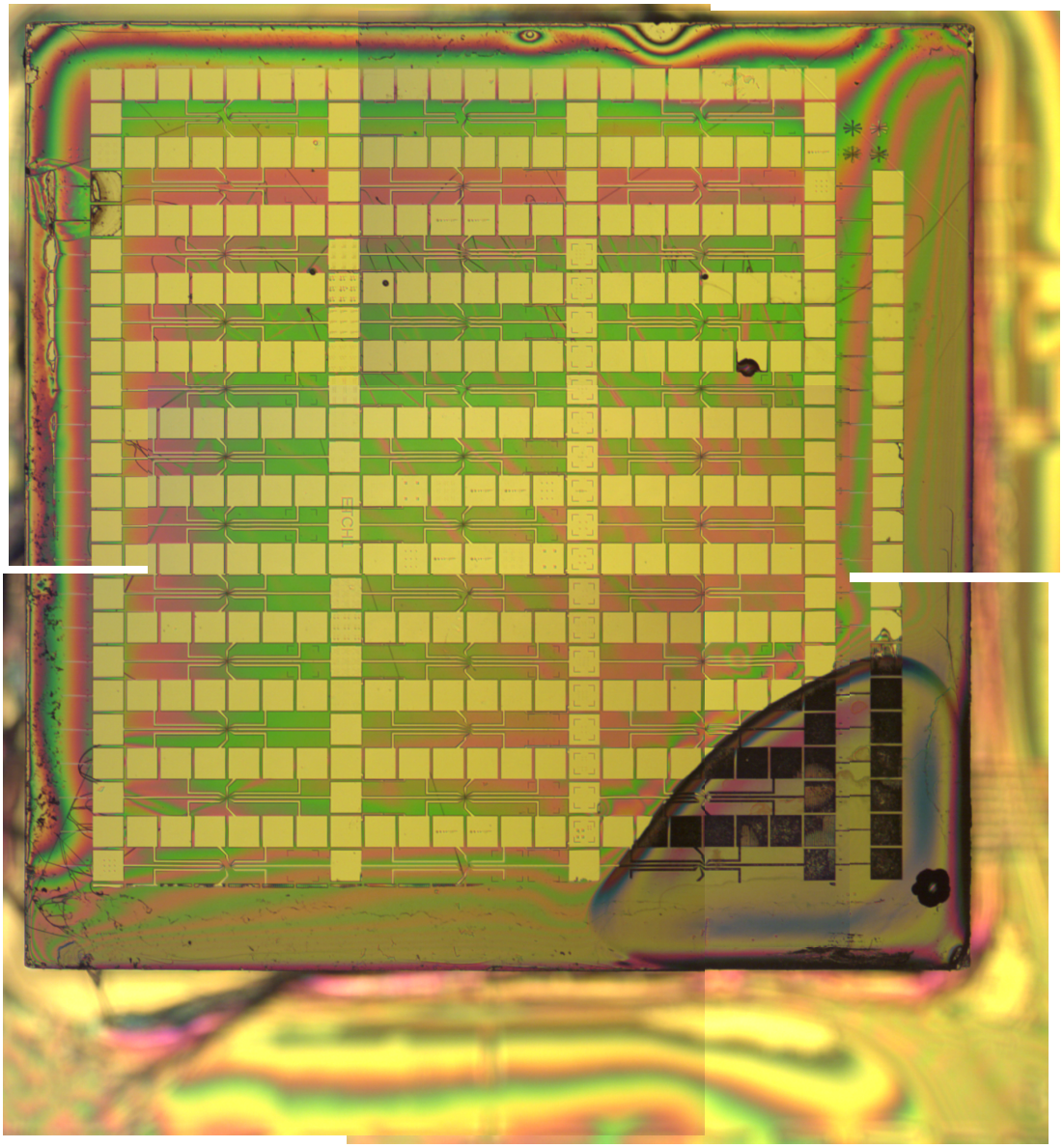

Figure 7.6: PMMA bilayer on $3.6mm^2$ diamond. Note the uniformity of the film and one concentrated edgebead caused by off axis spinning

A 10/20/100(nm) Ti/Pt/Au stack was evaporated by E-beam evaporation using standard recipes.

Fig.7.6 shows that lithography with a bilayer PMMA stack can be carried out across nearly all of the the 3.6mm square samples surface. Fig. 7.8 shows the lift off looking workable.

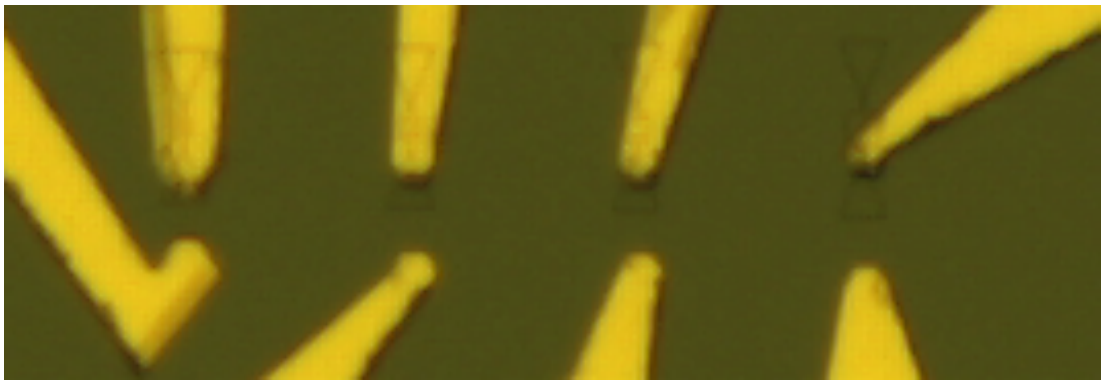

Figure 7.7: Metalisation after lift off mis-aligned. Time ran out at Yale and I had to start again, again at LCN on different machines

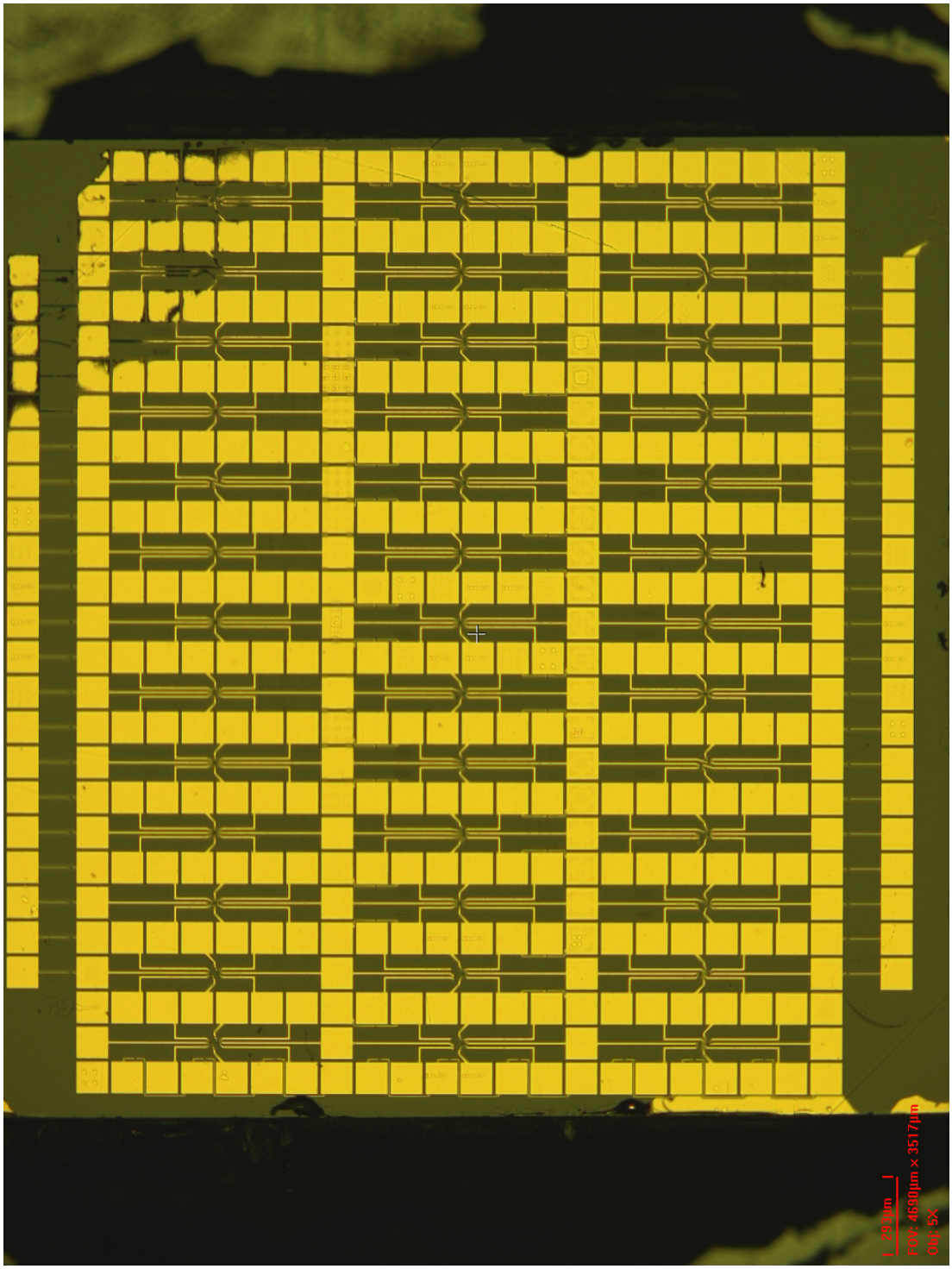

Figure 7.8: Close up of metalisation after lift off on $3.6mm^2$ diamond with etched features. Metal is Ti/Pt/Au stack. There are flags (folded edges on the metal), these are caused by evaporating too much metal relative to the bilayer stack height. More imporatntly the alignment is off, with the devices being covered by metal, the misalignment in this case was only in the y direction.

Sadly, I ran out of time at Yale and had to abandon this process as I no longer had access to the equipment and aligning the first layer to a second proved to be just not possible as seen in Fig.7.8

7.2.2 The UCL approach

The UCL clean room has a Raith 150-Two EBL system. This is a converted SEM which does have some drawbacks but also results in a very adaptable, versatile system. The drawbacks are that the writefield stitching is poor (compared to a purpose-designed EBL such as the EPBG system at Yale) and the possible beam accelerating voltages are relatively low, a maximum of 30keV. This results in lower beam currents and longer write times. The achievable spot size is also slightly larger as the inciendent electrons are absorbed closer to the surface producing more secondary electrons which can escape and create proximity exposed regions. Also, general stability issues caused by vibration and stray fields broaden the spot size. The positives are that the gun is capable of producing electrons across a range of energies and the sample holder is easily adapted to accommodate a range of sample shapes and sizes.

7.2.3 Electrically Addressable Diamond Lateral NanoWires and devices

The first step in fabrication is as always to thoroughly clean the substrate using a standard RCA clean. Next a bilayer of PMMA is span onto the chip and global and local alignment marks are patterned. The global marks are placed towards the edge of the chip and the local ones placed near features that will require a high degree of alignment on subsequent layers. The chip is then placed in a thermal evaporator and 50nm of Au is carefully evaporated. The chip is then put in 1165 (a strong solvent) for lift off. HSQ is then spun onto the chip and the second layer is exposed on the EBL. This layer aligns to the first layer minimising stitching errors and ensuring the pattern is as well positioned as possible. The sample is then developed in MF319, which, due to the surfactant minimises surface tension. The sample is then exposed to an oxygen plasma as descried in section 7.2.1 and then placed in hydrofluoric acid for 1 min to remove the HSQ. Bi-layer PMMA is then spun onto the chip, which is subsequently coated with a 5nm Au charge dissipation layer. This layer works as a little Faraday cage, stopping charging from effecting the incoming electrons from the EBL. This is

essential as most of the sample is now not doped and highly insulating. The sample is now patterned to fabricate the contact metal. This layer is designed to be tolerant to misalignment. The metal is then evaporated and lifted off.

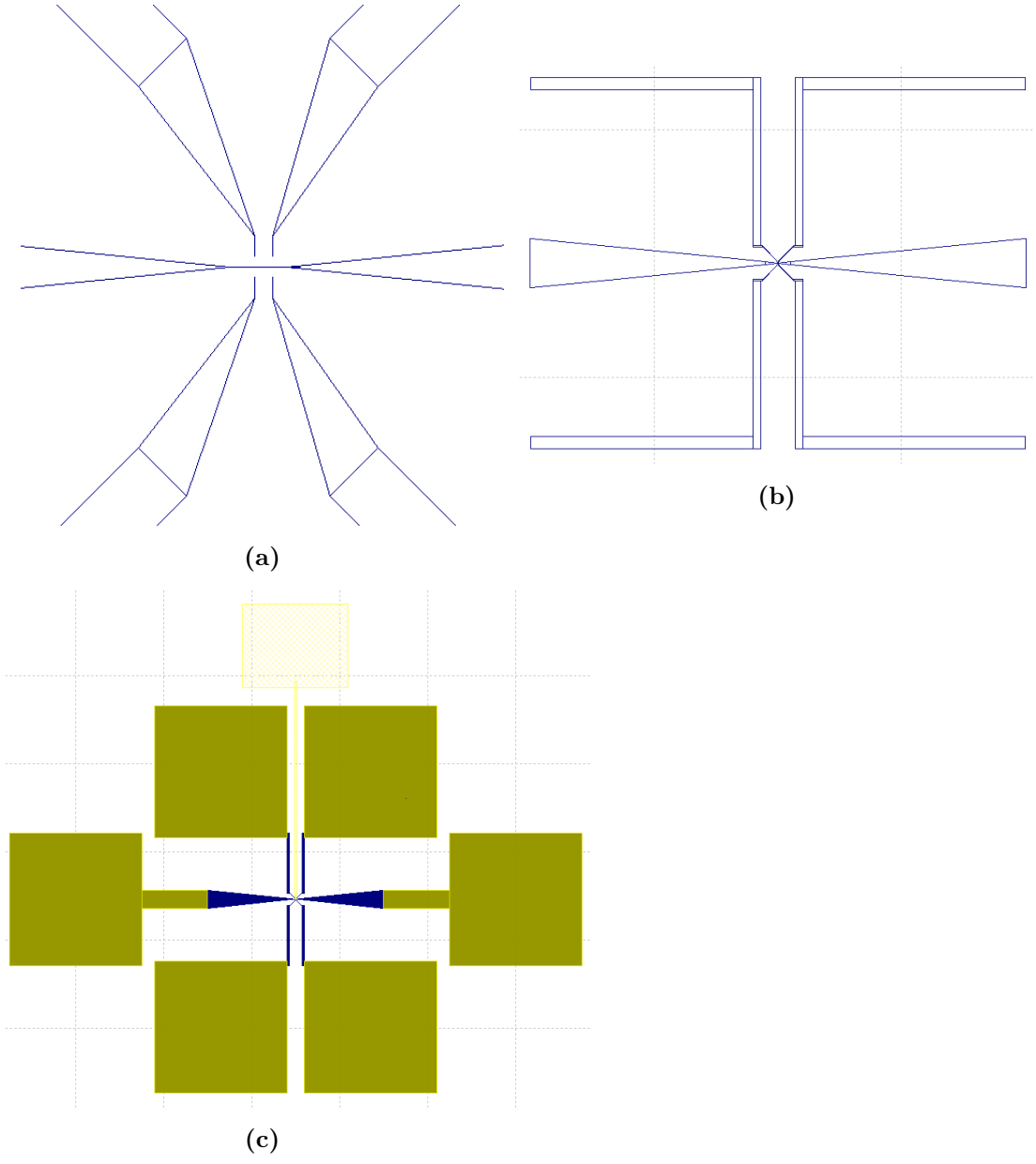

Figure 7.9: (a)Design showing NanoWire Single electron Transistor, single pixel lines are used to define the nanowires and the in plane gates. (b) Design showing Mesa design, large fan outs enable more tolerance for misalignment and larger surface are for metallisation, charge is injected into the doped layer from an edge 1 μm across. (c) Design showing whole SET; Mesa etch, Contact metallisation was realised the next steps would be a growing a dielectric via atomic layer deposition (not shown for clarity)and depositing a Top Gate

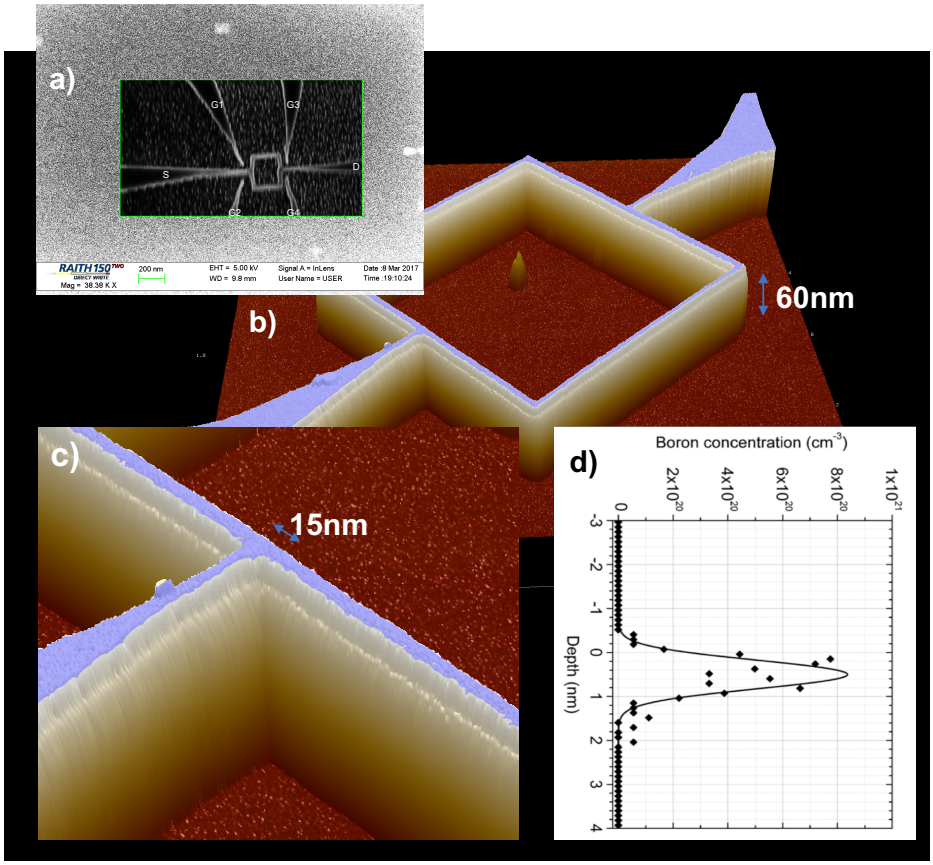

Figure 7.10: The first non-alignment layer of the sample is the HSQ after etching a lateral structure will look like this. a) SEM of ring showing top down view of a ring with side gates. b)AFM scan of Mesa etched ring. Blue colour is artificial to illustrate the surface doped layer etch is approx 60nm deep. c) Close up showing wire thickness to be less then 15nm. d) SIMS profile showing dopant profile in z.

7.2.4 Fabrication

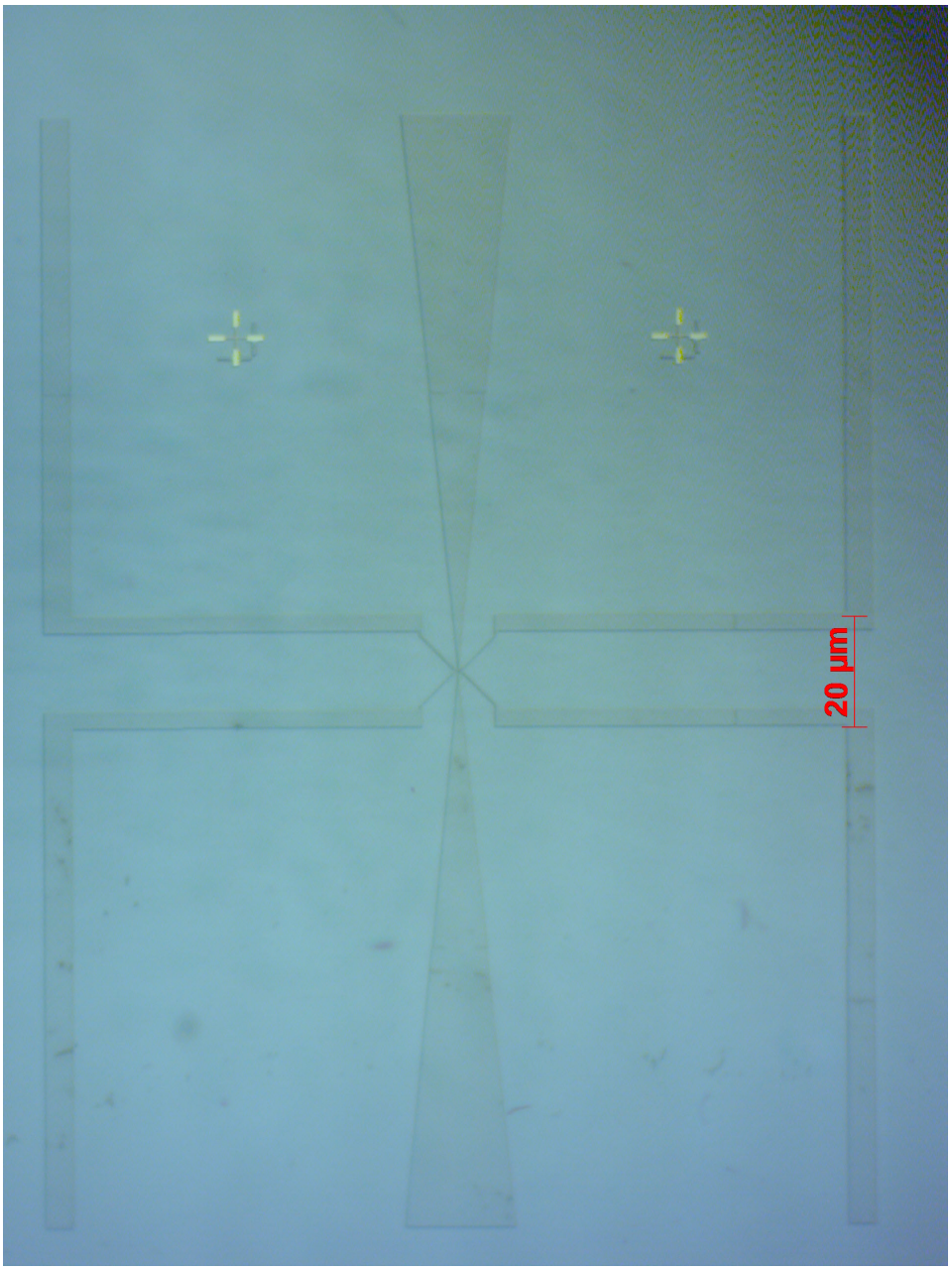

Figure 7.11: Optical microscope image of mesa etched delta layer after HSQ has been removed. Etch deth is 60nm. Au Alignment marks are used for aligning all layers, these are the Au crosses. The automatic scan lines leave from the alignment procedure can be seen as dark rectangles across the arms of the crosses.

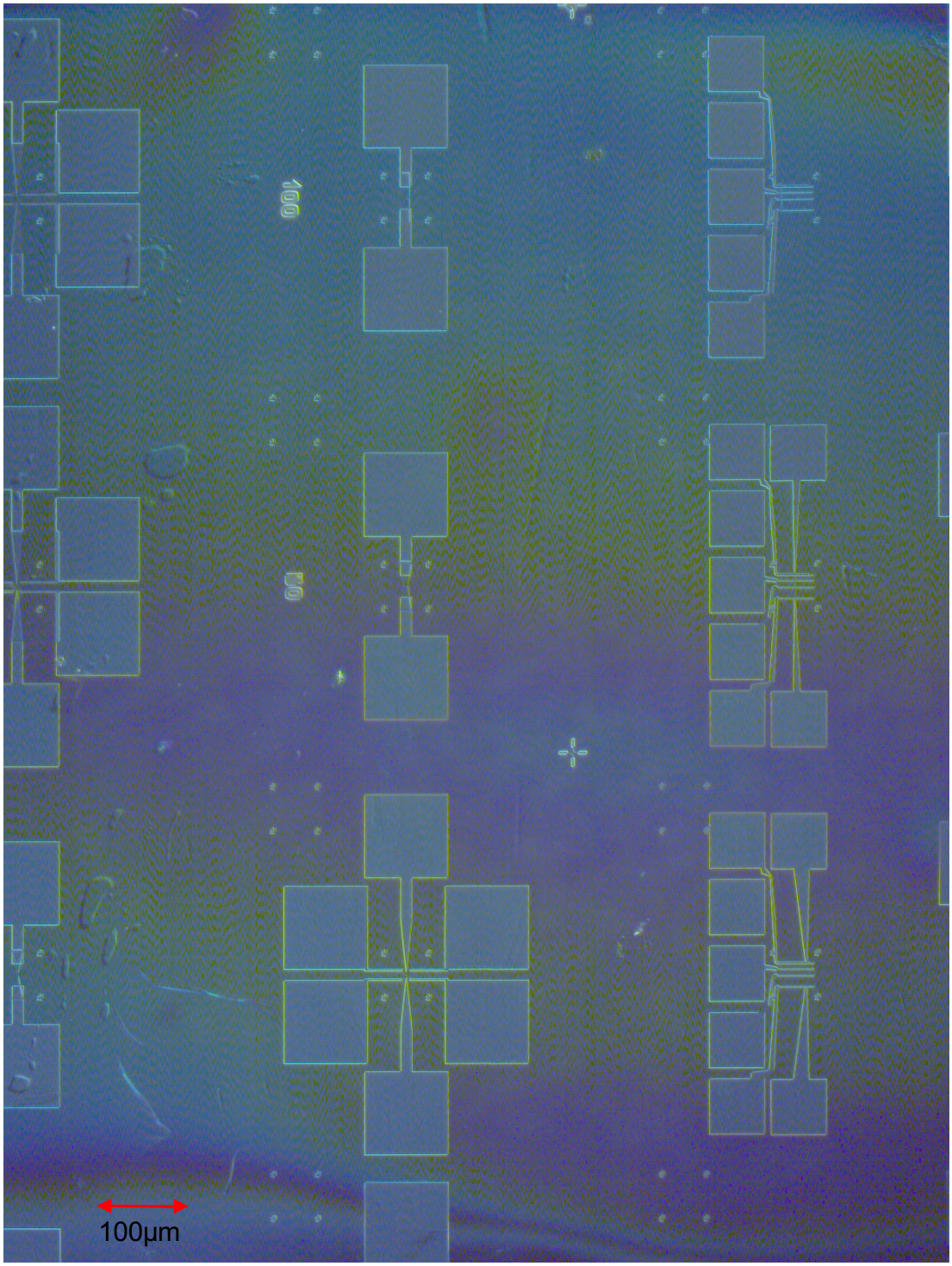

Figure 7.12: Bi-layer PMMA showing excellent alignment and visible undercut to help with lift off. The undercut is visible in the contrast at the edges between the continous film and the features

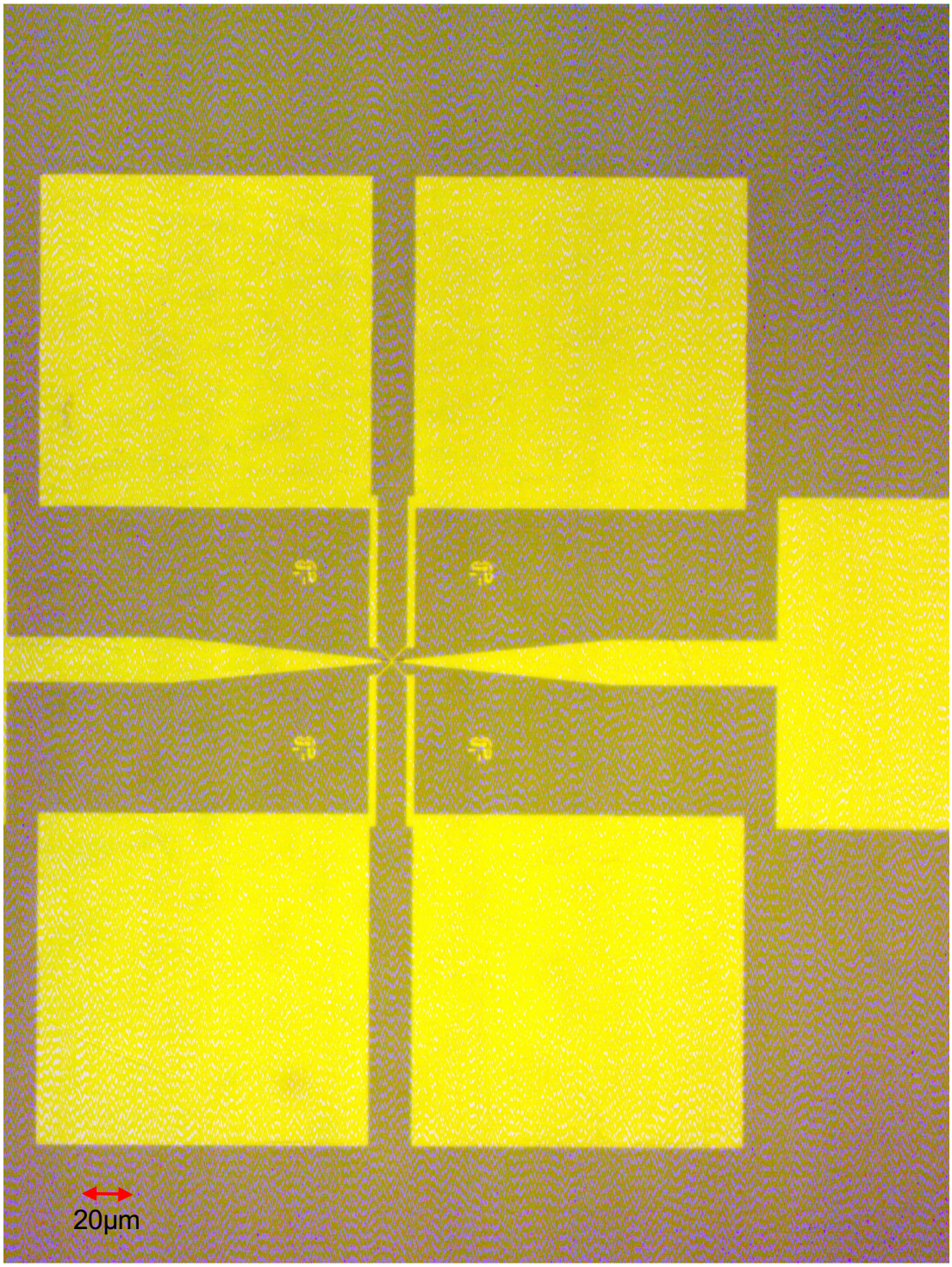

Figure 7.13: Good clean lift off of Ti/Pt/Au contact no flags or other artifacts.

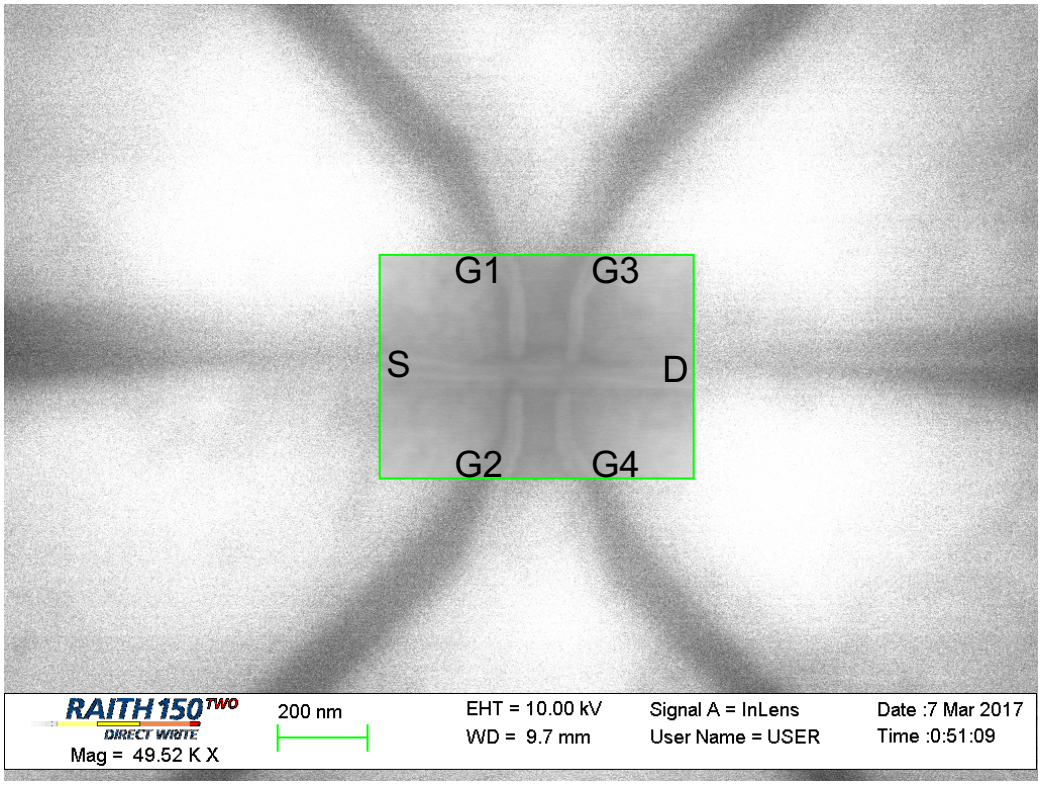

Figure 7.14: Mesa etched delta layer after HSQ has been removed, patterned to a multiple in-plane side gated nanowire FET structure. Imaging is challenging as the majority of the substrate is not conductive and the wires are electrically floating. S is a source, D is a drain, G1,2,3,4 are potential gates or physical tunnel juntions

7.2.5 Electrical Characterisation of NanoWire and NanoWire Devices

7.2.5.1 Contact Resistance

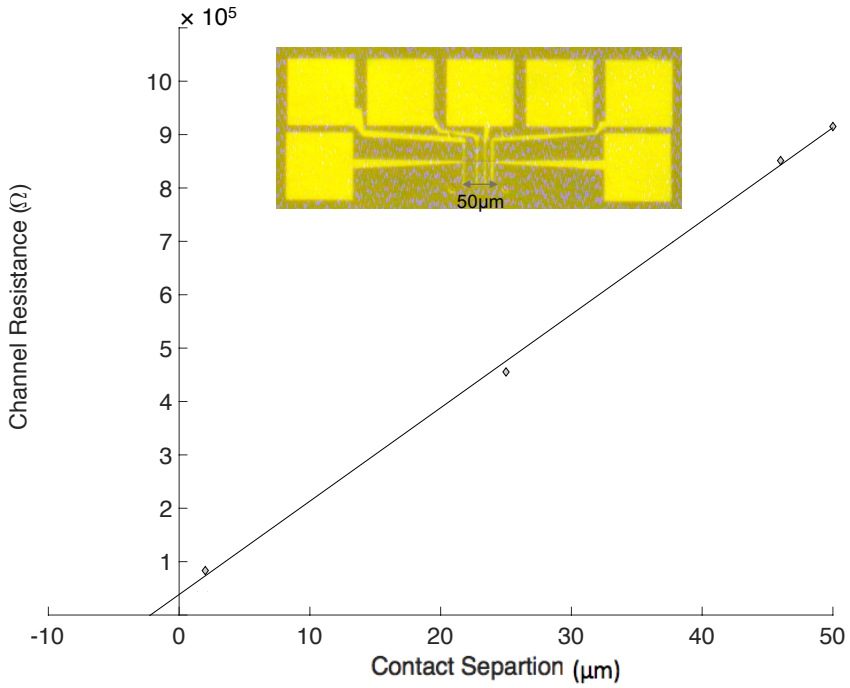

Figure 7.15: By varying the legnth of a 1 μm wide mesa etched channel and measuring the resistance for each chanel length we are able to work out the contact resisance. This is the transmission line model.

Electrical characterisation was performed on an Everbeing EB-6 high precision probe station using a Keithley 4200 semiconductor analysis system, connected by triax cabling. From the transmission line the sheet resistance eq. 7.2 can be calculated to be of the order of 20 kΩ. This is of the same order that measured on a wafer-scale two probe measurement. So, with a device 1μm wide transport is not yet dominated by edge effects.

From Fig.7.15 we find the gradient $= 1.7492E^{10}$ $\Omega/\mu m$ and at x = 0, y = 38400Ω;

$$\begin{aligned} R_C &= 38400/2 \\ &= 19200\Omega \end{aligned} \tag{7.1}$$

$$
\begin{aligned}
R_s &= slope \times width\Omega/\square \\
R_s &= 1.7492^{10} \times 1 \times 10^{-6}\Omega/\square \\
&= 17492\Omega/\square
\end{aligned}
\tag{7.2}
$$

$$
\begin{aligned}
when R_T &= 0 \\
L_T &= 38400/2 \times 1.7492^{10} \\
&= 1.0976\mu m
\end{aligned}
\tag{7.3}
$$

$$
\begin{aligned}
\rho_C &= R_C.L_T.W \\
&= 19200 \times 1.0976 \times 10^{-6} \times 1 \times 10^{-6} \\
&= 2.1075 \times 10^{-8}\Omega m^2 \\
&= 2.1075 \times 10^{-4}\Omega cm^2
\end{aligned}
\tag{7.4}
$$

7.2.5.2 Results from a Single NanoWire

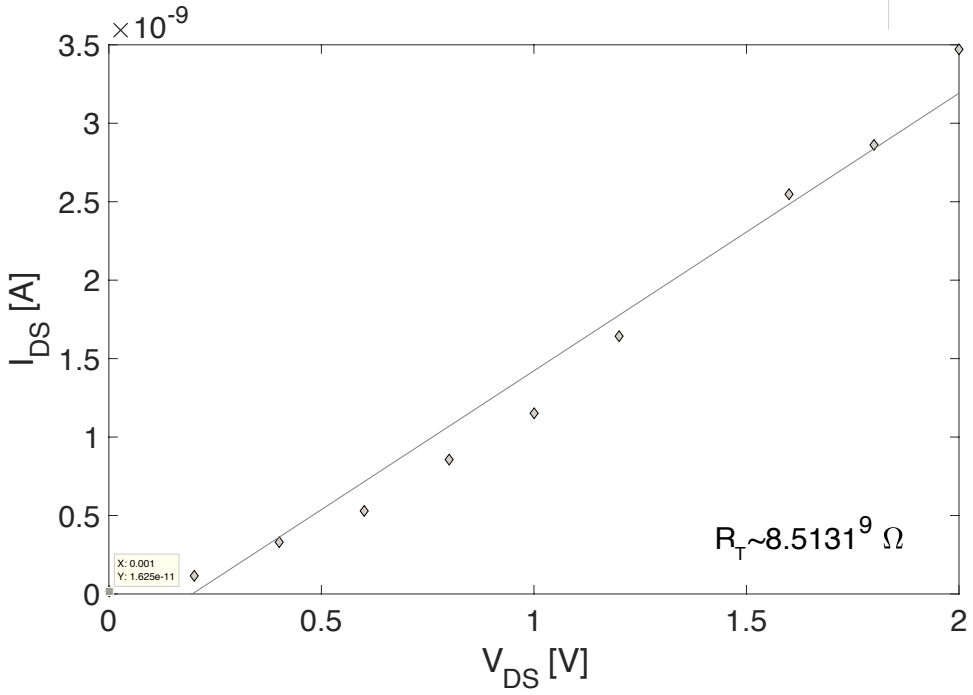

Using Equation 3.5 the sheet resistance for the nanowire is calculated to be $R_S = 4.6962E^6\Omega/\square$ This is an order of magnitude higher then the sheet resistance measured

for a 1μ wide channel. This suggests the carrier mean free path is somewhere above 20nm and below 1μm.

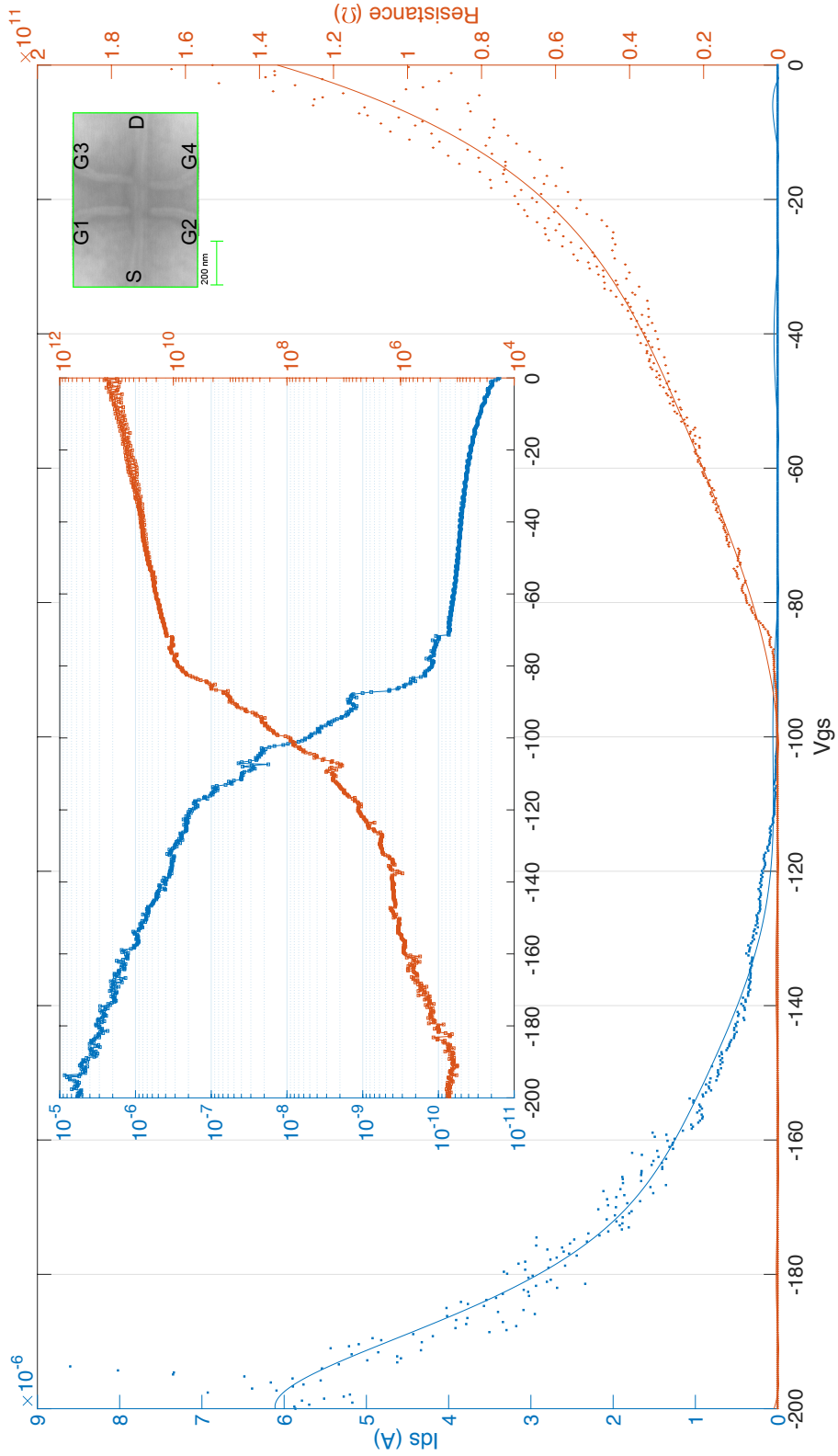

Figure 7.16: Modulation of nanowire resistance by application of gate voltage to V to $G_1, d\&G_2, d$. Inset; SEM of device and semi-log plots showing order of magnitude of transresistance effect $V_{ds} = 3.25$.

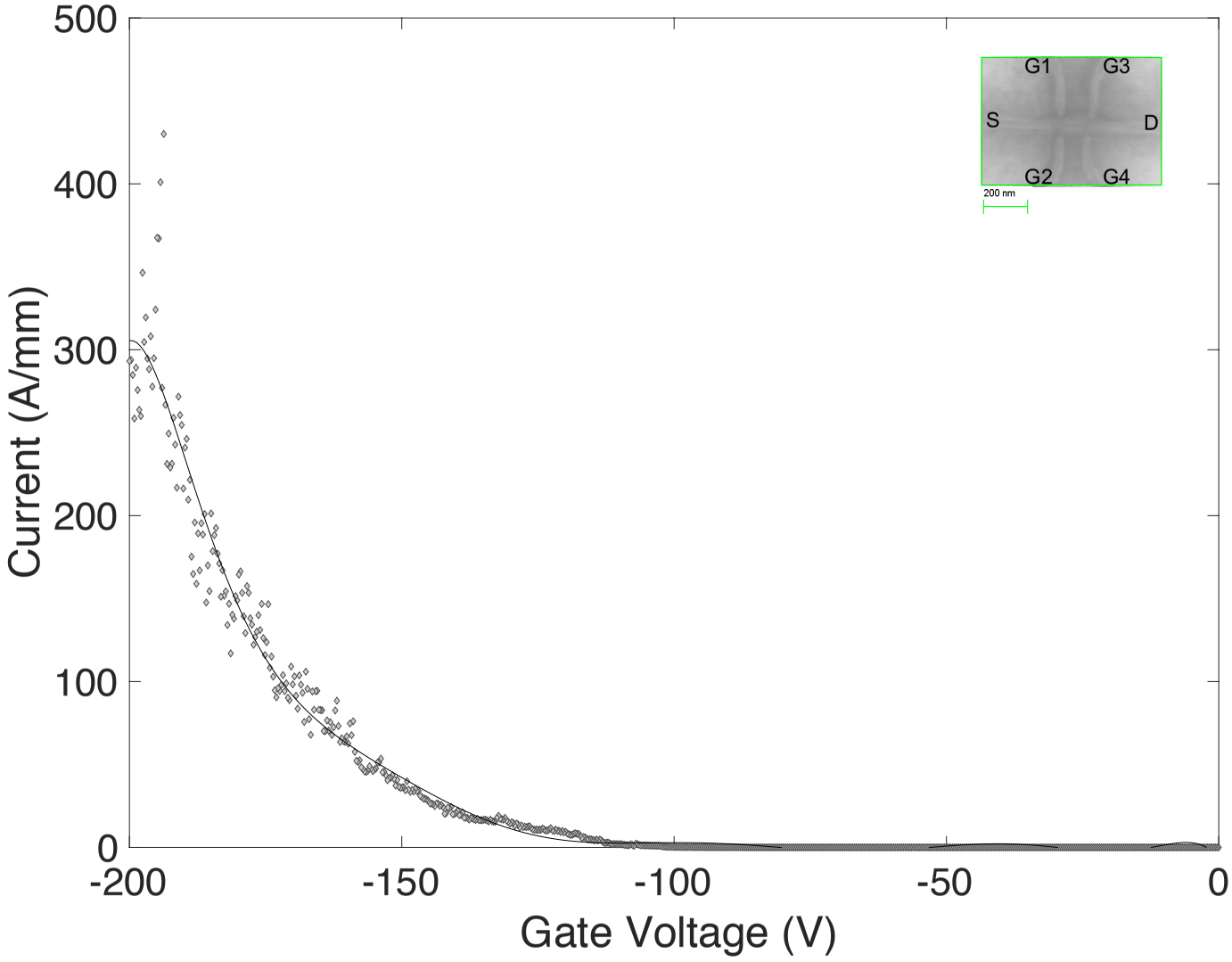

Figure 7.17: $3.25V_{ds}$, Modulation of nanowire resistance by application of gate voltage to $V$to $G_1, \& G_2$ allows a large current density in the nano wire. Inset. The line is polynomial fit.

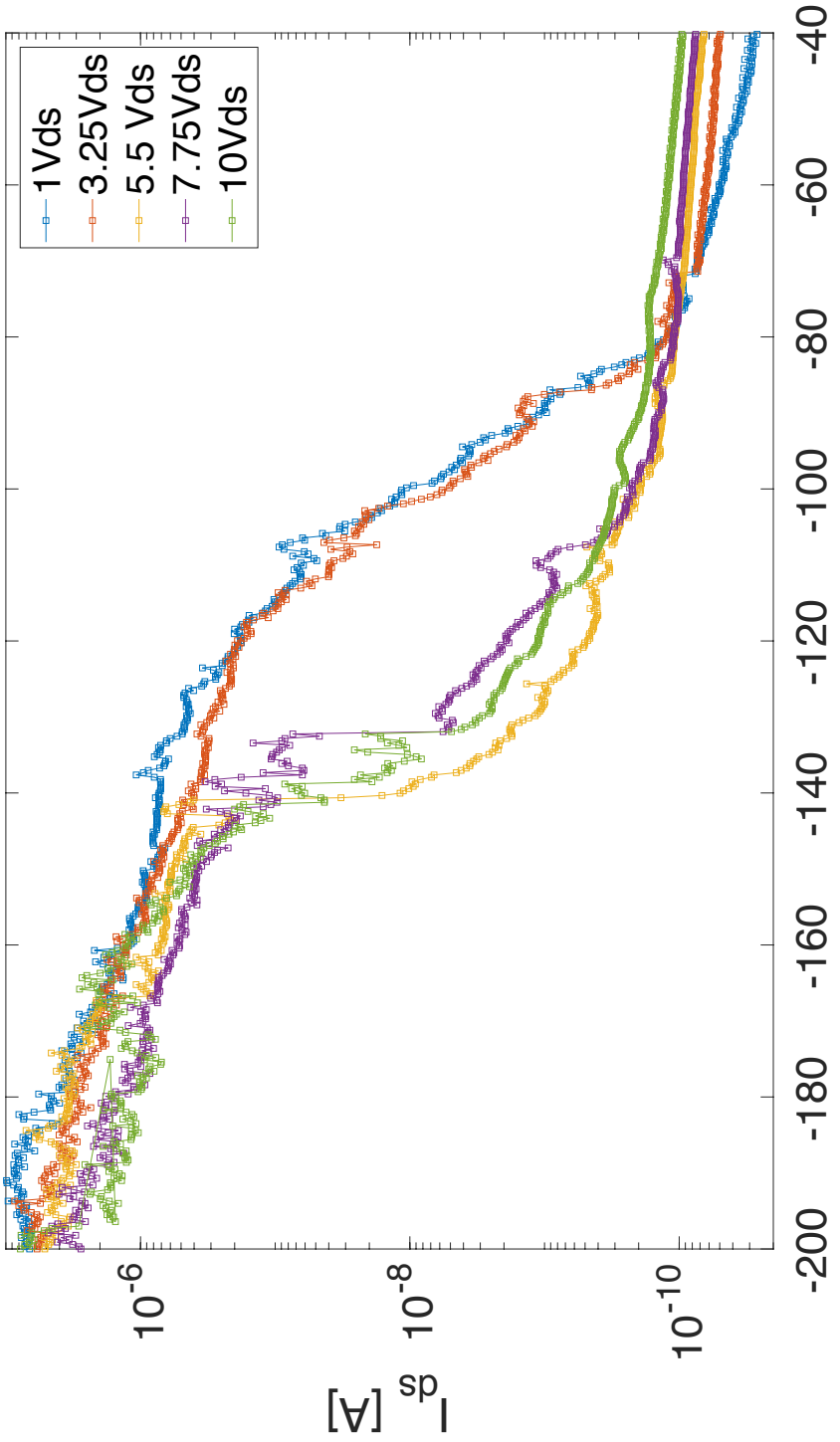

Figure 7.18: Range of V_{ds}, applied to l-dNwFET

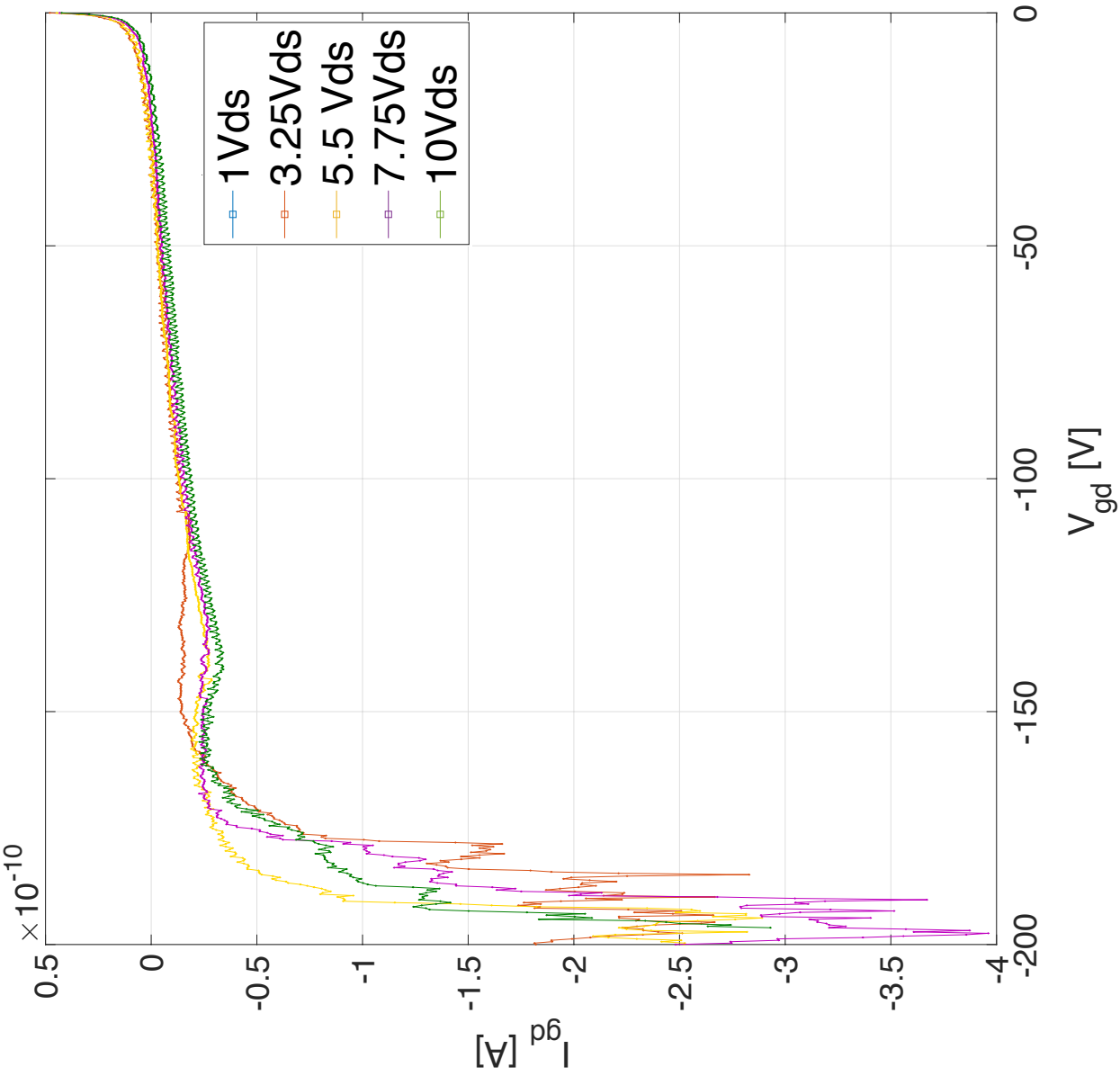

Figure 7.19: Gate to drain leakage current I_{gd} for range of V_{gd} applied to l-dNwFET

By careful process engineering, alingment of multiple layers with tolerences of a few nanometers is shown to be possible (Fig.7.11, 7.12, 7.13). This enables us to build wires and devices and electrically probe/manipulate them. Ohmic contacts are made to the wires with contact resistacnces comparable to the literature for carbide-forming metals [47]. These nanometrically small wires are shown to have Ohmic properties although conduction is dominated by width of the channel, resulting in a large sheet resistance. (Fig.7.16) shows clear modulation of the channel resistance and Fig.7.19 shows that there is very little current leaking from the gates. The large voltages for switching are, however, suspicious and no similar devices can be found by the author in the literature. What can be said for sure is that these nanowires are capable of handling incredibly high current density Fig. 7.17. Short channel effects (visible in Fig. 7.18) due to the channel length being possibly similar in size to the depletion layer width of the source and drain could be responsible for limiting the current handling. The current density is at least of the order of $300A/mm^2$. This amount of current can be handled by the nanowire with no noticeable damage (repeatable measurements over time suggest no degradation) and is comparable to the breakdown currents reported for graphene nanoribbons and silicon nanowires [117], as well as being of the same order of magnitude as reported current handling capabilities for carbon nanowires ($10^6 - 10^8 A/cm^2$).

7.3 Conclusions

Here it has been shown that highly doped nanowires still behave in an Ohmic way and that some sort of field effect trans-resistance is possible. Also, these nanowires show a very high current density handling capability, an important feature, as most nanowires suffer from the effects of electromigration at significantly lower current values. Moving the source and drain further apart may allow significantly more current to be carried down such a wire without significantly affecting the resistance, which is probably dominated by edge effects rather then by channel length. Having multiple wires may also stop current crowding. Some progress has been made towards this but further optimisation is required. This has proved difficult as each substrate currently requires dose optimisation as each suffers from charging effects in a different way depending on the doping level and quality of growth. By adding a charge dissipation layer above the HSQ (not easy, as metal tends to react in direct contact to HSQ, so a soluble bi-layer

will be required) doses should be normalised across all substrates.

Aligning to a carrier wafer would have allowed a process flow that could easily be ported to an industrial fab. Redesigning the devices to allow more tolerance for misalignment would make this approach feasible on a similar EBL system. It would not, however, work on the Raith 150-two, as the drift and stitching errors would be too large. It is demonstrated that very small features and devices can be fabricated in diamond using a variety of electron beam lithography systems. Although there are many challenges, proving this concept opens up a wide range of future projects and prospects both on highly doped single crystal diamond and other similar material systems. Fully understanding the results presented will require the fabrication of more devices.

8

Summary The Future and Other Work

The work contained herein, like most interesting science leads to more questions then it provides answers. Following on from the novel processing and experimental techniques developed I, colleagues and the diamond community will do a series of experiments to further understand both the boron doped diamond system as a whole and the new lateral nanowires specifically.

8.1 ARPES

Extending the range of incident photon energies will make it clearer if the non-dispersive '2D' features are real or just very flat bands. This data will be taken at an up coming beam time all ready allocated at the Swiss light source. More careful analysis and more data around the bulk gamma point will also be interesting as it is expected that this is where any delta state should be.

8.2 Lateral NanoWires and Nano-Structures

More repeatable measurements in more varied experimental conditions should be carried out to understand the physics of this system. Once we understand the nanowire itself, it will be possible to move on to that sort of experiment on the nano-Hall bar, followed by the other devices described. In particular looking at the affects of magnetic

fields and low temperatures could be interesting. It should also be possible to reduce NW width perhaps all the way down to single atom chains using STM lithography.

8.2.1 MultiGate and FinFet Structures

One interesting direction to take this type of nanowire for future work will be to make the first FinFet type transistors in diamond. Some work was done to test the principle and patterning procedures as shown in Fig. 8.1 and Fig.8.2.

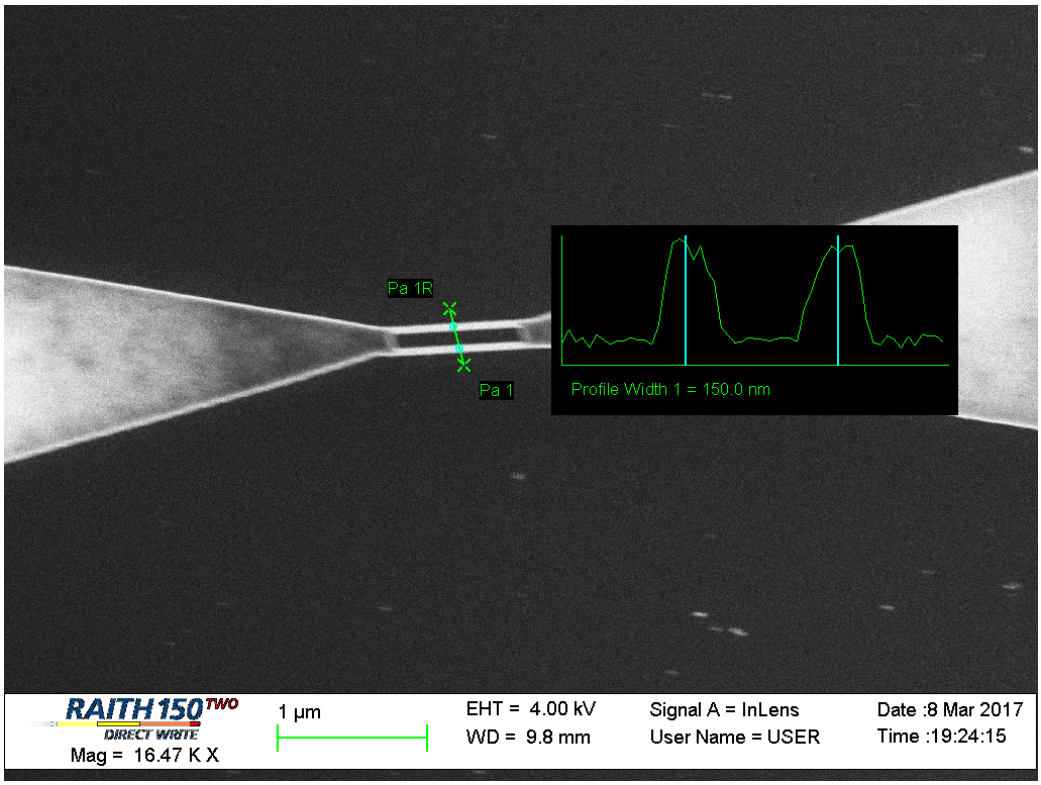

Figure 8.1: Mesa Etched Delta Layer after HSQ has been removed, patterned to a double nanowire for a mutiple FinFET structure, wide pitch would allow gate dielectric to be conformall grown and result in lower leakage currents

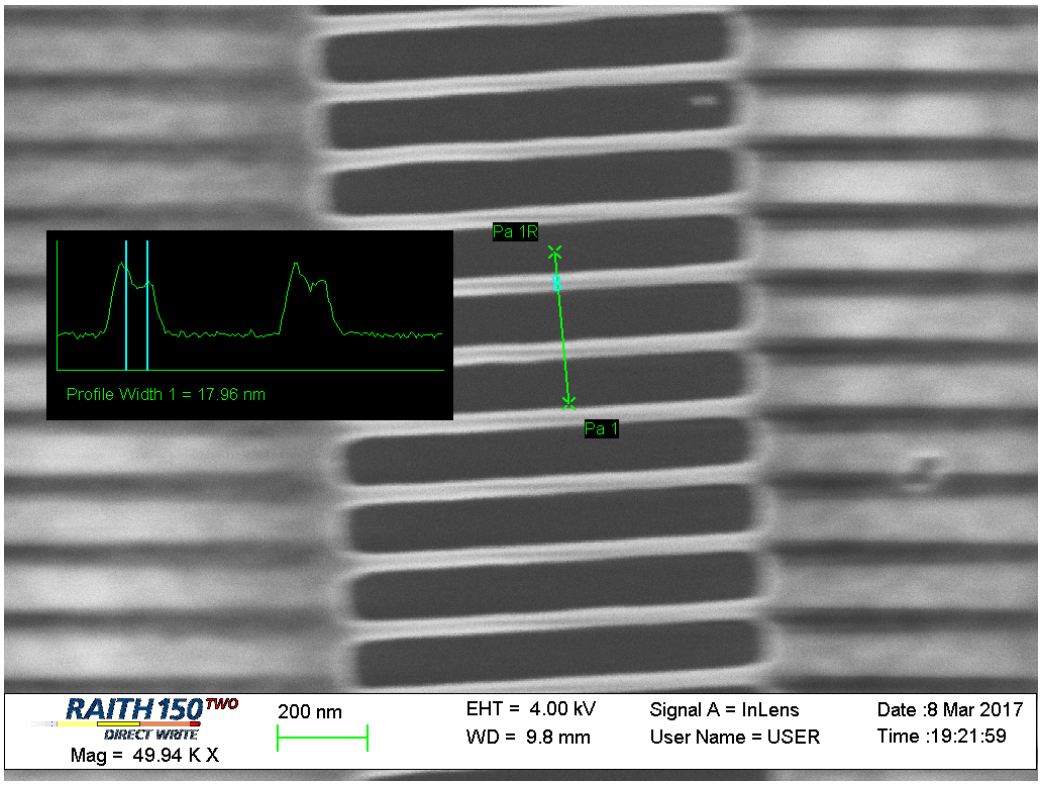

Figure 8.2: Mesa Etched Delta Layer after HSQ has been removed, wires between 15-20nm wide at top of mesa.

As can be seen in Fig. 8.2 more care is required in assigning doses to arrays of lines. However due to time constraints this set of devices was metallised with the intent of proving the concept. As not all the devices came out on this chip a cost saving choice was made and chrome/gold was thermally evaporated rather then using e-beam evaporated Ti/Pt/Au which is a significantly more expensive process. This still made for Ohmic contacts Fig. 7.2.5.2, however it is probable that the series resistance is significantly higher then if Ti/Pt/Au had been used.

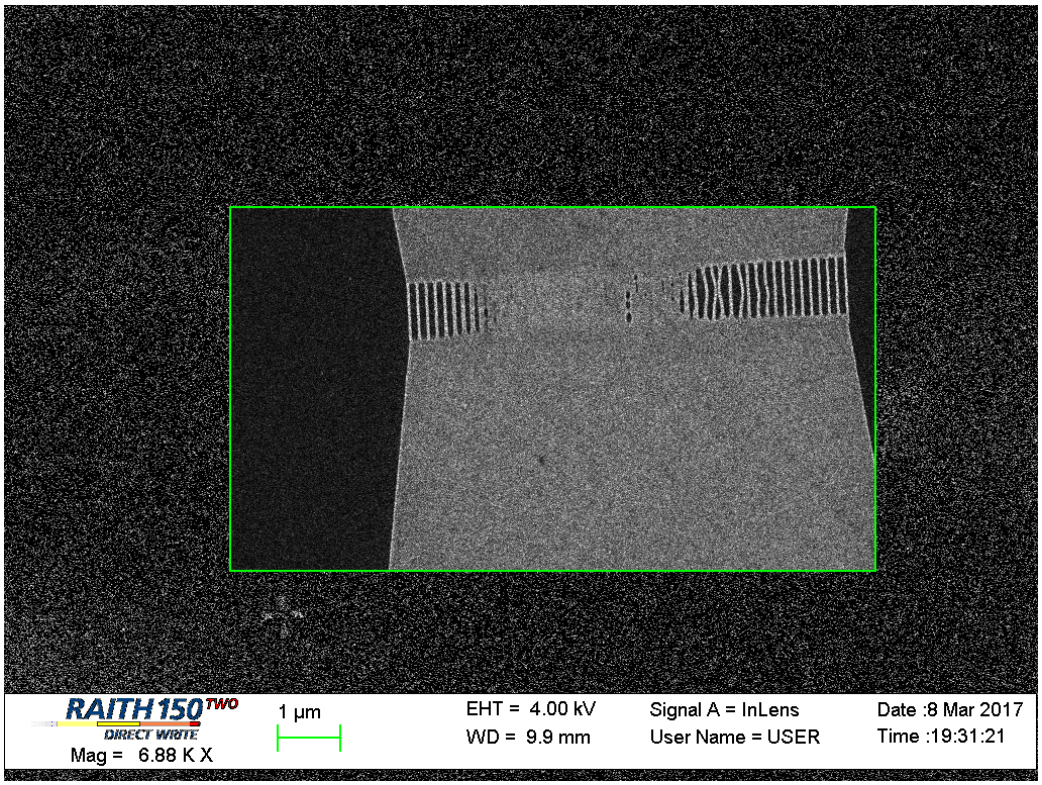

Figure 8.3: Mesa Etched Delta Layer after HSQ has been removed, small amounts of HSQ must have been over exposed. This results in significant masking in areas where the proximity effect is largest

8.2.2 Aharonov Bohm Ring or Sqiuds

The high Debeye temperature of diamond also mean it is possible that quantum effects may be visible at high temperatures. Signs of these are visible but not quite so visible in the transport measurements but not so clear as to be reported here. Further mea-

surements and fabrication is required to characterise the multi-nanoWire devices Figs. 8.1 8.2 as well as the Aharonov−Bohm ring Fig. 8.4.

Another interesting structure that I can pattern is an Aharonov Bohm Ring (see Fig.8.4), this experiment will look for interference phenomena that may be emergent in this material on these length scales.

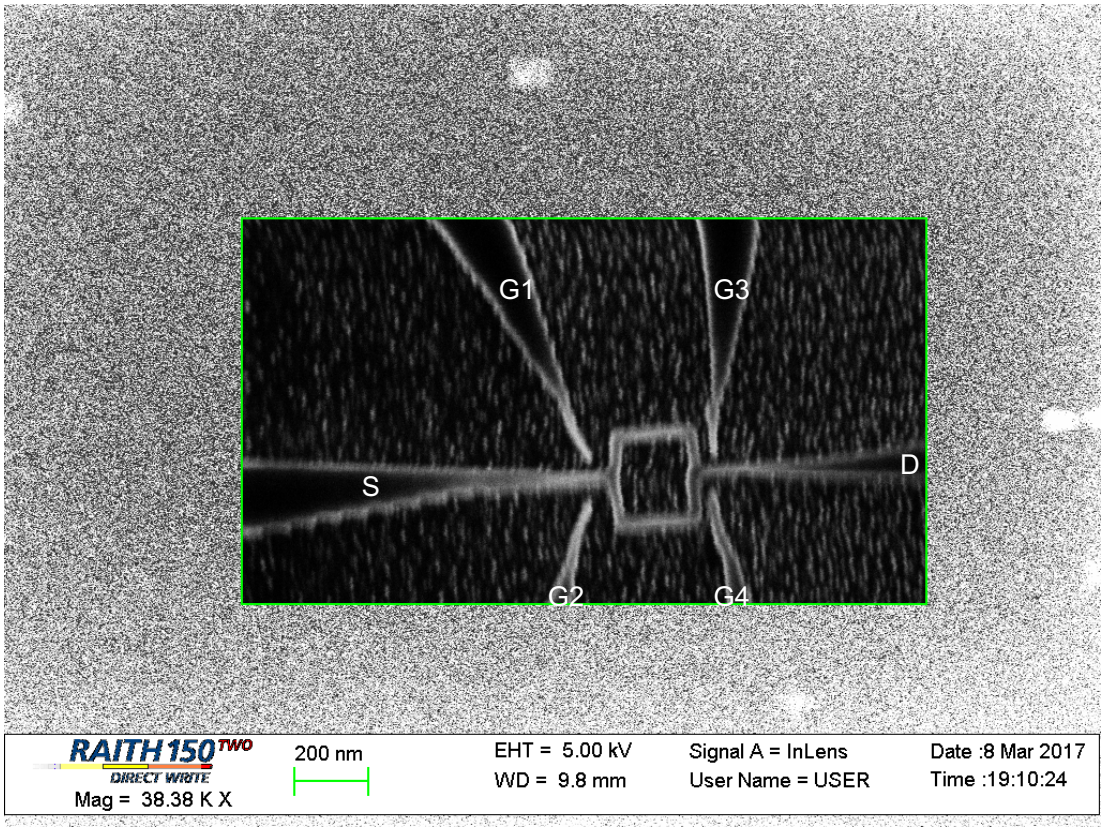

Figure 8.4: Mesa Etched Delta Layer after HSQ has been removed, patterned to a mutltiple in-plane side gated nanowire AB ring/FET structure. nano-grass is clear, this is probably from metal sputtered from the metal alignment marks.

The Aharonov Bohm Ring is also similar to the superconducting quantum interference device (SQUID), by slight changes to the design SQUIDS could be made using the processes developed herein. With smaller weak links then previously reported.

8.3 Diamond on Silicon Nano-Wires

A four inch SOI wafer was fabricated by me at Yale university under the supervision of Mary Mu a PhD student in the Reed group (I didn't have full unsupervised access to their clean room at the beginning of my time there) following processes developed by the Reed lab. I did however alter their masks in a subtle but important way after deciding the real unique selling point of diamond was that we could use it as a passivation layer. In the normal Si-NW (Silicon Nanowire) process only a small amount of the chip would be left heavily boron doped. Metal contact pads and leads would break out and onto these regions which would in turn contact to the active region of the device. My adaptation was to run the boron doped channels all the way out to the contact pads. The whole chip could then be covered in diamond. The diamond over the contact pads could then be selectively etched away. These contact pads would be far away from the device, far enough away that they would not need to be electrically isolated by a passivation material which can cause problems for the stability and reproducibility of a device.

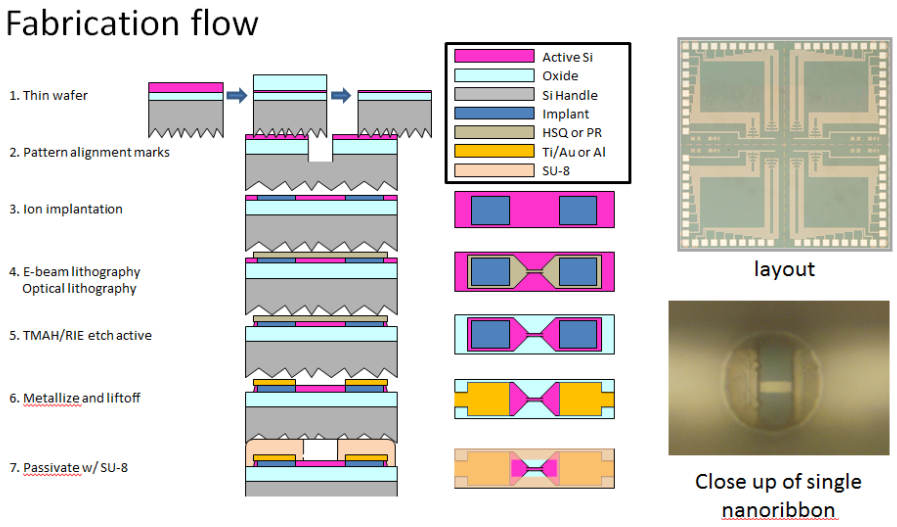

Figure 8.5: Previous Process flow developed by the Reed lab at Yale to produce Si nanoribon ISFETS. Note the use of SU8 Pasivation. Repropuced with permision

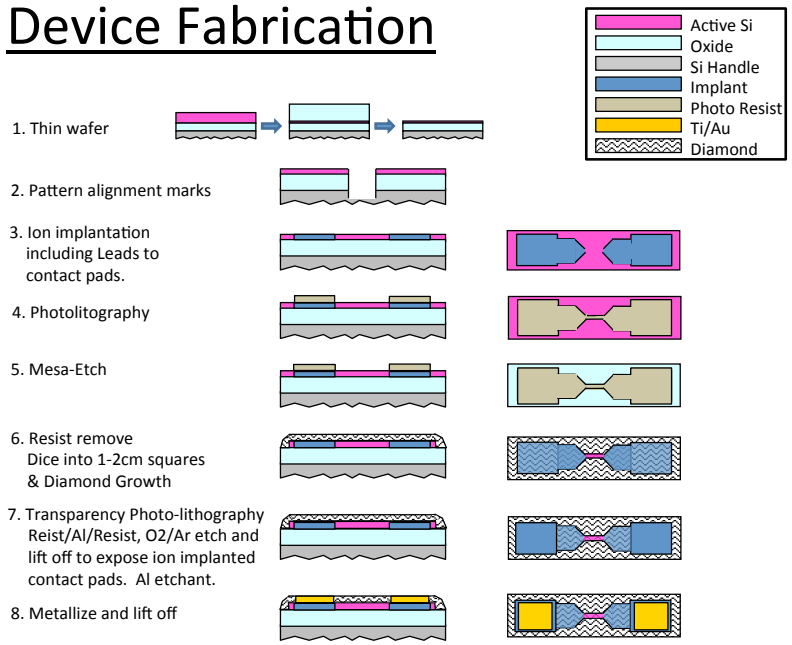

Figure 8.6: Modified Process flow developed by me in collaboration with the Reed lab at Yale to produce diamond dielectric/passivated Si nanoribon ISFETS

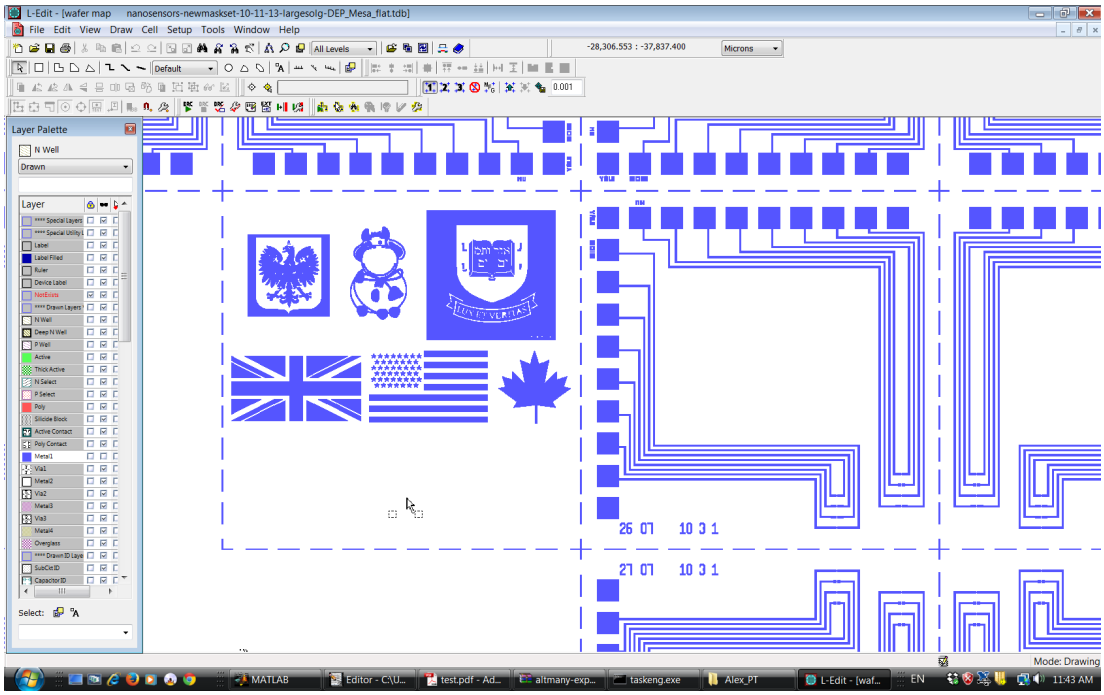

Figure 8.7: Modified mask for Boron Ion implatation, showing the countries of people who have over the years contributed as well as a chip with multiple devices

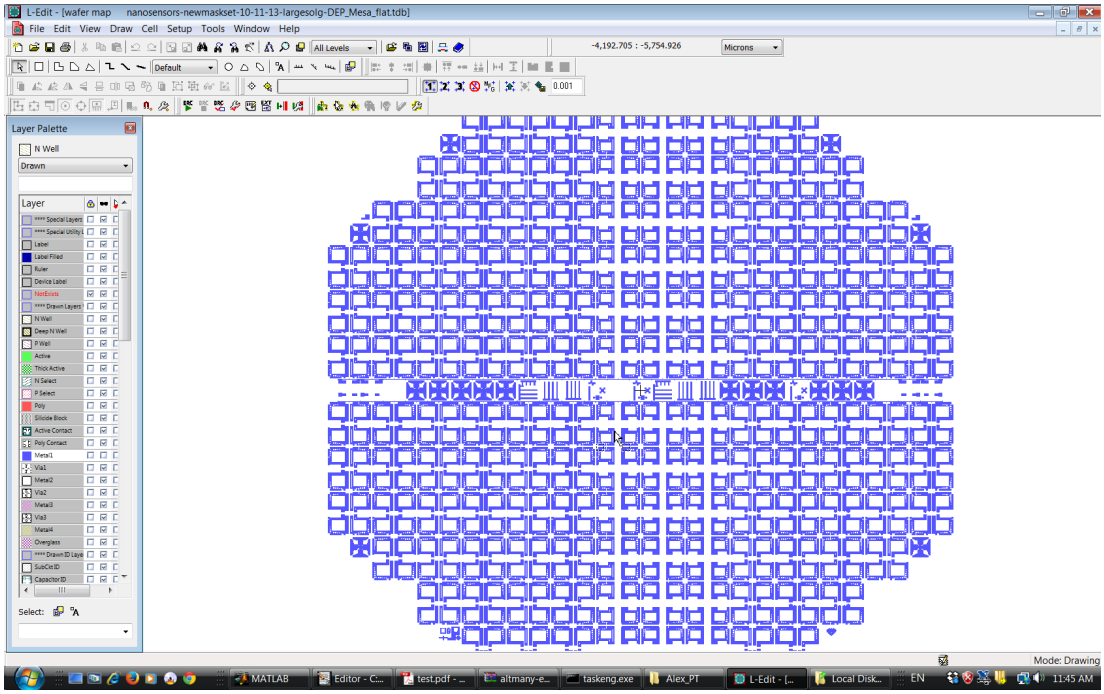

Figure 8.8: Modified mask for Boron Ion implatation, showing complete 4" wafer

8.4 Other on going or related Work

GreenDiamond- Power eletronics Resonant Inelastic Scattering X-ray Spectroscopy on Diamond and Graphite, looking for Multi phonon scattering. Solvothermal production of Nitrogen Doped Graphene from diamandoid precursors. ARPES on Phosorus Doped Si. Hard X-ray ARPES on Capped Delta Layers. Cryogenic Temperature ARPES on Delta Layers. ARPES on new single and multi-layer delta doped samples. UPS investigation into co-doping of diamond with MgO and N. Grazing Incidence X-ray spectroscopy in the search for a process to optimise substrate preparation prior to growth.

References

[1] User:Itub, "Diamond and graphite.jpg," *Wikimedia, Creative Commons Attribution-Share Alike 3.0 Unported*, 2009. viii, 3

[2] F. P. Bundy, "The p, t phase and reaction diagram for elemental carbon, 1979," *Journal of Geophysical Research: Solid Earth*, vol. 85, no. B12, pp. 6930–6936, 1980. [Online]. Available: http://dx.doi.org/10.1029/JB085iB12p06930 viii, 4

[3] J. E. Butler, R. L. Woodin, L. M. Brown, and P. Fallon, "Thin film diamond growth mechanisms [and comment]," *Philosophical Transactions of the Royal Society of London A: Mathematical, Physical and Engineering Sciences*, vol. 342, no. 1664, pp. 209–224, 1993. [Online]. Available: http://rsta.royalsocietypublishing.org/content/342/1664/209 viii, 6

[4] Z. Zhang and J. T. Yates Jr., "Band Bending in Semiconductors: Chemical and Physical Consequences at Surfaces and Interfaces," *Chemical Reviews*, vol. 112, no. 10, pp. 5520–5551, Oct. 2012. [Online]. Available: http://pubs.acs.org/doi/abs/10.1021/cr3000626 viii, 8, 9, 10, 11

[5] J. Bardeen, "Research leading to point-contact transistor," *Nobel Lecture*, 1956. [Online]. Available: http://www.nobelprize.org/nobel_prizes/physics/laureates/1956/bardeen-lecture.html viii, 10

[6] W. A. Smith, I. D. Sharp, N. C. Strandwitz, and J. Bisquert, "Interfacial band-edge energetics for solar fuels production," *Energy Environ. Sci.*, vol. 8, pp. 2851–2862, 2015. [Online]. Available: http://dx.doi.org/10.1039/C5EE01822F ix, 12

[7] R. S. Balmer, I. Friel, S. Hepplestone, J. Isberg, M. J. Uren, M. L. Markham, N. L. Palmer, J. Pilkington, P. Huggett, S. Majdi, and R. Lang, "Transport behavior of holes in boron delta-doped diamond structures," *Journal of Applied Physics*, vol. 113, no. 3, 2013. [Online]. Available: http://scitation.aip.org/content/aip/journal/jap/113/3/10.1063/1.4775814 ix, xiii, 14, 15, 53, 55, 63, 67, 71, 81, 94

[8] A. C. P.-T. M.-L. H. J. S. N. Black, "Green diamond, the vide0," *youtube*, vol. vol-11, 2016. [Online]. Available: https://www.youtube.com/watch?v=qbpohTjthjE ix, 17

[9] A. M. Morales and C. M. Lieber, "A laser ablation method for the synthesis of crystalline semiconductor nanowires," *Science*, vol. 279, no. 5348, pp. 208–211, 1998. [Online]. Available: http://science.sciencemag.org/content/279/5348/208 x, 20

[10] L. E. Jensen, M. T. BjÃűrk, S. Jeppesen, A. I. Persson, B. J. Ohlsson, and L. Samuelson, "Role of surface diffusion in chemical beam epitaxy of inas nanowires," *Nano Letters*, vol. 4, no. 10, pp. 1961–1964, 2004. [Online]. Available: http://dx.doi.org/10.1021/nl048825k x, 20

[11] D. Whang, S. Jin, Y. Wu, and C. M. Lieber, "Large-scale hierarchical organization of nanowire arrays for integrated nanosystems," *Nano Letters*, vol. 3, no. 9, pp. 1255–1259, 2003. [Online]. Available: http://dx.doi.org/10.1021/nl0345062 x, 20

[12] Y. Li, J. Xiang, F. Qian, S. GradeÄDak, Y. Wu, H. Yan, D. A. Blom, and C. M. Lieber, "Dopant-free gan/aln/algan radial nanowire heterostructures as high electron mobility transistors," *Nano Letters*, vol. 6, no. 7, pp. 1468–1473, 2006, pMID: 16834431. [Online]. Available: http://dx.doi.org/10.1021/nl060849z x, 20

[13] M. Kasu, K. Ueda, Y. Yamauchi, A. Tallaire, and T. Makimoto, "Diamond-based RF power transistors: Fundamentals and applications," *Diamond & Related Materials*, vol. 16, no. 4-7, pp. 1010–1015, Apr. 2007. [Online]. Available: http://linkinghub.elsevier.com/retrieve/pii/S0925963506005309 x, 21

[14] T. Matsumoto, H. Kato, K. Oyama, T. Makino, M. Ogura, D. Takeuchi, T. Inokuma, N. Tokuda, and S. Yamasaki, "Inversion channel diamond metal-oxide-semiconductor field-effect transistor with normally off characteristics," *Scientific Reports*, vol. 6, no. 1, p. 2357, Aug. 2016. [Online]. Available: http://www.nature.com/articles/srep31585 x, 21, 22, 23

[15] Moxfyre, "Raman energy levels," *Wikipedia*, 2009. [Online]. Available: https://en.wikipedia.org/wiki/Raman_spectroscopy x, 27

[16] K. Ushizawa, G. Mikka N., K. Watanabe, I. Sakaguchi, Y. Sato, and T. Ando, "Raman spectroscopic study on 100 facet of boron-doped chemical-vapour-deposited diamond crystals with fano line fitting," *Journal of Raman Spectroscopy*, vol. 30, no. 10, pp. 957–961, 1999. [Online]. Available: http://dx.doi.org/10.1002/(SICI)1097-4555(199910)30:10<957::AID-JRS469>3.0.CO;2-Q xi, 28

[17] R. GmbH, "Raith150 manual," *Wikimedia, Creative Commons Attribution-Share Alike 3.0 Unported*, 2005. [Online]. Available: www.raith.com xi, 33, 34

[18] B. Edwards, "Installation and maintenance instructuions," *Manual*, 2017. [Online]. Available: http://mfc.engr.arizona.edu/documents/E-beam/E090_72_880F.pdf xi, 39, 40

[19] D. Martien, "Inroduction to ac susceptibility," *Quantum Design*, 2017. [Online]. Available: https://www.qdusa.com/sitedocs/appNotes/ppms/1078-201.pdf xi, 41, 42

[20] G. Turtle, "ee432 semiconductor fabrication," *Iowa State University*, 2017. [Online]. Available: http://tuttle.merc.iastate.edu/ee432/topics/metals/tlm_measurements.pdf xi, xii, 44, 45, 46, 47, 48

[21] R. Balmer, I. Friel, S. Woollard, C. Wort, G. Scarsbrook, S. Coe, H. El-Hajj, A. Kaiser, A. Denisenko, E. Kohn, and J. Isberg, "Unlocking diamond's potential as an electronic material," *Philosophical Transactions of the Royal Society of London A: Mathematical, Physical and Engineering Sciences*, vol. 366, no. 1863, pp. 251–265, 2008. [Online]. Available: http://rsta.royalsocietypublishing.org/content/366/1863/251 xii, 54

[22] J. E. Butler, A. Vikharev, A. Gorbachev, M. Lobaev, A. Muchnikov, D. Radischev, V. Isaev, V. Chernov, S. Bogdanov, M. Drozdov, E. Demidov, E. Surovegina, V. Shashkin, A. Davidov, H. Tan, L. Meshi, A. C. Pakpour Tabrizi, M. L. Hicks, and R. B. Jackman, "Nanometric diamond delta doping with boron," *Physica Status Solidi (RRL) - Rapid Research Letters*, vol. 11, no. 1, p. 1600329, Jan. 2017. [Online]. Available: http://onlinelibrary.wiley.com/doi/10.1002/pssr.201600329/full xv, 7, 55, 88, 90

[23] J. E. Field, "The properties of natural and synthetic diamond," *Academic, New York*, 1992. 5, 53, 80

[24] S. N. Ahmed, *Physics and Engineering of Radiation Detection, Elsevier, second edition.* 5

[25] R. Linares, "Cvd-grown synthetic diamonds, part 1: History," 2013. [Online]. Available: http://www.gia.edu/news-research-CVD-grown-part1 5

[26] Y. Takano, M. Nagao, T. Takenouchi, H. Umezawa, I. Sakaguchi, M. Tachiki, and H. Kawarada, "Superconductivity in polycrystalline diamond thin films," *Diamond and Related Materials*, vol. 14, pp. 1936–1938, Nov. 2005. 5

[27] W. Schottky, "Halbleitertheorie der Sperrschicht," *Naturwissenschaften*, vol. 26, pp. 843–843, Dec. 1938. 8

[28] N. F. Mott, "The theory of crystal rectifiers," *Proceedings of the Royal Society of London A: Mathematical, Physical and Engineering Sciences*, vol. 171, no. 944, pp. 27–38, 1939. [Online]. Available: http://rspa.royalsocietypublishing.org/content/171/944/27 8

[29] F. Maier, M. Riedel, B. Mantel, J. Ristein, and L. Ley, "Origin of surface conductivity in diamond," *Phys. Rev. Lett.*, vol. 85, pp. 3472–3475, Oct 2000. [Online]. Available: http://link.aps.org/doi/10.1103/PhysRevLett.85.3472 12

[30] V. Chakrapani, S. Eaton, A. Anderson, M. Tabib-Azar, and J. Angus, "Diamond surface conductivity: Effect of ph, temperature, and humidity," in *Proceedings of the 9th International Symposium on Diamond Materials*, 2004, pp. 3–8. 13

[31] W. Gajewski, P. Achatz, O. A. Williams, K. Haenen, E. Bustarret, M. Stutzmann, and J. A. Garrido, "Electronic and optical properties of boron-doped nanocrystalline diamond films," *Physical Review B*, vol. 79, no. 4, p. 045206, 2009. 13, 81

[32] O. A. Williams, S. Curat, J. E. Gerbi, D. M. Gruen, and R. B. Jackman, "n-type conductivity in ultrananocrystalline diamond films," *Applied Physics Letters*, vol. 85, no. 10, pp. 1680–1682, 2004. 13

[33] M. Salvadori, W. W. R. d. Araujo, F. d. S. Teixeira, M. Cattani, A. Pasquarelli, E. Oks, and I. Brown, "Termination of diamond surfaces with hydrogen, oxygen and fluorine using a small, simple plasma gun," *Diamond and Related Materials*, vol. 19, no. 4, pp. 324–328, 2010. 13

[34] M. V. Hauf, P. Simon, M. Seifert, A. W. Holleitner, M. Stutzmann, and J. A. Garrido, "Low dimensionality of the diamond surface conductivity," *arXiv preprint arXiv:1310.8616*, 2013. 13

[35] T. Yokoya, T. Nakamura, T. Matsushita, T. Muro, Y. Takano, M. Nagao, T. Takenouchi, H. Kawarada, and T. Oguchi, "Origin of the metallic properties of heavily boron-doped superconducting diamond," *Nature*, vol. 438, no. 7068, pp. 647–650, 12 2005. [Online]. Available: http://dx.doi.org/10.1038/nature04278 13, 24, 43, 71, 79

[36] M. Polo, J. Cifre, and J. Esteve, "Boron incorporation effects in cvd diamond film growth," *Vacuum*, vol. 45, no. 10, pp. 1013–1014, 1994. 13

[37] R. Kalish, "The search for donors in diamond," *Diamond and Related Materials*, vol. 10, pp. 1749–1755, 2001. 14

[38] R. Edgington, S. Sato, Y. Ishiyama, R. Morris, R. B. Jackman, and H. Kawarada, "Growth and electrical characterisation of Ĩt-doped boron layers on (111) diamond surfaces," *Journal of Applied Physics*, vol. 111, no. 3, 2012. [Online]. Available: http://scitation.aip.org/content/aip/journal/jap/111/3/10.1063/1.3682760 14

[39] E. F. Schubert, *Delta-doping of Semiconductors*, 1996. 14

[40] J. J. Harris, "Delta-doping in semiconductor," *Journal of Materials Science: Materials in Electronics*, vol. 4, no. 2, pp. 93–105, 1993. 14

[41] M. Fuechsle, J. A. Miwa, S. Mahapatra, H. Ryu, S. Lee, O. Warschkow, L. C. L. Hollenberg, G. Klimeck, and M. Y. Simmons, "A single-atom transistor," *Nat Nano*, vol. 7, no. 4, pp. 242–246, 04 2012. [Online]. Available: http://dx.doi.org/10.1038/nnano.2012.21 14

[42] B. Weber, H. Ryu, Y.-H. M. Tan, G. Klimeck, and M. Y. Simmons, "Limits to metallic conduction in atomic-scale quasi-one-dimensional silicon wires," *Phys. Rev. Lett.*, vol. 113, p. 246802, Dec 2014. [Online]. Available: http://link.aps.org/doi/10.1103/PhysRevLett.113.246802 14

[43] B. Weber, S. Mahapatra, H. Ryu, S. Lee, A. Fuhrer, T. C. G. Reusch, D. L. Thompson, W. C. T. Lee, G. Klimeck, L. C. L. Hollenberg, and M. Y. Simmons, "Ohm's law survives to the atomic scale," *Science*, vol. 335, no. 6064, pp. 64–67, 2012. [Online]. Available: http://www.sciencemag.org/content/335/6064/64.abstract 14

[44] Y. Kozuka, M. Kim, C. Bell, B. G. Kim, Y. Hikita, and H. Y. Hwang, "Two-dimensional normal-state quantum oscillations in a superconducting heterostructure," *Nature*, vol. 462, no. 7272, pp. 487–490, 11 2009. [Online]. Available: http://dx.doi.org/10.1038/nature08566 14

[45] F. Mazzola, C. M. Polley, J. A. Miwa, M. Y. Simmons, and J. W. Wells, "Disentangling phonon and impurity interactions in Îŧ-doped si(001)," *Applied Physics Letters*, vol. 104, no. 17, pp. –, 2014. [Online]. Available: http://scitation.aip.org/content/aip/journal/apl/104/17/10.1063/1.4874651 14

[46] J. A. Miwa, O. Warschkow, D. J. Carter, N. A. Marks, F. Mazzola, M. Y. Simmons, and J. W. Wells, "Valley splitting in a silicon quantum device platform," *Nano Letters*, vol. 14, no. 3, pp. 1515–1519, 2014, pMID: 24571617. [Online]. Available: http://dx.doi.org/10.1021/nl404738j 14

[47] J. Nakanishi, A. Otsuki, T. Oku, O. Ishiwata, and M. Murakami, "Formation of ohmic contacts to pâĂŘtype diamond using carbide forming metals," *Journal of Applied Physics*, vol. 76, no. 4, pp. 2293–2298, 1994. [Online]. Available: http://dx.doi.org/10.1063/1.357649 16, 122

[48] V. Venkatesan and K. Das, "Ohmic contacts on diamond by b ion implantation and ti-au metallization," *IEEE Electron Device Letters*, vol. 13, no. 2, pp. 126–128, Feb 1992. 16

[49] W. Wang, C. Hu, F. Li, S. Li, Z. Liu, F. Wang, J. Fu, and H. Wang, "Palladium ohmic contact on hydrogen-terminated single crystal diamond film," *Diamond and Related Materials*, vol. 59, pp. 90 – 94, 2015. [Online]. Available: http://www.sciencedirect.com/science/article/pii/S0925963515300431 16

[50] H. Kiyota, E. Matsushima, K. Sato, H. Okushi, T. Ando, M. Kamo, Y. Sato, and M. Iida, "Electrical properties of schottky barrier formed on asâĂŘgrown and oxidized surface of homoepitaxially grown diamond (001) film," *Applied Physics Letters*, vol. 67, no. 24, pp. 3596–3598, 1995. [Online]. Available: http://dx.doi.org/10.1063/1.115329 16

[51] C. Mead and T. McGill, "Schottky barrier heights on p-type diamond and silicon carbide (6h)," *Physics Letters A*, vol. 58, no. 4, pp. 249 – 251, 1976. [Online]. Available: http://www.sciencedirect.com/science/article/pii/0375960176900888 16

[52] M. C. Hicks, C. R. Wronski, S. A. Grot, G. S. Gildenblat, A. R. Badzian, T. Badzian, and R. Messier, "The barrier height of schottky diodes with a chemical-vapor-deposited diamond base," *Journal of Applied Physics*, vol. 65, no. 5, pp. 2139–2141, 1989. [Online]. Available: http://dx.doi.org/10.1063/1.342864 16

[53] D. A. Evans, O. R. Roberts, A. R. Vearey-Roberts, D. P. Langstaff, D. J. Twitchen, and M. Schwitters, "Direct observation of schottky to ohmic transition in al-diamond contacts using real-time photoelectron spectroscopy," *Applied Physics Letters*, vol. 91, no. 13, p. 132114, 2007. [Online]. Available: http://dx.doi.org/10.1063/1.2790779 16

[54] D. K. Schroder, "Mobility in semiconductor material and device characterization, 3rd ed," *IEEE, New Jersey,*, 2006. [Online]. Available: http://www.nobelprize.org/nobel_prizes/physics/laureates/1956/bardeen-lecture.html 18

[55] Y. Cui, Z. Zhong, D. Wang, W. U. Wang, and C. M. Lieber, "High performance silicon nanowire field effect transistors," *Nano Letters*, vol. 3, no. 2, pp. 149–152, 2003. [Online]. Available: http://dx.doi.org/10.1021/nl0258751 18

[56] G. A. Asres, A. Dombovari, T. Sipola, R. Puskás, A. Kukovecz, Z. Kónya, A. Popov, J.-F. Lin, G. S. Lorite, M. Mohl, G. Toth, A. Lloyd Spetz, and K. Kordas, "A novel ws_2 nanowire-nanoflake hybrid material synthesized from wo3 nanowires in sulfur vapor," vol. 6, 05 2016. 18

[57] F. Patolsky and C. M. Lieber, "Nanowire nanosensors," *Materials Today*, vol. 8, no. 4, pp. 20 – 28, 2005. [Online]. Available: http://www.sciencedirect.com/science/article/pii/S1369702105007911 18

[58] R. Huang, R. Wang, J. Zhuge, C. Liu, T. Yu, L. Zhang, X. Huang, Y. Ai, J. Zou, Y. Liu, J. Fan, H. Liao, and Y. Wang, "Characterization and analysis of gate-all-around si nanowire transistors for extreme scaling," in *2011 IEEE Custom Integrated Circuits Conference (CICC)*, Sept 2011, pp. 1–8. 18

[59] S. Chuang, Q. Gao, R. Kapadia, A. C. Ford, J. Guo, and A. Javey, "Ballistic inas nanowire transistors," *Nano Letters*, vol. 0. [Online]. Available: http://dx.doi.org/10.1021/nl3040674@proofing 18

[60] L. P. Rokhinson, X. Liu, and J. K. Furdyna, "The fractional a.c. josephson effect in a semiconductor-superconductor nanowire as a signature of majorana particles," *Nat Phys*, vol. 8, no. 11, pp. 795–799, 11 2012. 19

[61] Y. Coffinier, E. Galopin, S. Szunerits, and R. Boukherroub, "Preparation of superhydrophobic and oleophobic diamond nanograss array," *J. Mater. Chem.*, vol. 20, pp. 10 671–10 675, 2010. [Online]. Available: http://dx.doi.org/10.1039/C0JM01296C 19

[62] W. Wang, C. Hu, S. Y. Li, F. N. Li, Z. C. Liu, and F. Wang, "Diamond based field-effect transistors of Zr gate with SiN x dielectric layers," 2015. [Online]. Available: http://dl.acm.org/citation.cfm?id=2930567 21

[63] T. Klein, P. Achatz, J. Kacmarcik, C. Marcenat, F. Gustafsson, J. Marcus, E. Bustarret, J. Pernot, F. Omnes, B. E. Sernelius, C. Persson, A. Ferreira da Silva, and C. Cytermann, "Metal-insulator transition and superconductivity in boron-doped diamond," *Phys. Rev. B*, vol. 75, p. 165313, Apr 2007. [Online]. Available: http://link.aps.org/doi/10.1103/PhysRevB.75.165313 24, 43, 79, 80, 81

[64] E. A. Ekimov, V. A. Sidorov, E. D. Bauer, N. N. Mel'nik, N. J. Curro, J. D. Thompson, and S. M. Stishov, "Superconductivity in diamond," *Nature*, vol. 428, no. 6982, pp. 542–545, 04 2004. [Online]. Available: http://dx.doi.org/10.1038/nature02449 24, 43, 79

[65] M. Calandra and F. Mauri, "High-T_c superconductivity in superhard diamondlike bc_5," *Phys. Rev. Lett.*, vol. 101, p. 016401, Jun 2008. [Online]. Available: http://link.aps.org/doi/10.1103/PhysRevLett.101.016401 24, 43, 79

[66] H. Okazaki, T. Wakita, T. Muro, T. Nakamura, Y. Muraoka, T. Yokoya, S.-i. Kurihara, H. Kawarada, T. Oguchi, and Y. Takano, "Signature of high Tcabove 25K in high quality superconducting diamond," *Applied Physics Letters*, vol. 106, no. 5, p. 052601, Feb. 2015. [Online]. Available: http://aip.scitation.org/doi/10.1063/1.4907411 24, 67

[67] A. V. Sumant, O. Auciello, R. W. Carpick, S. Srinivasan, and J. E. Butler, "Ultrananocrystalline and nanocrystalline diamond thin films for mems/nems applications," *MRS Bulletin*, vol. 35, no. 4, pp. 281–288, 2010. 24

[68] S. Mandal, T. Bautze, O. A. Williams, C. Naud, Ã. Bustarret, F. OmnÃÍs, P. RodiÃÍre, T. Meunier, C. BÃđuerle, and L. Saminadayar, "The diamond superconducting quantum interference device," *ACS Nano*, vol. 5, no. 9, pp. 7144–7148, 2011, pMID: 21800905. [Online]. Available: http://dx.doi.org/10.1021/nn2018396 24

[69] C. E. Nebel, B. Rezek, D. Shin, H. Uetsuka, and N. Yang, "Diamond for bio-sensor applications," *Journal of Physics D: Applied Physics*, vol. 40, no. 20, p. 6443, 2007. 24

[70] X. Wang, A. R. Ruslinda, Y. Ishiyama, Y. Ishii, and H. Kawarada, "Higher coverage of carboxylic acid groups on oxidized single crystal diamond (001)," *Diamond and Related Materials*, vol. 20, no. 10, pp. 1319 – 1324, 2011. [Online]. Available: http://www.sciencedirect.com/science/article/pii/S0925963511002974 26

[71] A. Fiori, F. Jomard, T. Teraji, G. Chicot, and E. Bustarret, "Improved depth resolution of secondary ion mass spectrometry profiles in diamond: A quantitative analysis of the delta-doping," *Thin Solid Films*, vol. 557, pp. 222–226, Apr. 2014. [Online]. Available: http://linkinghub.elsevier.com/retrieve/pii/S0040609013016878 29

[72] C. Su and J. C. Lin, "Thermal desorption of hydrogen from the diamond C(100) surface," *Surface Science*, vol. 406, no. 1, pp. 149–166, May 1998. [Online]. Available: http://linkinghub.elsevier.com/retrieve/pii/S0039602898001071 29

[73] A. V. Hamza, G. D. Kubiak, and R. H. Stulen, "Hydrogen chemisorption and the structure of the diamond C(100)-(2 ? 1) surface," *Surface Science*, vol. 237, no. 1-3, pp. 35–52, Nov. 1990. [Online]. Available: http://linkinghub.elsevier.com/retrieve/pii/003960289090517C 29, 70

[74] B. J. Hausmann, M. Khan, Y. Zhang, T. M. Babinec, K. Martinick, M. McCutcheon, P. R. Hemmer, and M. Lončar, "Fabrication of diamond nanowires for quantum information processing applications," *Diamond and Related Materials*, vol. 19, pp. 621–629, 2010. [Online]. Available: http://www.sciencedirect.com/science/article/pii/S0925963510000312 34

[75] H. Hoff, G. Waytena, C. Vold, J. Suehle, I. Isaacson, M. Rebbert, D. Ma, and K. Harris, "Ohmic contacts to semiconducting diamond using a ti/pt/au trilayer metallization scheme," *Diamond and Related Materials*, vol. 5, no. 12, pp. 1450 – 1456, 1996. [Online]. Available: http://www.sciencedirect.com/science/article/pii/S0925963596005663 39

[76] A. Damascelli, "Probing the electronic structure of complex systems by arpes," *Physica Scripta*, vol. T109, no. 61–74, 2004. 43, 71, 73

[77] H. Guyot, P. Achatz, A. Nicolaou, P. Le Fèvre, F. Bertran, A. Taleb-Ibrahimi, and E. Bustarret, "Band structure parameters of metallic diamond from angle-resolved photoemission spectroscopy," *Phys. Rev. B*, vol. 92, p. 045135, Jul 2015. [Online]. Available: http://link.aps.org/doi/10.1103/PhysRevB.92.045135 43, 71

[78] K.-W. Lee and W. E. Pickett, "Superconductivity in boron-doped diamond," *Phys. Rev. Lett.*, vol. 93, p. 237003, Nov 2004. [Online]. Available: http://link.aps.org/doi/10.1103/PhysRevLett.93.237003 43, 53, 64, 75

[79] X. Blase, C. Adessi, and D. Connétable, "Role of the dopant in the superconductivity of diamond," *Phys. Rev. Lett.*, vol. 93, p. 237004, Nov 2004. [Online]. Available: http://link.aps.org/doi/10.1103/PhysRevLett.93.237004 43, 64, 75

[80] K. Ishizaka, R. Eguchi, S. Tsuda, T. Yokoya, A. Chainani, T. Kiss, T. Shimojima, T. Togashi, S. Watanabe, C.-T. Chen, C. Q. Zhang, Y. Takano, M. Nagao, I. Sakaguchi, T. Takenouchi, H. Kawarada, and S. Shin, "Observation of a superconducting gap in boron-doped diamond by laser-excited photoemission spectroscopy," *Phys. Rev. Lett.*, vol. 98, p. 047003, Jan 2007. [Online]. Available: http://link.aps.org/doi/10.1103/PhysRevLett.98.047003 43

[81] L. Boeri, J. Kortus, and O. K. Andersen, "Three-dimensional mgb_2-type superconductivity in hole-doped diamond," *Phys. Rev. Lett.*, vol. 93, p. 237002, Nov 2004. [Online]. Available: http://link.aps.org/doi/10.1103/PhysRevLett.93.237002 43

[82] J. E. Graebner, *Thermal Conductivity of Diamond*. Boston, MA: Springer US, 1995, pp. 285–318. [Online]. Available: http://dx.doi.org/10.1007/978-1-4615-2257-7_7 53, 80

[83] M. Gabrysch, S. Majdi, D. J. Twitchen, and J. Isberg, "Electron and hole drift velocity in chemical vapor deposition diamond," *Journal of Applied Physics*, vol. 109, no. 6, p. 063719, 2011. [Online]. Available: http://dx.doi.org/10.1063/1.3554721 53, 80

[84] R. S. Balmer, J. R. Brandon, S. L. Clewes, H. K. Dhillon, J. M. Dodson, I. Friel, P. N. Inglis, T. D. Madgwick, M. L. Markham, T. P. Mollart, N. Perkins, G. A. Scarsbrook, D. J. Twitchen, A. J. Whitehead, J. J. Wilman, and S. M. Woollard, "Chemical vapour deposition synthetic diamond: materials, technology and applications," *Journal of Physics: Condensed Matter*, vol. 21, no. 36, p. 364221, 2009. [Online]. Available: http://stacks.iop.org/0953-8984/21/i=36/a=364221 53, 80

[85] M. Kamo, Y. Sato, S. Matsumoto, and N. Setaka, "Diamond synthesis from gas phase in microwave plasma," *Journal of Crystal Growth*, vol. 62, no. 3, pp. 642 – 644, 1983. [Online]. Available: http://www.sciencedirect.com/science/article/pii/0022024883904116 53

[86] S. N. Demlow, R. Rechenberg, and T. Grotjohn, "The effect of substrate temperature and growth rate on the doping efficiency of single crystal boron doped diamond," *Diamond and Related Materials*, vol. 49, pp. 19 – 24, 2014. [Online]. Available: http://www.sciencedirect.com/science/article/pii/S0925963514001241 57

[87] S. A. Solin and A. K. Ramdas, "Raman spectrum of diamond," *Phys. Rev. B*, vol. 1, pp. 1687–1698, Feb 1970. [Online]. Available: http://link.aps.org/doi/10.1103/PhysRevB.1.1687 67

[88] G. Bachelier, I. Russier-Antoine, E. Benichou, C. Jonin, N. Del Fatti, F. Vallée, and P.-F. Brevet, "Fano profiles induced by near-field coupling in heterogeneous dimers of gold and silver nanoparticles," *Phys. Rev. Lett.*, vol. 101, p. 197401, Nov 2008. [Online]. Available: http://link.aps.org/doi/10.1103/PhysRevLett.101.197401 67

[89] J. W. A. III, W. Walukiewicz, M. McCluskey, M. A. Plano, and M. I. Landstrass, "Fano interference of the raman phonon in heavily boronâĂŘdoped diamond films grown by chemical vapor deposition," *Applied Physics Letters*, vol. 66, no. 5, pp. 616–618, 1995. [Online]. Available: http://dx.doi.org/10.1063/1.114031 67

[90] R. Singh, R. Lal, U. C. Upreti, D. K. Suri, A. V. Narlikar, V. P. S. Awana, J. Albino Aguiar, and M. Shahabuddin, "Superconductivity in Zn-doped tetragonal LaBaCaCu3O7δsystems," *Physical Review B*, vol. 55, no. 2, pp. 1216–1222, Jan. 1997. [Online]. Available: https://link.aps.org/doi/10.1103/PhysRevB.55.1216 67

[91] M. Bianchi, R. C. Hatch, J. Mi, B. B. Iversen, and P. Hofmann, "Simultaneous quantization of bulk conduction and valence states through adsorption of nonmagnetic impurities on bi_2se_3," *Phys. Rev. Lett.*, vol. 107, p. 086802, Aug 2011. [Online]. Available: http://link.aps.org/doi/10.1103/PhysRevLett.107.086802 73

[92] J. A. Miwa, P. Hofmann, M. Y. Simmons, and J. W. Wells, "Direct measurement of the band structure of a buried two-dimensional electron gas," *Phys. Rev. Lett.*, vol. 110, p. 136801, Mar 2013. [Online]. Available: http://link.aps.org/doi/10.1103/PhysRevLett.110.136801 73, 77

[93] F. Mazzola, M. T. Edmonds, K. Høydalsvik, D. J. Carter, N. A. Marks, B. C. C. Cowie, L. Thomsen, J. Miwa, M. Y. Simmons, and J. W. Wells, "Determining the electronic confinement of a subsurface metallic state," *ACS Nano*, vol. 8, no. 10, pp. 10 223–10 228, 2014, pMID: 25243326. [Online]. Available: http://dx.doi.org/10.1021/nn5045239 73

[94] F. J. Himpsel, "Experimental determination of bulk energy band dispersions," *Appl. Opt.*, vol. 19, pp. 3964–3970, 1980. 73

[95] F. Mazzola, J. W. Wells, R. Yakimova, S. Ulstrup, J. A. Miwa, R. Balog, M. Bianchi, M. Leandersson, J. Adell, P. Hofmann, and T. Balasubramanian, "Kinks in the σ band of graphene induced by electron-phonon coupling," *Phys. Rev. Lett.*, vol. 111, p. 216806, Nov 2013. [Online]. Available: http://link.aps.org/doi/10.1103/PhysRevLett.111.216806 73

[96] E. L. Shirley, L. J. Terminello, A. Santoni, and F. J. Himpsel, "Brillouin-zone-selection effects in graphite photoelectron angular distributions," *Phys. Rev. B*, vol. 51, pp. 13 614–13 622, May 1995. [Online]. Available: http://link.aps.org/doi/10.1103/PhysRevB.51.13614 73

[97] F. Mazzola, M. T. Edmonds, K. Høydalsvik, D. J. Carter, N. A. Marks, B. C. C. Cowie, L. Thomsen, J. Miwa, M. Y. Simmons, and J. W. Wells, "Determining the electronic confinement of a subsurface metallic state," *ACS Nano*, vol. 8, no. 10, pp. 10 223–10 228, 2014, pMID: 25243326. [Online]. Available: http://dx.doi.org/10.1021/nn5045239 77

[98] T. Valla, P. D. Johnson, Z. Yusof, B. Wells, Q. Li, S. M. Loureiro, R. J. Cava, M. Mikami, Y. Mori, M. Yoshimura, and T. Sasaki, "Coherence-incoherence and dimensional crossover in layered strongly correlated metals," *Nature*, vol. 417, no. 6889, pp. 627–630, 06 2002. [Online]. Available: http://dx.doi.org/10.1038/nature00774 79

[99] M. M. Qazilbash, J. J. Hamlin, R. E. Baumbach, L. Zhang, D. J. Singh, M. B. Maple, and D. N. Basov, "Electronic correlations in the iron pnictides," *Nat Phys*, vol. 5, no. 9, pp. 647–650, 09 2009. [Online]. Available: http://dx.doi.org/10.1038/nphys1343 79

[100] P. D. C. King, H. I. Wei, Y. F. Nie, M. Uchida, C. Adamo, S. Zhu, X. He, I. Bozovic, D. G. Schlom, and K. M. Shen, "Atomic-scale control of competing electronic phases in ultrathin lanio3," *Nat Nano*, vol. 9, no. 6, pp. 443–447, 06 2014. [Online]. Available: http://dx.doi.org/10.1038/nnano.2014.59 79

[101] D. Jâerome and L. G. Caron, "Low dimensional conductors and superconductors," *Plenum, New York*, 1987. 79

[102] J. Kortus, "Superconductivity: Where are the electrons?" *Nat Mater*, vol. 4, no. 12, pp. 879–880, 12 2005. [Online]. Available: http://dx.doi.org/10.1038/nmat1542 79

[103] P. Muret, P.-N. Volpe, T.-N. Tran-Thi, J. Pernot, C. Hoarau, F. Omnès, and T. Teraji, "Schottky diode architectures on p-type diamond for fast switching, high forward current density and high breakdown field rectifiers," *Diamond and Related Materials*, vol. 20, no. 3, pp. 285–289, 2011. 80

[104] S. Koizumi, T. Teraji, and H. Kanda, "Phosphorus-doped chemical vapor deposition of diamond," *Diamond and Related Materials*, pp. 935 – 940, 2000. [Online]. Available: http://www.sciencedirect.com/science/article/pii/S092596350000217X 80

[105] A. Denisenko and E. Kohn, "Diamond power devices. concepts and limits," *Diamond and Related Materials*, vol. 14, no. 3, pp. 491 – 498, 2005, proceedings of Diamond 2004, the 15th European Conference on Diamond, Diamond-Like Materials, Carbon Nanotubes, Nitrides and Silicon Carbide. [Online]. Available: http://www.sciencedirect.com/science/article/pii/S0925963505000087 81

[106] C. I. Pakes, J. A. Garrido, and H. Kawarada, "Diamond surface conductivity: Properties, devices, and sensors," *MRS Bulletin*, vol. 39, no. 6, p. 542âĂŞ548, 2014. 81

[107] A. Fiori, J. Pernot, E. Gheeraert, and E. Bustarret, "Simulations of carrier confinement in boron Ît-doped diamond devices," *Physica Status Solidi (a)*, vol. 207, no. 9, pp. 2084–2087, 2010. [Online]. Available: http://dx.doi.org/10.1002/pssa.201000062 81

[108] J. Scharpf, A. Denisenko, C. I. Pakes, S. Rubanov, A. Bergmaier, G. Dollinger, C. Pietzka, and E. Kohn, "Transport behaviour of boron delta-doped diamond," *Physica Status Solidi (a)*, vol. 210, no. 10, pp. 2028–2034, 2013. [Online]. Available: http://dx.doi.org/10.1002/pssa.201300093 81

[109] G. Chicot, A. Fiori, P. N. Volpe, T. N. T. Thi, J. C. Gerbedoen, J. Bousquet, M. P. Alegre, J. C. PiÃśero, D. AraÃžjo, F. Jomard, A. Soltani, J. C. D. Jaeger, J. Morse, J. HÃđrtwig, N. Tranchant, C. Mer-Calfati, J. C. Arnault, J. Delahaye, T. Grenet, D. Eon, F. OmnÃís, J. Pernot, and E. Bustarret, "Electronic and physico-chemical properties of nanometric boron delta-doped diamond structures," *Journal of Applied Physics*, vol. 116, no. 8, p. 083702, 2014. [Online]. Available: http://dx.doi.org/10.1063/1.4893186 81, 82

[110] A. L. Vikharev, A. M. Gorbachev, M. A. Lobaev, A. B. Muchnikov, D. B. Radishev, V. A. Isaev, V. V. Chernov, S. A. Bogdanov, M. N. Drozdov, and J. E. Butler, "Novel microwave plasma-assisted cvd reactor for diamond delta doping," *physica status solidi (RRL) âĂŞ Rapid Research Letters*, vol. 10, no. 4, pp. 324–327, 2016. [Online]. Available: http://dx.doi.org/10.1002/pssr.201510453 82

[111] S. C. Eaton, A. B. Anderson, J. C. Angus, Y. E. Evstefeeva, and Y. V. Pleskov, "Co-doping of diamond with boron and sulfur," *Electrochemical and Solid-State Letters*, vol. 5, no. 8, pp. G65–G68, 2002. [Online]. Available: http://esl.ecsdl.org/content/5/8/G65.abstract 82

[112] A. B. Muchnikov, A. L. Vikharev, J. E. Butler, V. V. Chernov, V. A. Isaev, S. A. Bogdanov, A. I. Okhapkin, P. A. Yunin, and Y. N. Drozdov, "Homoepitaxial growth of cvd diamond after icp pretreatment," *physica status solidi (a)*, vol. 212, no. 11, pp. 2572–2577, 2015. [Online]. Available: http://dx.doi.org/10.1002/pssa.201532171 82

[113] J. P. D. E. Karl E. Spear (Editor), "Synthetic diamond: Emerging cvd science and technology," 1994. 96

[114] F. Dolde, I. Jakobi, B. Naydenov, N. Zhao, S. Pezzagna, C. Trautmann, J. Meijer, P. Neumann, F. Jelezko, and J. Wrachtrup, "Room-temperature entanglement between single defect spins in diamond," *Nature Physics*, vol. 9, no. 3, pp. 139–143, Feb. 2013. [Online]. Available: http://www.nature.com/doifinder/10.1038/nphys2545 96, 97

[115] D. G. England, K. A. G. Fisher, J.-P. W. MacLean, P. J. Bustard, R. Lausten, K. J. Resch, and B. J. Sussman, "Storage and Retrieval of THz-Bandwidth Single Photons Using a Room-Temperature Diamond Quantum Memory," *Physical review . . .*, vol. 114, no. 5, p. 053602, Feb. 2015. [Online]. Available: https://link.aps.org/doi/10.1103/PhysRevLett.114.053602 96

[116] X. Duan, Y. Li, N. K. Rajan, D. A. Routenberg, Y. Modis, and M. A. Reed, "Quantification of the affinities and kinetics of protein interactions using silicon nanowire biosensors," *Nat Nano*, vol. 7, no. 6, pp. 401–407, 06 2012. [Online]. Available: http://dx.doi.org/10.1038/nnano.2012.82 96

[117] R. Murali, Y. Yang, K. Brenner, T. Beck, and J. D. Meindl, "Breakdown current density of graphene nanoribbons," *Applied Physics Letters*, vol. 94, no. 24, p. 243114, 2009. [Online]. Available: http://dx.doi.org/10.1063/1.3147183 122